Faculty of Science and Engineering
Department of Petroleum Engineering

Pore-Scale Investigations of Rock and Fluid Microstructure and Fluid Displacement Processes in Geological Porous Media

TAUFIQURRAHMAN

This thesis is presented for the Degree of
Doctor of Philosophy
of
Curtin University

August 2018

DECLARATION OF ACADEMIC INTEGRITY

To the best of my knowledge and belief this thesis contains no material previously published by any other person except where due acknowledgment has been made.

This thesis contains no material which has been accepted for the award of any other degree or diploma in any university.

Taufiqurrahman,
1st of August 2018

COPYRIGHT

I warrant that I have obtained, where necessary, permission from the copyright owners to use any third-party copyright material reproduced in the thesis (e.g. questionnaires, artwork, unpublished letters), or to use any of my own published work (e.g. journal articles) in which the copyright is held by another party (e.g. publisher, co-author).

Taufiqurrahman,
1st of August 2018

DEDICATION

I would like to dedicate my thesis to my beloved family.

To my father, Mr. Anwar Abubakar BA. He is the best role model, and the greatest inspirator for my whole entire life.

To the people of Acheh who have sacrificed their lives for freedom, independence, sovereignty, justice, and dignity of their country!

ACKNOWLEDGMENT

I would like to express my deepest gratitude and appreciation to my principal supervisor Professor Stefan Iglauer for his continuous support, guidance, insightful comments, and encouragements. My gratitude also goes to Associate Professor Ahmed Barifcani for his continuous encouragement, and motivation to complete this thesis on schedule. I would like to express my sincere gratitude for Associate Professor Maxim Lebedev for his continuous guidance on X-Ray imaging data analysis and allowing me to use the facilities therein to conduct the required experimental work. My earnest thank also goes to Dr. Andrew Squelch, a Senior Visualisation Specialist at the Department of Petroleum Geophysics, Curtin University, for his continuous guidance and advice to operate Avizo software that is greatly needed in image processing. Thanks also goes to Associate Professor Mofazzal Hossain, Head of Department of Petroleum Engineering, Curtin University and Professor Brian even, former head of the Department, for their continuous support during my time at this department.

I am deeply indebted to my colleague at Department of Petroleum Engineering Curtin University, Ahmed Yaseri for his continuous unfailing advice, encouragement, constructive idea, inspiration, and kind assistance.

I would like to acknowledge the funding and support given to me by the Australian Federal Government, under the Research Training Schema, who has fully funded my PhD fees.

I would like to thank my family for their unconditional support and love. For my parents, Mr. Anwar Abubakar BA and Madam Fatmawati SPd; for my sisters, Hera Tursina Amd, Jannati SE, and drg. Maya Alfiana; for my wife Cut Rozalia Amd and our beloved baby boy Teuku Rafiq Rahman. You are my guiding light and inspiration.

ABSTRACT

Since the beginning of the industrial age, excessive use of fossil fuels has led to a significant increase in the atmospheric concentration of greenhouse gases. Sequestration of carbon dioxide in geological formations appears to be the most direct carbon-management strategy for reducing such anthropogenic CO_2 in the long term. Residual trapping mechanisms have been recognised as effective approaches for CO_2 geo-sequestration projects, as they immobilise micrometre-sized CO_2 bubbles in the pore network of the rock and increase the safety of the storage sites as they inhibit upward migration of CO_2, thus, minimising leakage potential. This mechanism has been proven to work in water-wet rocks with no existing works. However, no such work has been completed for (oil-wet) oil reservoirs, which are economically most important, and it was hypothesised that this significantly affects residual trapping.

Thus, this study evaluated the supercritical carbon dioxide trapping capacity of oil-wet formations at reservoir conditions via x-ray micro-computed tomography. The CO_2 clusters and their morphologies were analysed statistically and it was clear that residual saturations are approximately halved in oil-wet rock while cluster morphology changes into flatter clusters.

These findings need to be implemented in reservoir-scale models to obtain accurate results.

List of Publications included as part of the thesis

1. Al-Yaseri, A.Z., Roshan, H., Zhang, Y., **Rahman, T.,** Lebedev, M., Barifcani, A. and Iglauer, S., 2017. Effect of the Temperature on CO_2/Brine/Dolomite Wettability: Hydrophilic versus Hydrophobic Surfaces. Energy & Fuels, 31(6), pp.6329-6333.

2. Lebedev, M., Zhang, Y., Mikhaltsevitch, V., Inglauer, S. and **Rahman, T.,** 2017. Residual trapping of supercritical CO_2: direct pore-scale observation using a low-cost pressure cell for micro-computer tomography. Energy Procedia, 114, pp.4967-4974.

3. **Rahman, T**., Lebedev, M., Barifcani, A. and Iglauer, S., 2016. Residual trapping of supercritical CO_2 in oil-wet sandstone. Journal of Colloid and Interface Science, 469, pp.63-68.

4. Iglauer, S., **Rahman, T.,** Sarmadivaleh, M., Al-Hinai, A., Fernø, M.A. and Lebedev, M., 2016. Influence of wettability on residual gas trapping and enhanced oil recovery in three-phase flow: a pore-scale analysis by use of microcomputed tomography. SPE Journal, 21(06), pp.1-916.

List of Publications relevant to the thesis but not forming part of it

1. **Rahman, T.,** Lebedev, M., Zhang, Y., Barifcani, A. and Iglauer, S., 2017. Influence of rock microstructure on its electrical properties: an analysis using x-ray microcomputed tomography. Energy Procedia, 114, pp.5023-5031.

2. Zhang, Y., Lebedev, M., Sarmadivaleh, M., Barifcani, A., **Rahman, T**., and Iglauer, S., 2016. Swelling effect on coal microstructure and associated permeability reduction. Fuel, 182, pp.568-576.

TABLE OF CONTENTS

List of Figures

List of Tables

Chapter 1 Introduction

1.1 Background

Multiphase fluid flow and displacement in rock porous media is a highly applicable process in the energy and environment fields. Water imbibition processes have been used to displace and produce hydrocarbons, which are trapped by capillary forces in the pore spaces. However, in geological carbon capture and storage (CCS), there are many important trapping mechanisms that are rooted in interfacial phenomena, apparent at the scale of individual pores and throats.

Pore-scale imaging and modelling have been becoming a routine service in the oil and gas industry over the last 10 years because they have potential applications in contaminant transport and carbon dioxide storage; therefore, pore-scale modelling has developed rapidly (Blunt et al. 2013). Furthermore, three-phase fluid flow through porous media is an important topic in the oil and gas industry as it occurs in gas-assisted enhanced oil recovery (EOR) processes and carbon geo-storage.

Petrophysical properties can be used as an indication of the average rock wettability (Anderson, 1986); however, determining the distribution of wettability at the pore scale is complicated. Bakke and Øren (Bakke and Øren, 1997) reconstructed grain-size distribution and other petrographical data from 2D thin sections to 3D sandstones. Note that the reconstructed model reproduced important geometrical and connectivity properties. Valvatne and Blunt (Valvatne and Blunt, 2004) studied the change of wettability at the pore scale using two-phase capillary-dominated network models. They estimated relative permeability and oil recovery for the rock at different wettability. Further, Hui and Blunt (Hui and Blunt, 2000) discussed the effects of rock wettability on three-phase systems after analysing ten different fluid configurations in a single pore and estimating all possible displacements. Hui and Blunt found there is a significant influence of wettability on relative permeability estimation. Moreover, a three-dimensional mixed-wet network model was found by Piri and Blunt (Piri and Blunt, 2005) to simulate two- and three-phase

relative permeability using process-based techniques (Øren and Bakke, 2002) for the pore space in Berea sandstone.

In the oil and gas industry, micro-CT scans have been used to measure pore morphologies for rocks and to visualise porous media, as well as many other static petrophysical parameters (porosity and interface area) and dynamic properties (permeability, NMR response, formation factor, and capillary pressure). Morphologies of carbonate rocks were investigated using X-ray microtomography (Arns et al. 2005). Arns et al. (Arns et al. 2005) identified 32,000 separate vugs and measured the size distribution. In addition, the permeability, drainage capillary pressure, formation factor, and NMR response were estimated using micro-CT images. Cuttings of carbonate core plugs were scanned using micro-CT scans to measure the density and porosity (Siddiqui et al., 2005). Further, an environmental scanning electron microscope (ESEM), NMR spectrometer, and APEX were used for comparison to support pore-scale network modelling. X-ray microtomography was used to get the pore-scale images from rock samples at different resolutions (Blunt et al. 2013; Andrew et al. 2014), see figures 1.1, 1.2, and 1.3 below, which can provide a three-dimensional image of the pore space. However, these images cannot be directly input into network models (Dong and Blunt, 2009). It is, therefore, vital to deepen our understanding in this area to aid in developing better CCS and EOR schemes and to improve clean-up technologies for contaminated soils.

Pore-scale three-phase fluid flow has previously been studied theoretically (e.g. Van Dijke et al. 2011; Piri and Blunt 2004, 2005a, b; Al-Dhahli et al. 2012) or experimentally using 2D micromodels (e.g. Oren 1992, Oren and Pincewzski 1995, Dong et al. 1995, Keller et al. 1997); both approaches rely on strongly simplified pore morphologies. It is, however, well established that pore space morphology has a significant impact on the related fluid dynamics (Dullien 1979). In addition, it is clear that 3D flow characteristics cannot be fully captured by 2D models (e.g. the percolation threshold is significantly lower in 3D, Stauffer 1979). Only recently, with the advent of micro-computed tomography (μCT), can three-phase flow through porous media be studied in 3D at the pore-scale of realistic geological porous media (compare the recent reviews by Blunt et al. (2013), Wildenschild and Sheppard

(2013), and Cnudde and Boone (2013)), which is most relevant for industrial applications.

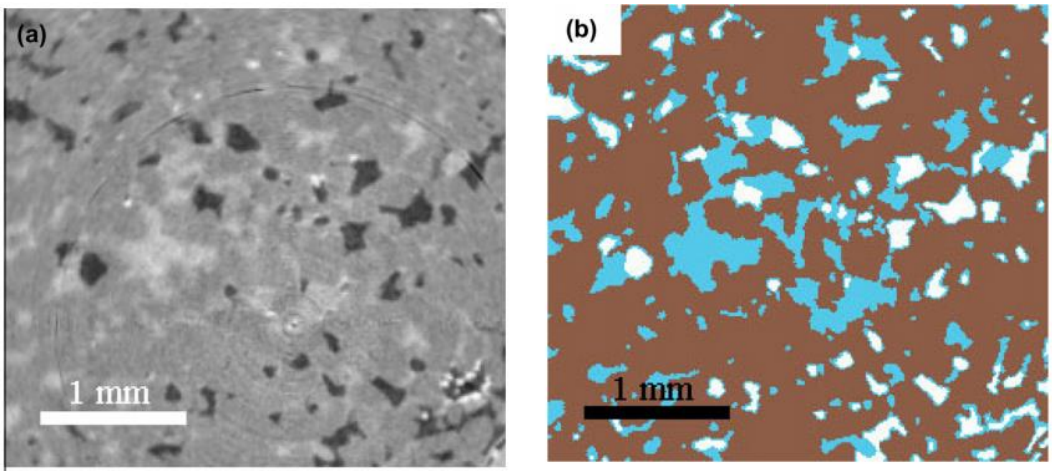

Figure 1-1 Images of CO_2 after waterflooding with CO_2 saturated brine, showing the trapped supercritical CO_2 clusters. The picture is a two-dimensional cross-section through a three-dimensional image; the area shown is 10.80 mm^2 (261 239 voxels). (a) A raw grey-scale image: supercritical CO_2 is black, brine is light grey, and sandstone is dark grey. The few white areas are minerals with high X-ray absorption. (b) The same slice with phases segmented. Supercritical CO_2 is white, brine light blue, and rock is brown (figure taken from Blunt et al. (2013)).

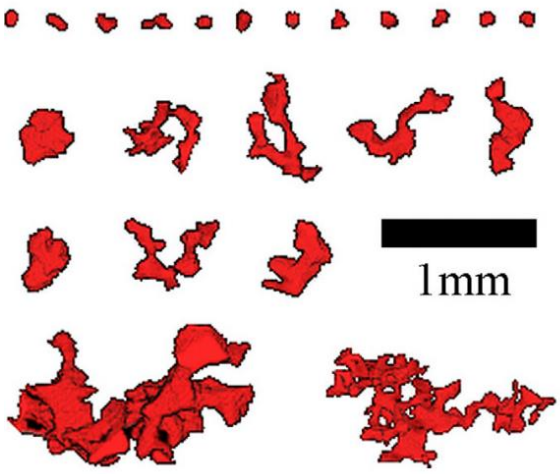

Figure 1-2 Images of CO_2 after waterflooding with CO_2 saturated brine showing selected trapped clusters of different sizes (figure taken from Blunt et al. (2013)).

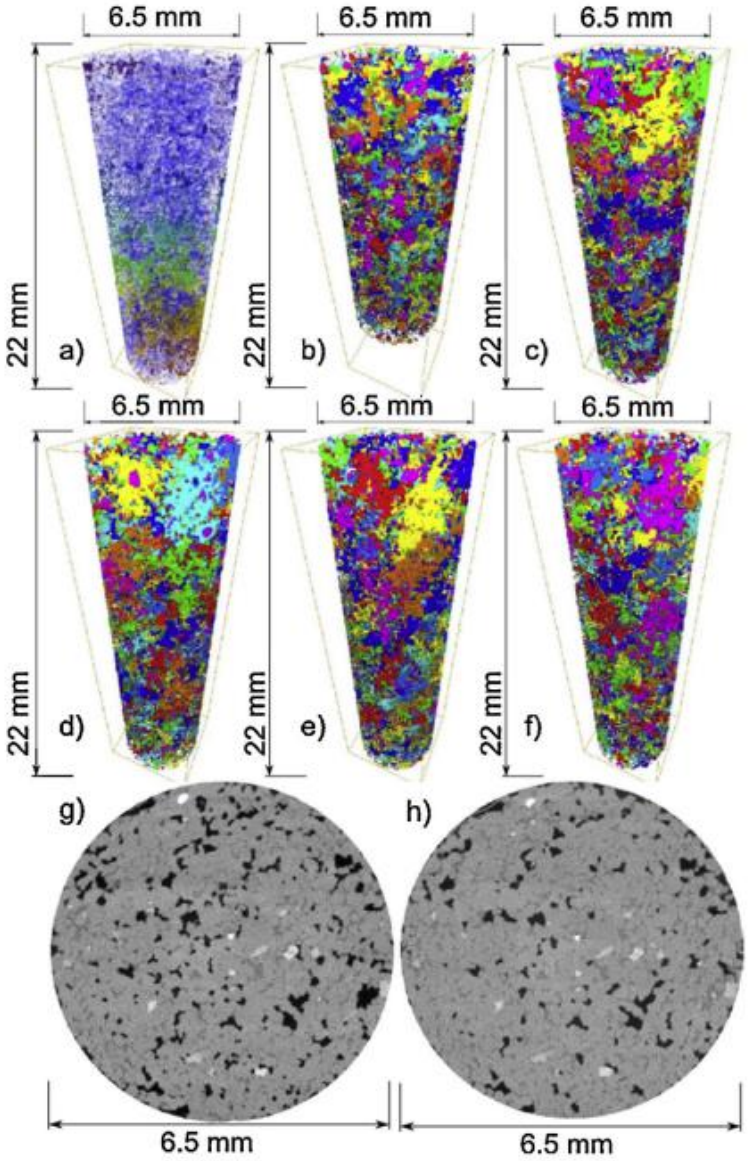

Figure 1-3 The CO_2 is black, rock is the lightest phase, and brine is intermediate (figure taken from Andrew et al. (2015)).

In the last few decades, high concentration of carbon dioxide emissions in our atmosphere has become a major issue worldwide as it leads to global warming and climate change. CO_2 emissions have dramatically increased since the industrial revolution (Iglauer et al. 2012) owing to increasing demand for energy. Fossil fuels are the major source of energy (International Energy Agency, 2010). They contribute to >80% of total energy consumption. However, fossil fuels are depleting at an increasing rate and this situation challenges us to develop advanced technologies to recover additional fossil fuels.

Further, anthropogenic CO_2 emissions can be cut by injecting CO_2 deep underground. This method, known as carbon capture and storage (CCS) (Metz et al. 2005), has the potential to significantly reduce CO_2 emissions in the atmosphere. Crude oil is the most important fossil fuel and is only recovered up to ~30% (BP Statistical Review of World Energy, 2014). However, several methods can be used to enhance recovery (EOR), such as miscible or partially miscible gas flooding, thermal stimulation (Lake, 2010), polymer flooding (Iglauer et al. 2010), and surfactant flooding (Iglauer et al. 2010). CO_2 enhanced oil recovery is attractive (Firoozabadi et al. 2010; Blunt et al. 1993), as it can be combined with CO_2 sequestration.

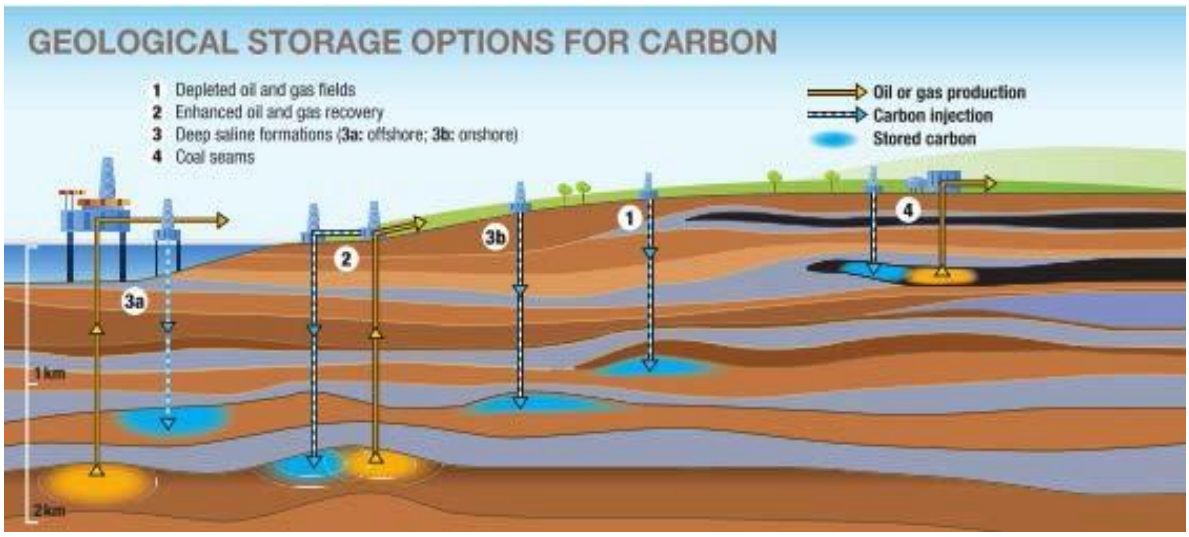

Figure 1-4 Geological storage mediums with typical depths (after Thomas and Benson, 2015)).

Residual trapping (Figure 1-5) refers to the physical immobilization of CO_2 in the pore spaces because of capillary forces that hold the buoyant CO_2 back (Hesse et al. 2008; Juanes et al. 2006; Pentland et al. 2011). Capillary trapping, which is a rapid and effective mechanism, occurs at the cessation of CO_2 injection into the targeted formation while the brine displaces and traps CO_2 as discontinuous droplets at the trailing edge of a rising CO_2 plume. Further, it was found that rock wettability (Farophpoor et al. 2013; Iglauer et al. 2013; Iglauer et al. 2015a) and interfacial tension

(Chalbaud et al. 2009) significantly influence capillary trapping. It was also reported that initial gas saturation, pore geometry, pore throat aspect ratio, and hysteresis can affect capillary trapping (Al-Menhali et al. 2015; Juanes et al. 2006; Suekane et al. 2010), Figure 1-5.

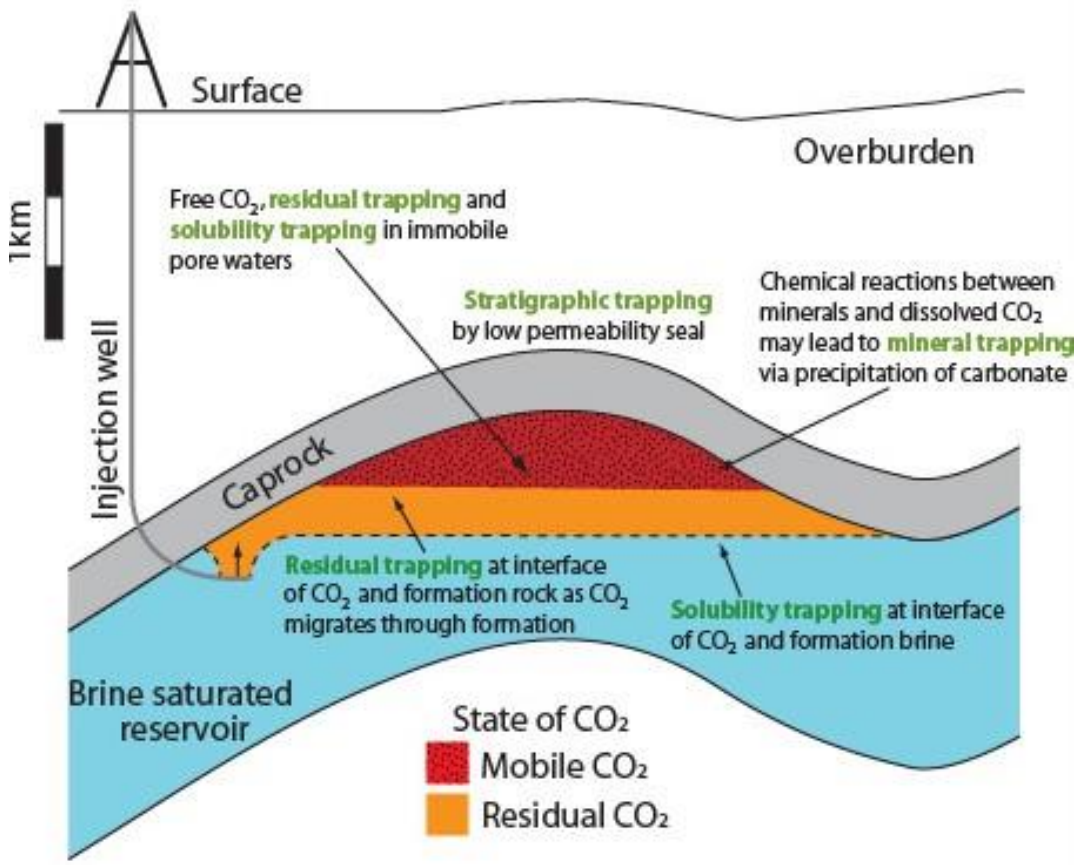

Figure 1-5 Conceptualization of in-situ trapping mechanisms (after Burnside & Naylor, 2011).

However, it is important to understand the nature of interaction between fluid and rock in order to safely store CO_2 in the ground and assess the CO_2's ability to increase the recovery (Oomole et al. 1983; Iglauer et al. 2015, 2015a). Therefore, the wettability of a rock–CO_2–water system was measured here because it is a key parameter in geological carbon capture and storage (CCS) owing to its impact on the three most important trapping mechanisms during the initial storage phase, i.e.

structural (Iglauer et al. 2015; Naylor et al. 2011), residual (Iglauer et al. 2011, 2016; Krevor et al. 2015; Chaudhary et al. 2013; Rahman et al. 2016; Al-Khdheeawi et al. 2016, 2017, 2017a), and dissolution trapping (Al-Khdheeawi et al. 2016, 2017, 2017a) (see Figure 1-6).

Anderson (1986 and 1987) and Salathiel (1973) described reservoir rock wettability measurement methods comprehensively by categorising the measurements into direct and indirect methods. Contact angle measurements represent the direct method, which refers to the relative amount of spontaneous (imbibition) and forced displacement (Amott, 1959). Relative permeability (Owens and Archer, 1970), capillary pressure (Slobod and Blum, 1952), flotation, glass slide, and NMR methods represent the indirect method. However, no satisfactory method exists for the in-situ measurement for the rock wettability. Therefore, it is important that it is measured in the laboratory.

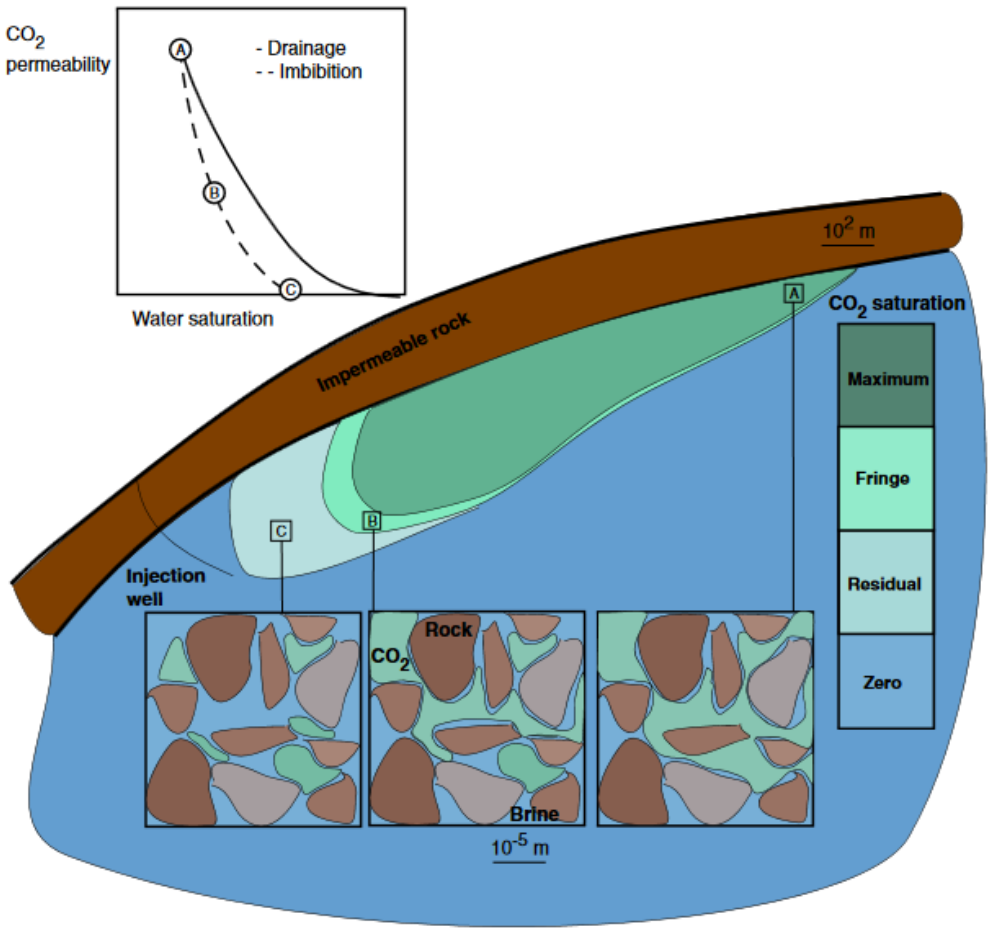

Figure 1-6 A sketch of key processes governed by capillary trapping after CO_2 injection has ceased at a storage site. Plume migration is limited by the trapping as large fractions of the plume are immobilised. Capillary trapping is secure over long timescales and avoids buoyant stress on overlying cap rock layers. Trapping is also key to parameterising hysteresis in relative permeability functions—more trapping leads to greater disconnection of fluid ganglia as CO_2 saturation in the pore space decreases (movement from A towards C in the figure) and, thus, a larger decrease in permeability as a function of saturation (figure taken from Krevor et al. (2015)).

The contact angle measurement (Figure 1-7) is the best quantitative method for characterising wettability, especially when pure mineral samples are used (Giraldo et al. 2013; Mittal, 2006; Kaveh et al. 2012; 2014). The captive bubble method and sessile drop method (Anderson, 1986) are the most popular in the petroleum industry. In that study, the tilting plate method—part of the sessile drop method—

was used because advancing and receding contact angles could be measured simultaneously (Lander et al. 1993). Practically, for a rock/CO_2/brine system, if θ is less than 50°, then the system is strongly water-wet, weakly water-wet for θ between 50-70°, and intermediate-wet for the θ range 70-110°. The system turns weakly CO_2-wet for the θ range 110-130° and strongly CO_2-wet for the θ range 130-180° (Table 1-1). However, pressure, temperature, brine salinity surface roughness, and many other parameters can influence wettability measurements.

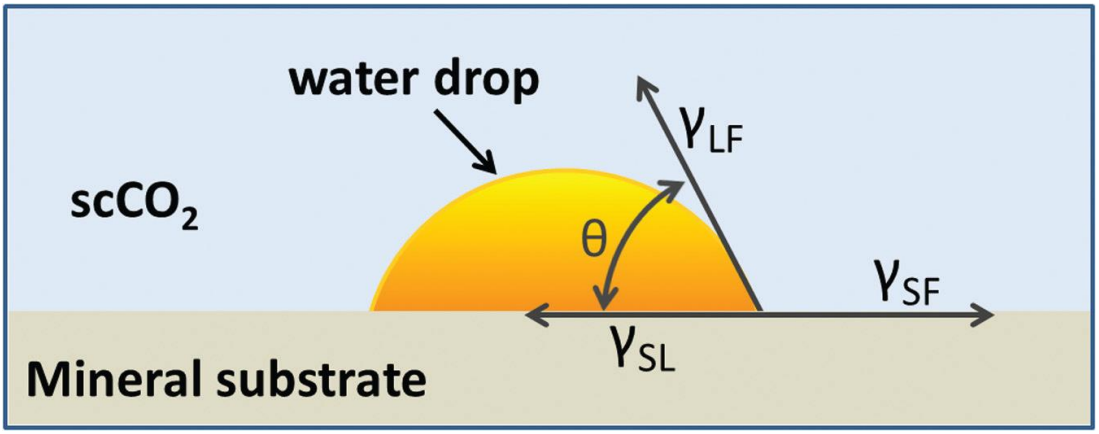

Figure 1-7 Forcefield acting on a three-phase mineral/CO_2/brine system. There are three different interfacial forces: solid/CO_2interfacial tension (γ_{sc}), solid/water interfacial tension (γ_{sw}), and CO_2/brine interfacial tension (γ_{cw}). This figure was taken from Iglauer et al. (2015).

Table 1-1 Wettability criteria based on the contact angle of rock/CO_2/brine systems (modified after Iglauer et al. (2015a)).

Wettability state	Water contact angle θ (°)
Complete wetting	0
Strongly water-wet	0 – 50
Weakly water-wet	50 – 70
Intermediate-wet	70 – 110
Weakly CO_2-wet	110 – 130
Strongly CO_2-wet	130 – 180
Complete non-wetting of water	180

1.1.1 Influence of wettability on residual trapping

Capillary trapping, which is proportional to the product of porosity times the residual saturation occurred when the capillary forces inside the porous medium trapped the non-wetting phase clusters. Principally, capillary trapping occurs during the imbibition process, i.e. at the trailing edge of the CO_2 plume. This residual CO_2 saturation, which is a function of wettability, is resolved through laboratory measurements of relative permeability and capillary pressure curves (Krevor et al. 2012; Pini and Benson, 2013) or through pore-scale models. Reservoir-scale simulation and 3D micro-CT imaging detect that water-wet rocks have a better residual trapping potential, which refers to trapping large residual/nonwetting phase clusters trapping by snap-off phenomenon, which occurs only in water-wet rocks (Chaudhary et al. 2013; Iglauer et al. 2013; Krevor et al. 2012; Krevor et al. 2015) (Figure 1-8).

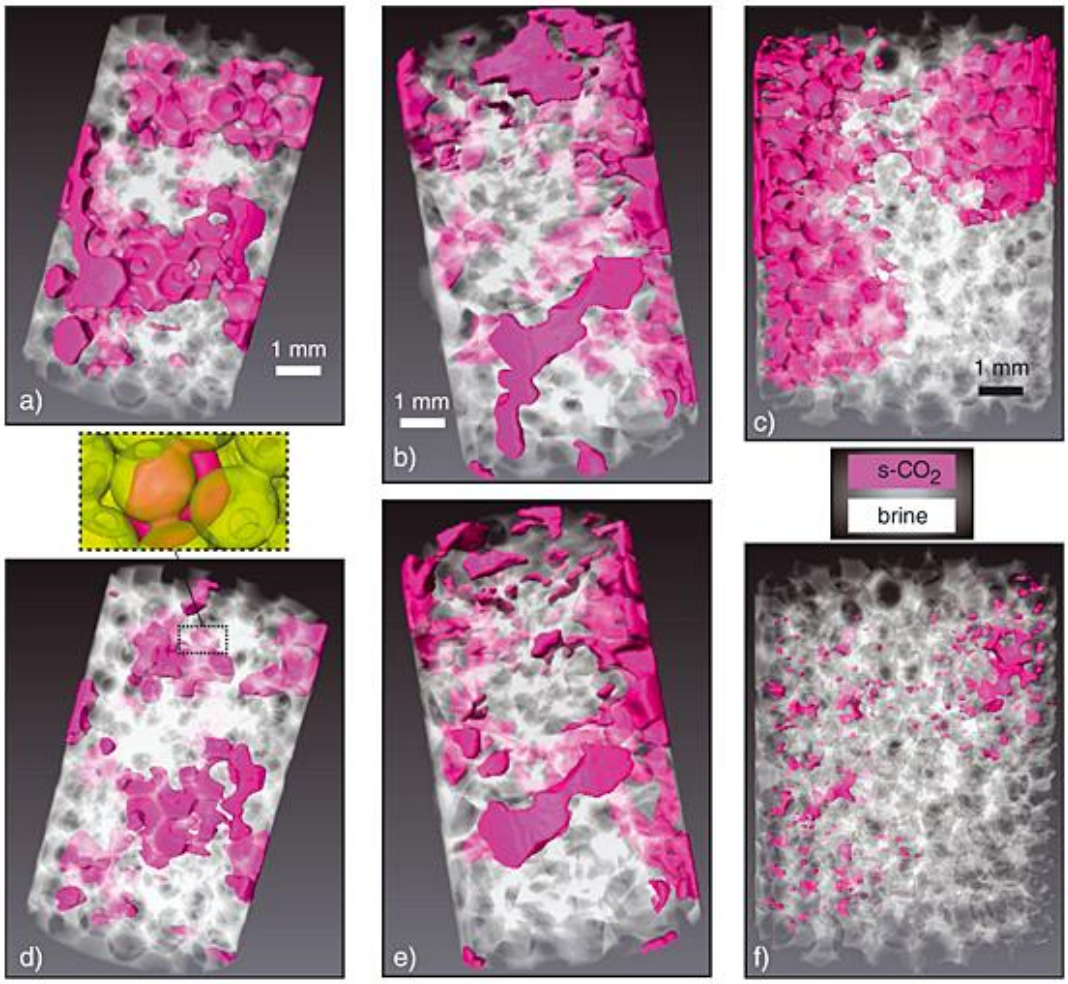

Figure 1-8 Three-dimensional segmented renderings of HRXCT data showing s-CO_2 saturation after s-CO_2 flood and the trapped s-CO_2 after the brine flood in (a, d) water-wet glass bead pack, (b, e) water-wet angular glass grain pack, and (c, f) CO_2-wet Teflon bead pack. The inset in figure (d) shows individually trapped s-CO_2 in a discrete pore. The scale (see white and black bars) is the same for all images. Solid media are rendered transparent. See the six corresponding animated versions of the images in the supporting information. This figure was taken from Chaudhary et al. (2013).

1.2 Research objective

The main objective of this research is to investigate pore-scale displacement processes associated with CO_2-EOR in rocks. This specifically includes the analysis of rocks' microstructure, which is a key factor in determining these flow processes. Various rock samples with different wettabilities were used. We analyse the capability of CO_2 trapping in oil reservoirs that is combined with enhanced oil recovery. We, thus, imaged residual CO_2 supercritical in oil-wet sandstone plug using high-resolution X-ray microcomputed tomography at reservoir conditions.
Specifically, the objectives of this research are:

1. Observing and describing pore-scale oil-CO_2-water displacement processes in rock.
2. Investigating the wettability of rocks influencing oil production and CO_2 sequestration.
3. Analysing the capability of rocks in trapping the residual of CO_2, using X-ray microcomputed tomography.

1.3 Thesis organisation

There are seven chapters in this thesis, starting with the introduction, literature review, results, and conclusion.

Chapter 1. Introduction
This first chapter presents the introduction of the background, the importance of understanding multiphase flow, describes pore-scale oil-CO_2-water displacement processes, and issues related to CO_2 sequestration and the solution. The objectives and thesis organisation are also included in this chapter.

Chapter 2 – Literature review.
In this second chapter, a brief summary of pore-scale analysis and the influence of wettability in residual CO_2 trapping processes is provided.

Chapter 3 – Effect of Temperature on CO_2/Brine/Dolomite Wettability: Hydrophilic vs Hydrophobic Surfaces

This chapter analyses the effect of temperature on CO_2/brine/dolomite wettability using two different types of surfaces.

Chapter 4 – Residual Trapping of Supercritical CO_2: Direct Pore-Scale Observation Using a Low-cost Pressure Cell for Microcomputer Tomography

This chapter describes the design and fabrication steps of a low-cost, modular experimental cell for flooding and X-ray tomography visualisation of the rock samples at reservoir conditions.

Chapter 5 – Residual Trapping of Supercritical CO_2 in Oil-Wet Sandstone

This chapter unravels the capability of the CO_2 residual trapping of CO_2 on water-wet rocks. CO_2 cluster morphologies and sizes are also presented in this chapter.

Chapter 6 – Influence of Wettability on Residual Gas Trapping and Enhanced Oil Recovery in Three-Phase Flow: A Pore-Scale Analysis Using Microcomputed Tomography

This chapter involves observing the capillary pressure, curvature, and residual saturation of CO_2 and oil phases in homogenous sandstone rocks.

Chapter 7 – This last chapter underlines the meaningfulness of the findings in this research study.

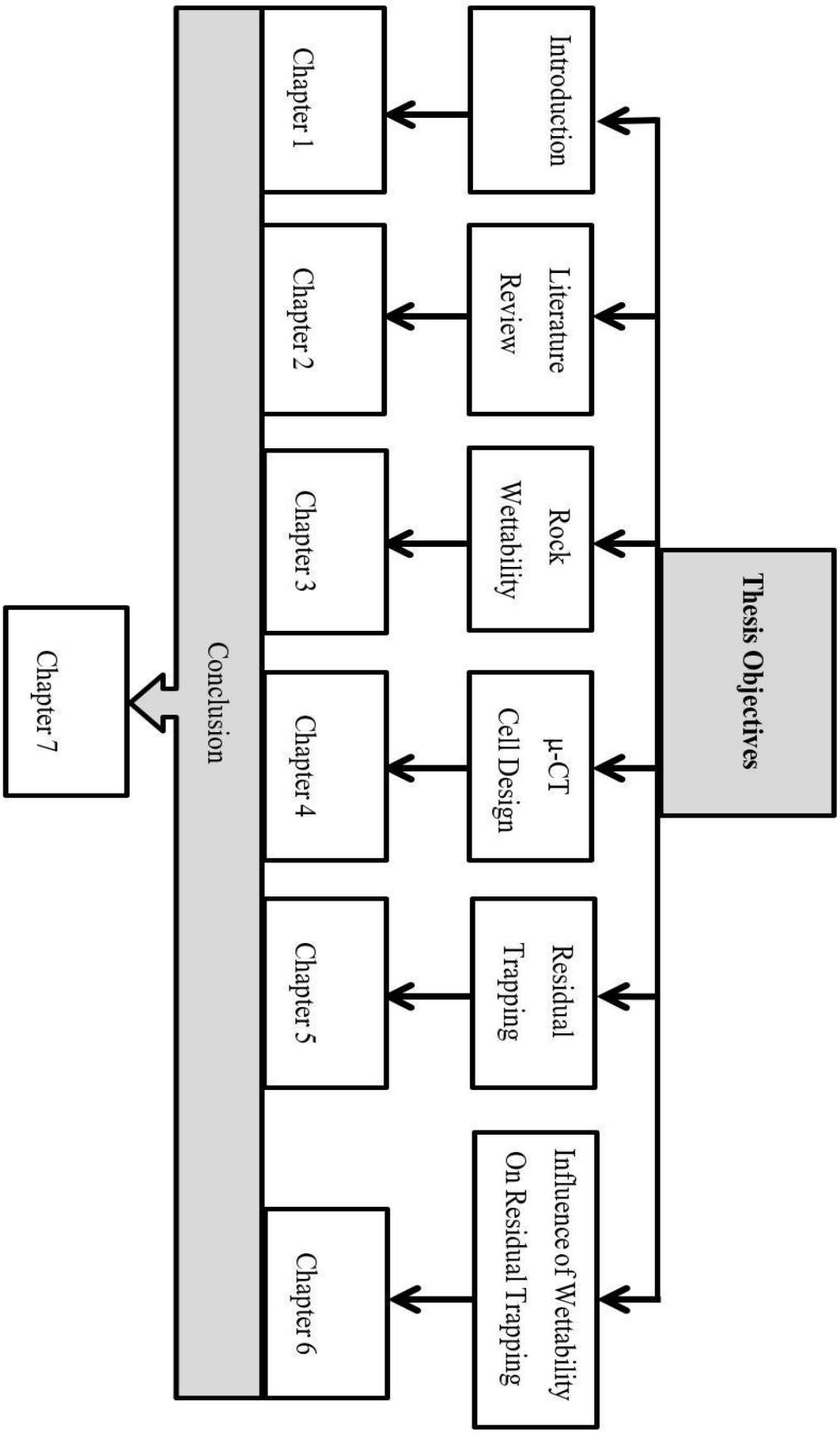

Figure 1-9 Layout of thesis objectives and structure

Chapter 2 Literature Review

2.1 Residual Trapping of Supercritical CO_2

CO_2 injection into the pore network of the hydrocarbon reservoir is a typical process to enhance oil recovery (Olenick et al. 1993; Babadagli 2006) and CO_2storage (Cantucci et al. 2009), which has been recently recognised as a major cause of climate change. CO_2 can be injected into deep saline aquifers for carbon geo-sequestration (CGS) only, which is a viable option for reducing CO_2 emissions (IPCC 2005, Lackner 2003). Further, it has been reported that deep saline sandstone formation is mostly water-wet even after CO_2 injection (Kaveh et al. 2014; Sarmadivaleh et al. 2015; Al-Yaseri et al. 2016) while most of the hydrocarbon reservoir rock is oil-wet or intermediate-wet (Hirasaki et al. 2004; Cantucci et al. 2009; Arif et al. 2016). However, most existing oil reservoirs have legal (permission from the related authorities to use the site) and supporting infrastructures already in place (Gurevich et al. 2014). Therefore, oil reservoirs have attracted considerable attention in recent years for CO_2 injection (Blunt 1993, Orr 2009, Lake 2010, and Iglauer 2012). On the other hand, pore-scale residual trapping of CO_2 in oil-wet reservoirs has not yet been proven (Cantucci et al. 2009). Moreover, safely trapping CO_2 is greatly required in the sequestration process because it can prevent the CO_2 from leaking to the surface. In addition, the trapping capability, which refers to how much CO_2 can be securely stored as a residual phase without reliance on cap rock seals is important in CCS projects (Iglauer et al. 2009; Iglauer et. al 2011b; Iglauer et. al. 2015a).

In saline sandstone formations, which are mostly water-wet, CO_2 would be trapped when it is displaced by the aquifer's brine water (Ennis-King and Peterson, 2005; Kumar et al. 2005). However, in oil reservoirs, which are mostly oil-wet, the effective movement of CO_2 is lower. However, this allows for more of the formations to be contacted by CO_2 while the chase brine rapidly and effectively traps the CO_2 (Qi et al. 2009). Moreover, Al-Menhali et al. (2016) used cylindrical small samples (5 mm diameter and 15 mm length) of Estaillades limestone (97.9% calcite and 2.1 quartz) with average permeability of 140 mD and 25% porosity. The

measurements were tested on strongly water-wet and intermediate-wet (Arabian medium crude oil was used for wettability alteration) samples. CO_2+brine or N_2+brine (7 wt% KI brine) was injected at 10 MPa pore pressure, 13 MPa confining pressure, and a temperature of 298 K for N_2 and 323 K for CO_2. Then, the micro CT (μCT) scanner (Versa XRM-500 X-ray microscope, Zeiss X-ray Microscopy, CA, USA) was used for imaging at $(4.9\ \mu m)^3$ (resolution). They reported an average initial CO_2 saturation of 29% pore volume, which was similar for both water-wet and intermediate-wet samples. However, the remaining CO_2 after water flooding in the intermediate-wet sample (14%) was significantly lower than the saturation in the water-wet sample (21%). Moreover, the initial and residual N_2 saturations in the water-wet sample were 33% and 24%, respectively, and 20% and 13% for the intermediate-wet sample. Further, a homogenous sandstone (80 mD permeability and 11.1% porosity) outcrop (96 wt% quartz with a small amount of k-fedspar, ankerite and calcite) was selected by Iglauer et al. (2013) for their experiments, which was assumed to be water-wet rock. N_2 gas, brine (10 wt% KI), and oil (bromododecane) were used as fluid phases to study the efficiency of oil recovery using μCT. Two GEOR flooding sequences were also used for comparison: 1) gas was directly injected into a core at connate water saturation followed by a chase brine injection (gw sequence); 2) gas was injected into a water flooded core at residual oil saturation followed by chase brine injection (wgw sequence). The μCT scanner was used for imaging at $(9\ \mu m)^3$. Their results showed that more oil can be produced in the gw process (S_{or} = 21.6%) compared to the wgw process (S_{or} = 29.3%). In 2011, Iglauer et al. also ran their experiment in a homogeneous Doddington sandstone (98 wt% quartz, 2 wt % K-feldspar and traces of kaolinite) sample (4.95 mm diameter and 9 mm length) with a porosity of 20.7% and a brine permeability of 1.6 Darcy. The core sample was initially fully saturated with brine, then CO_2 was injected and finally followed by live brine (10 wt% KI brine saturated with CO_2) injection at 9 MPa pore pressure, 11.75 MPa confining pressure, and temperature of 323 K. The core was then scanned with μCT at nominal resolution of $(13.156\ \mu m)^3$, which showed a low CO_2 residual saturation (24.9 % pore volume) for a strongly water-wet system.

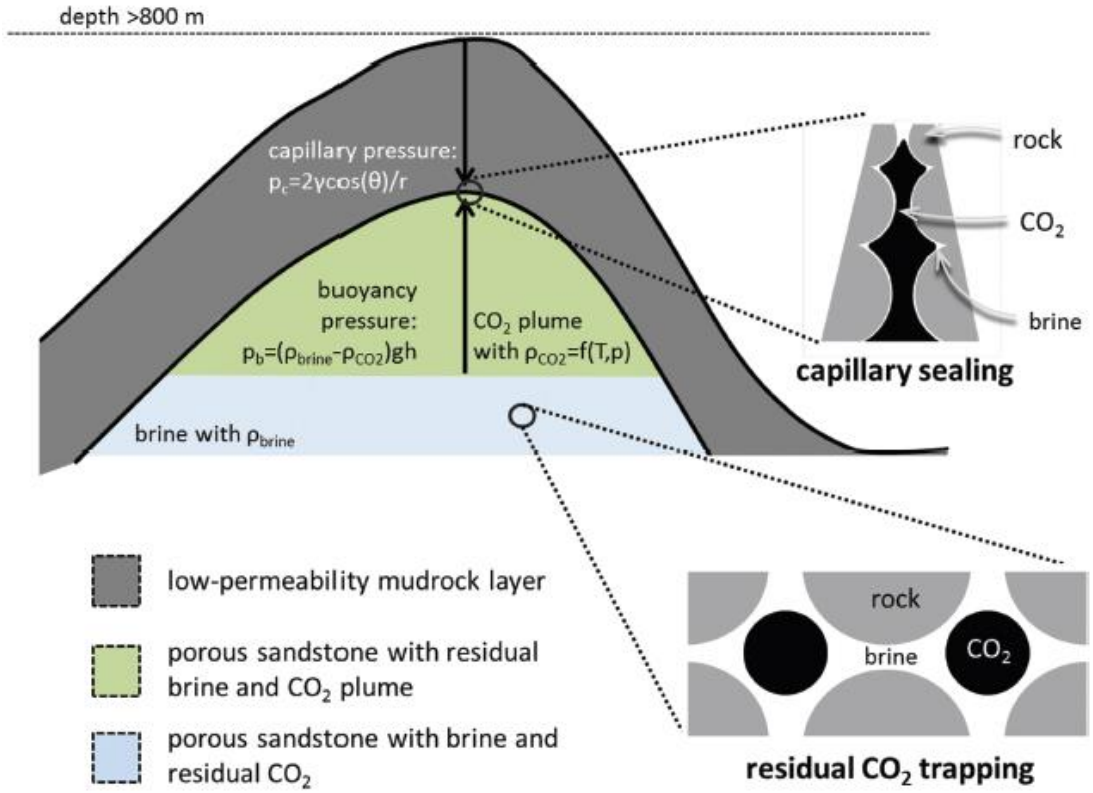

Figure 2-1 Pressures acting on a fluid column at the reservoir-seal interface for structural trapping. If CO_2 has migrated upward through the underlying water column, then a fraction of the CO_2 is residually trapped in the pore space of the reservoir rock. Note that at depths below 800 m, CO_2 is in the supercritical state. The insets on the right side schematically illustrate the pore-scale fluid configurations for a water-wet condition. This figure was taken from Iglauer et al. (2015).

a

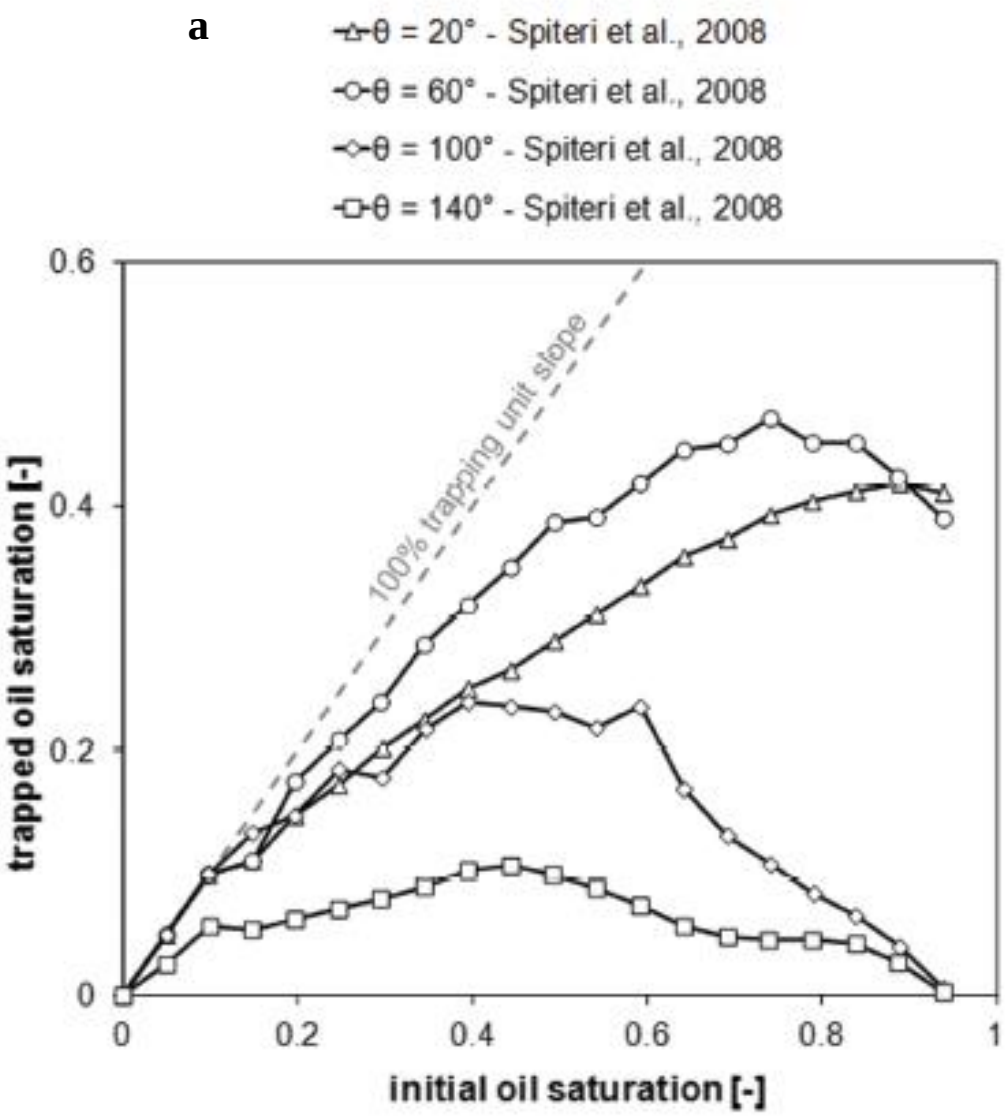
θ = 20° - Spiteri et al., 2008
θ = 60° - Spiteri et al., 2008
θ = 100° - Spiteri et al., 2008
θ = 140° - Spiteri et al., 2008
100% trapping unit slope
trapped oil saturation [-]
initial oil saturation [-]
0
0.2
0.4
0.6
0.8
1

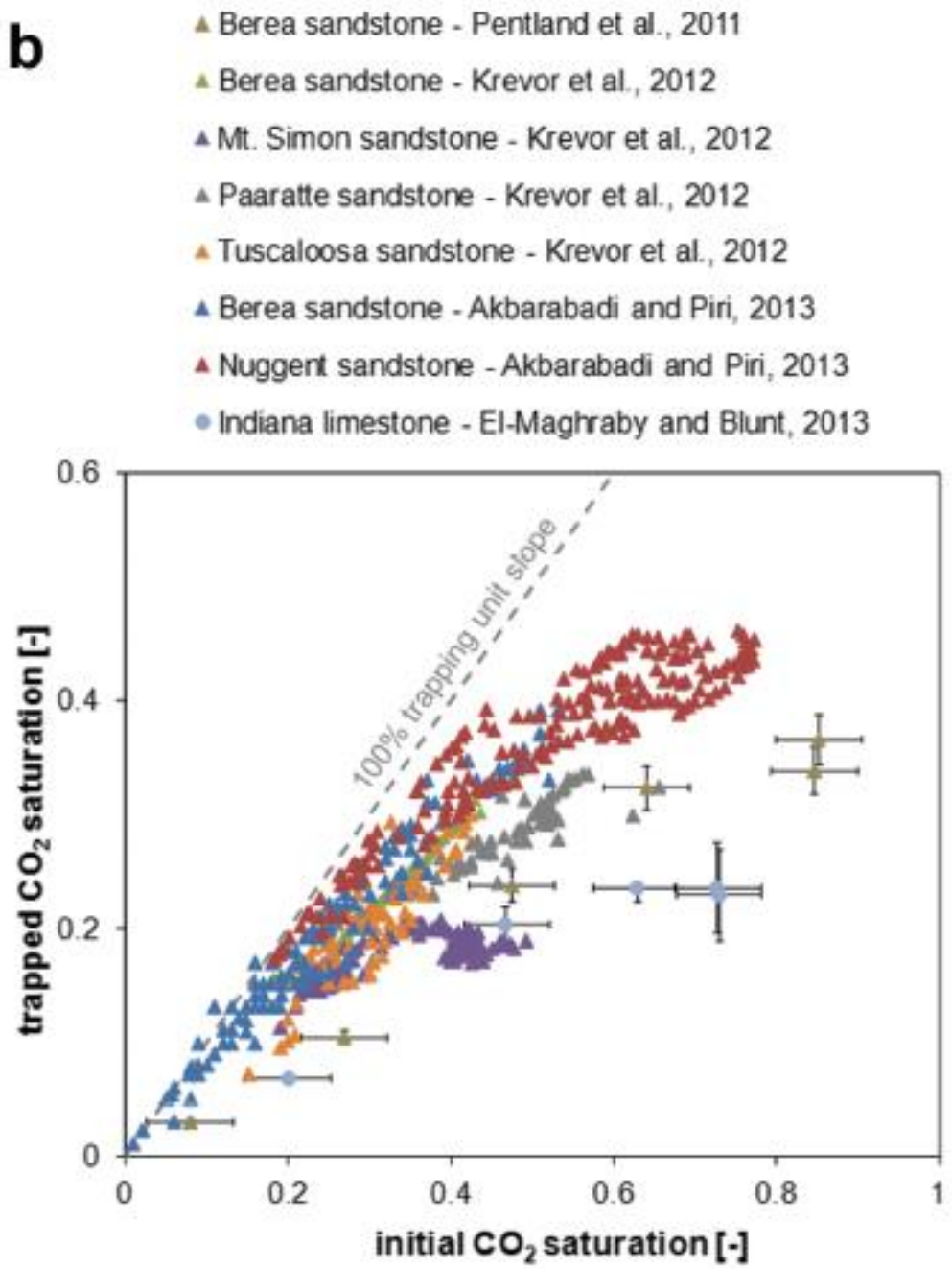

Figure 2-2 Initial-residual saturation relationships from (a) pore-network modelling and (b) laboratory measurements. In the pore network modelling study, the initial residual saturation relationship of oil is shown for a range of contact angles. Most data exhibit water-wet behaviour with the exception of the illite-rich Mt. Simon sandstone and possibly Indiana limestone. This figure was taken from Iglauer et al. (2015).

2.1.1 Storage Mechanisms

There are various physical and chemical mechanisms for storing CO_2 in the porous medium. These include structural trapping, residual trapping, solubility trapping, mineral trapping, and adsorption trapping (Figure 2-3).

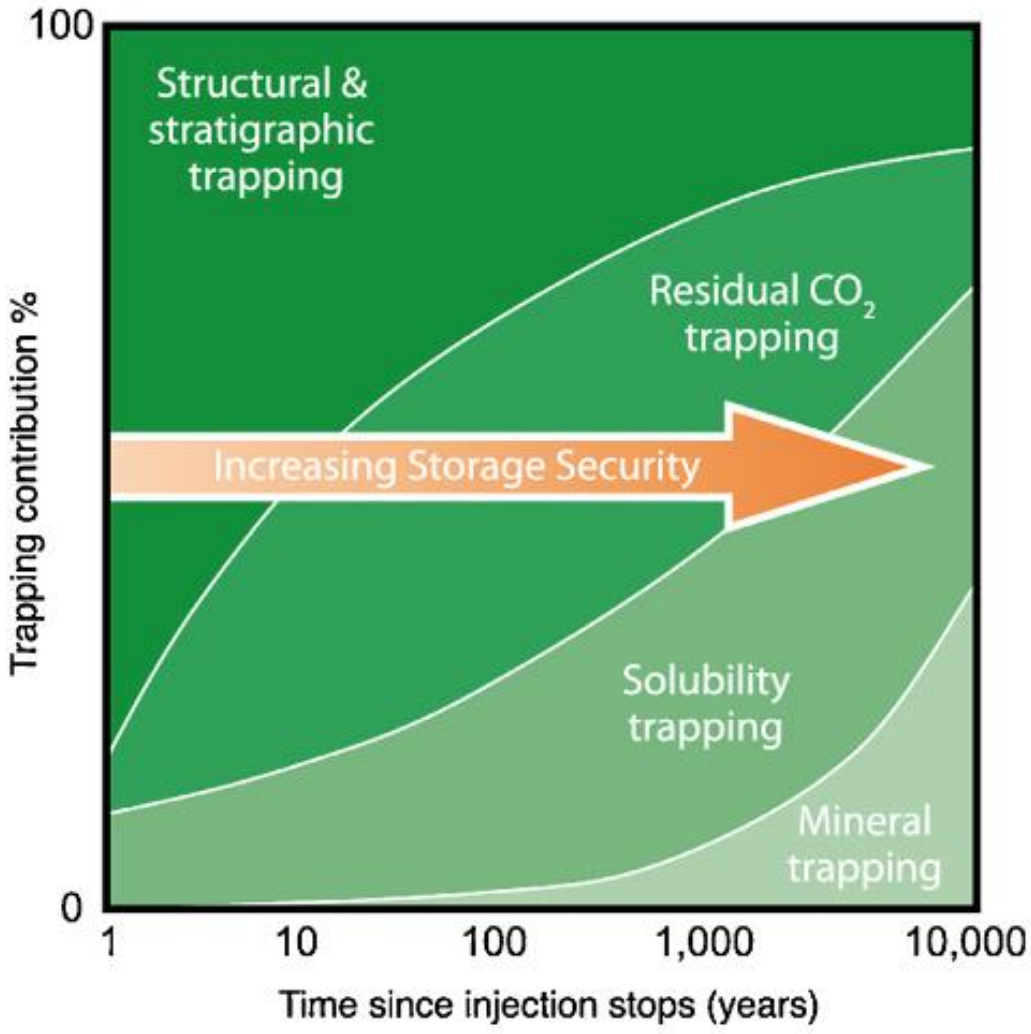

Figure 2-3 A schematic of the relative importance of various trapping mechanisms over time (from Benson et al. (2005, 2012)). Residual trapping is significant both in the amount of trapping capacity it provides, as well as for the speed in which residual trapping takes place, simultaneously with water influx into the migrating plume.

2.1.1.1 Structural trapping

CO_2 will rise after it is injected into porous formations because of the imbalance of buoyancy and capillary forces. Where buoyancy forces exceed capillary forces, the CO_2 will be retained into the porous medium. Meanwhile, the CO_2 plume migrates up-structure and becomes thick and fine-textured in low permeability rock (cap rock) (Neuzil, 1994). This low permeability cap rock or seal prevents CO_2 from upward migration and then CO_2 is structurally trapped. Therefore, structural CO_2 trapping is one of the most dominant storage mechanisms because it can contribute to the total CO_2 trapped volume throughout the storage project life and is most significant in the first decade. Note, it was found that if injection pressure of CO_2 exceeds the fracture pressure of the cap rock, cap rock would fail, which would lead to reduced cap rock sealing efficiency (Chiquet et al. 2007) and the effective storage volume would be limited (Underschultz and Strand, 2016). Further, the rock wettability and interfacial tension can control the capillary sealing efficiency of cap rock (Chiquet et al. 2007; Broseta et al. 2012; Iglauer et al. 2015a, b; Yang et al. 2007).

2.1.1.2 Residual trapping

Residual trapping is the physical immobilisation of CO_2 in the pore spaces because of capillary forces that hold the buoyant CO_2 back (Hesse et al. 2008; Juanes et al. 2006; Pentland et al., 2011). Capillary trapping is one of the most effective storage mechanisms that occurs at the cessation of CO_2 injection to storage formation while the brine displaces and traps CO_2 as discontinuous droplets at the trailing edge of a rising CO_2 plume. The residual CO_2 estimation represents the capillary trapping potential (Kumar et al. 2005; Qi et al., 2009; Saadatpoor et al. 2010) in laboratory practice because high pressure is used to inject brine through the core held. Moreover, capillary trapping is an effective mechanism for a CO_2 storage project. Note that capillary trapping can be demonstrated by wettability (Farophpoor et al. 2013; Iglauer et al. 2013; Iglauer et al. 2015a) and interfacial tension (Chalbaud et al. 2009). Capillary trapping is also influenced by pore throat aspect ratio, pore geometry, initial gas saturation, and hysteresis (Al-Menhali et al. 2015; Juanes et al. 2006; Suekane et al. 2010).

2.1.1.3 Solubility trapping

The dissolution of CO_2 in brine formation leads to a higher density of CO_2 saturated brine, which sinks to the bottom of the reservoir and can be referred to as solubility trapping. Solubility trapping is a geochemical storage mechanism that has several benefits. Dissolved CO_2 does not exist as a separate phase. Thereby, upwards CO_2 plume migration owing to buoyancy is non-existent (Iglauer, 2011c; IPCC, 2005). However, solubility trapping is controlled by operating pressure, temperature, and brine salinity (Koschel et al. 2006; Lagneau et al. 2005) specifically from mid to long-term scales (Gilfillan et al. 2009).

2.1.1.4 Mineral trapping

Mineral trapping or mineralization is an important mechanism for long timescales (thousands of years), where carbon dioxide is dissolved in formation brine, resulting in a weak carbonic acid (Bachu et al. 1994; Xu et al. 2001) that can react with different minerals inside the reservoir rock (carbonate or silicate). However, this will not affect storage security during the CO_2 injection project because the time scale of this trapping needs thousands of years. The following reaction equations explain the mineral- trapping process (Bachu et al. 1994; Xu et al. 2001):

First, the injected CO_2 dissolves in formation brine forming carbonic acid as depicted by the following chemical reaction:

$$CO_2 + H_2O \leftrightarrow H_2CO_3$$

Next, the carbonic acid undergoes a rapid dissociation to form the bicarbonate ions as follows:

$$H_2CO_3 \leftrightarrow HCO_3^- + H^+$$

Then the increased acidity promotes dissolution of the primary minerals in the host rock, which results in a bicarbonate complex as follows:

$$Ca^{2+} + HCO_3^- = CaHCO_3^-$$

Finally, the dissolved bicarbonates react with the divalent mineral cations to result in carbonate precipitation, e.g. the formation of calcium carbonate as follows:

$$HCO_3^- + Ca^{2+} = CaCO_3 + H^+$$

2.1.1.5 Adsorption trapping

This type of mechanism is only applicable in coal bed CO_2 storage by which means the injected CO_2 will displace attached methane from coal because CO_2 has a greater affinity to coal than methane (Busch et al., 2004; Clarkson and Bustin, 2000). However, coal has a very small storage capacity.

2.2 Influence of Wettability on Residual Gas Trapping and EOR

Three-phase flow through porous media is an important topic in the oil and gas industry as it occurs in gas-assisted enhanced oil recovery (EOR) processes, and carbon geo-storage (CCS), when CO_2 is injected into oil reservoirs for storage and incremental oil recovery (Blunt et al. 1993, IPCC 2005). Further, three-phase flow also occurs in soils contaminated by organic solvents (Sleep and McClure 2001). In this context, a significant amount of work has been completed to study such three-phase flow at the reservoir scale (e.g. compare Qi et al. 2009; Moortgat et al. 2011; Beygi et al. 2013) and the mesoscale (centimetres up to several metres sized structures) (e.g. Oak et al. 1990; Egermann et al. 2000; Caubit et al. 2004; Al-Mansoori et al. 2009; Amaechi et al. 2014). However, the detailed pore-scale (micrometre scale) fluid dynamics was poorly understood despite that pore-scale flow determines the overall reservoir-scale (kilometre scale) flow, in addition to other larger scale mechanisms, e.g. reservoir heterogeneity or gravity segregation (Bear, 1988). Therefore, it is vital to deepen our understanding in this area to aid the development of better storage mechanism techniques of CCS and EOR schemes, and to improve clean-up technologies for contaminated soils (see figures 2-4 and 2-5 below).

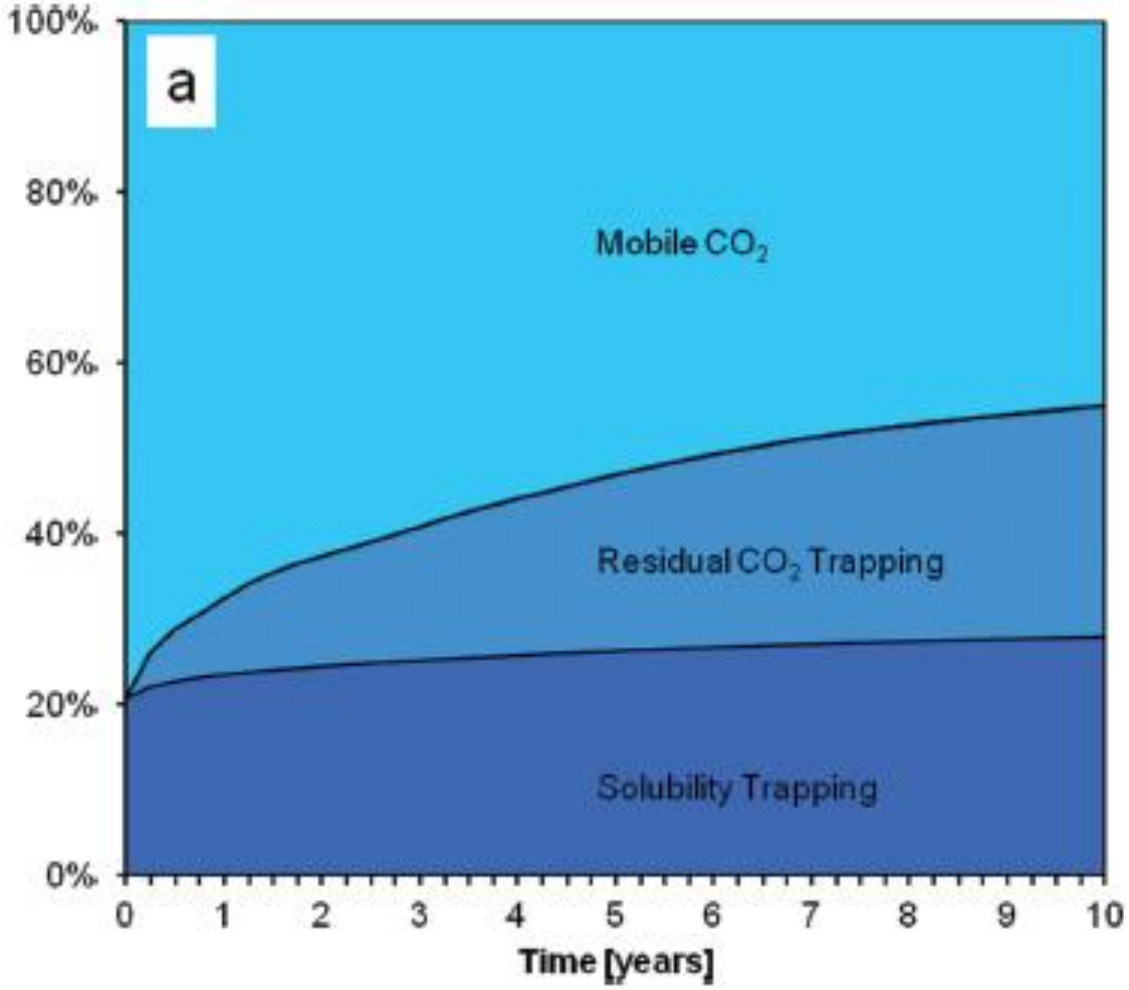
a
100%
80%
60%
40%
20%
0%
Mobile CO_2
Residual CO_2 Trapping
Solubility Trapping
0
1
2
3
4
5
6
7
8
9
10
Time [years]

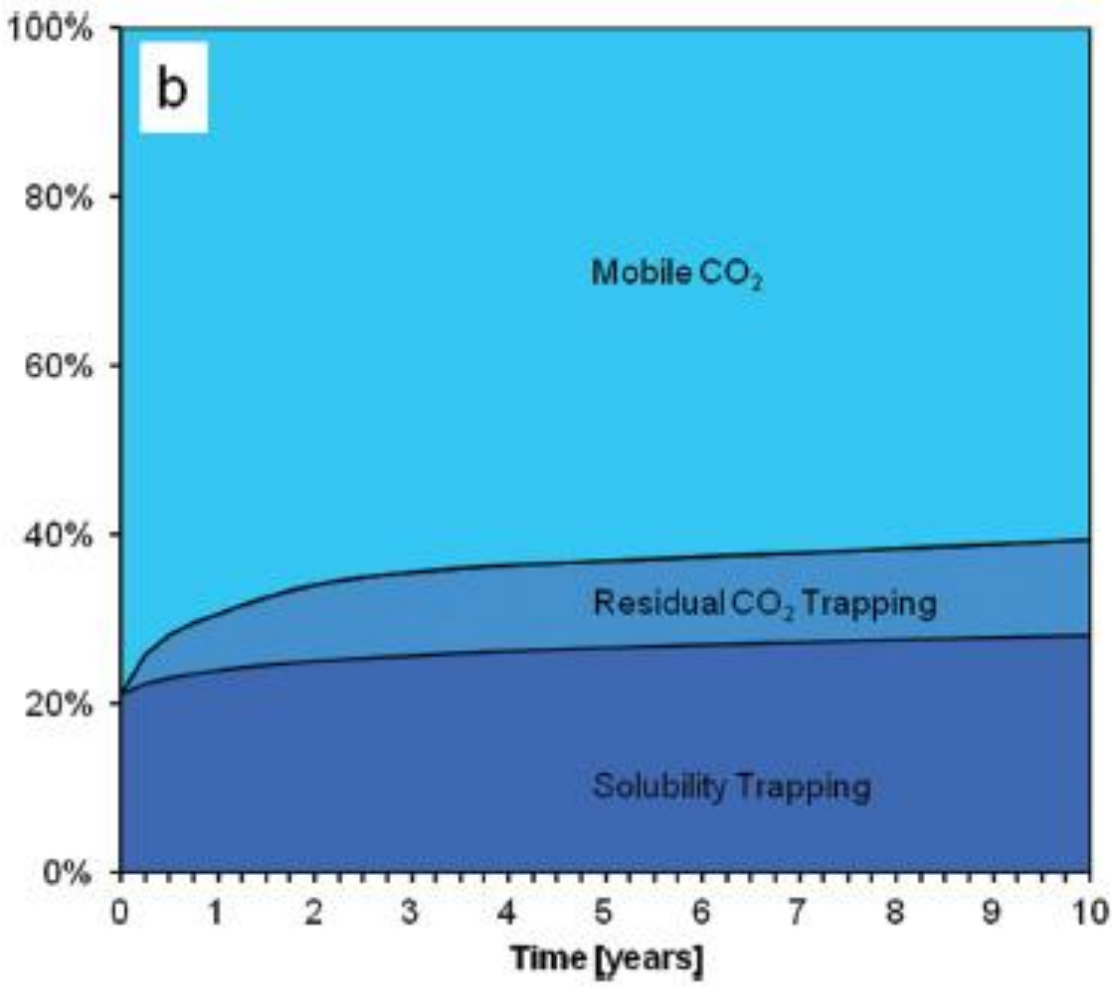

Figure 2-4 CO_2 fate simulation results from the modified tenth SPE Comparative Solution Project model using saturation functions derived from the contact angle to simulation workflow illustrated in Figure 2-5. (a) In the water-wet scenario, significantly more CO_2 is immobilised as a residually trapped phase than (b) in the CO_2-wet scenario, leading to significantly reduced CO_2 leakage risk. This figure was taken from Iglauer et al. (2015).

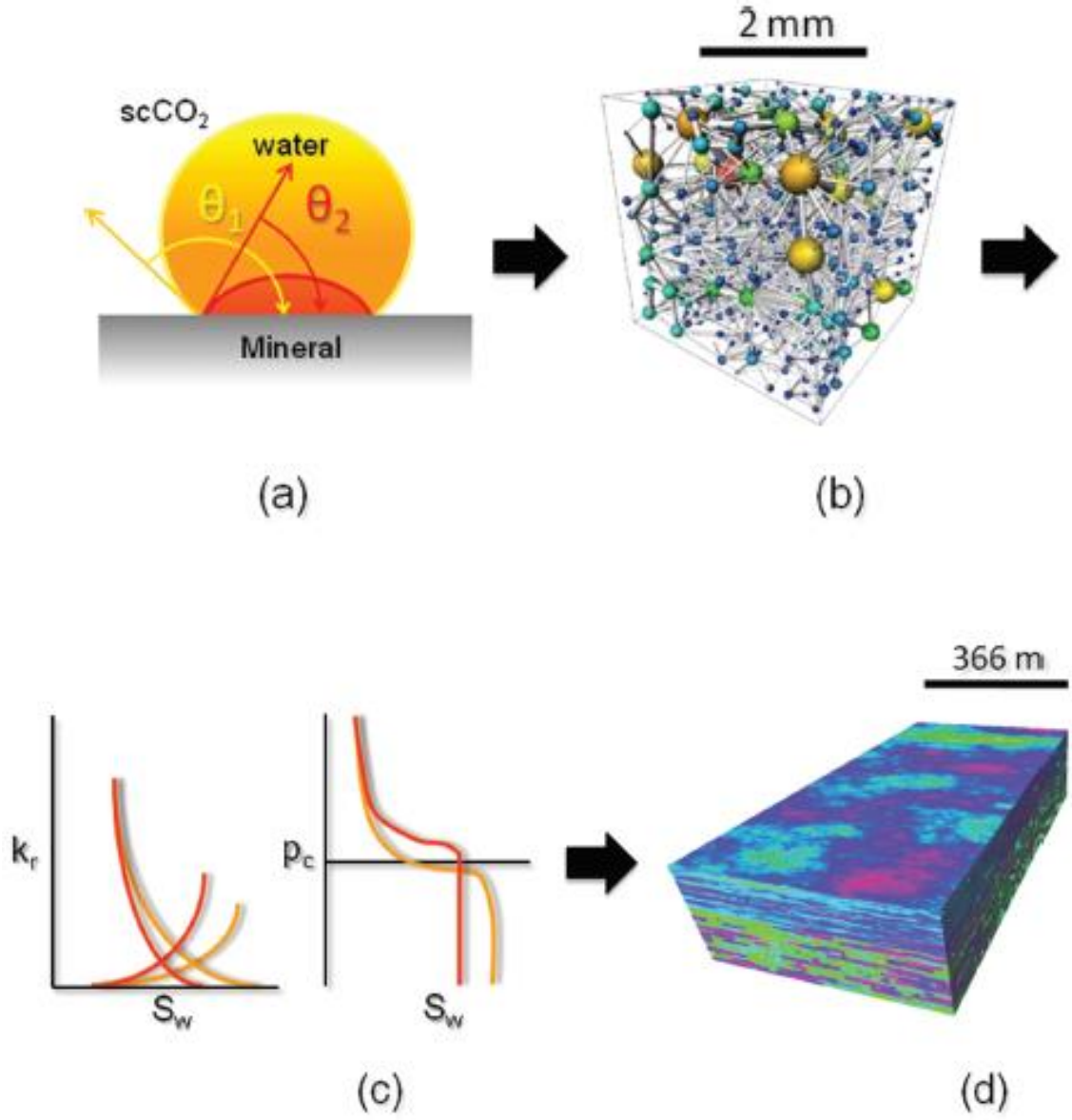

Figure 2-5 An example workflow leading from (a) millimetre-scale contact angle measurements to (d) hectometre-scale pilot-project simulation via (b) millimetre-scale pore-network modelling and (c) the predicted macroscale saturation functions for relative permeability and capillary pressure. The image of a pore network model was reproduced from Blunt et al. (2013). The permeability array is displayed per grid-block on a logarithmic scale in the pilot-scale model (d): the permeability scale is from 0.001 mD (green) to 10,000 mD (red) (9.87×10^{-19} - 9.87×10^{-12} m^2). This figure was taken from Iglauer et al. (2015).

2.3 Dolomite Wettability after CO_2 injection

Wettability of a rock–CO_2–water system is a key parameter for CO_2 geo-sequestration and enhancing oil recovery owing to its impact on the three most important trapping mechanisms during the initial storage phase, i.e. structural (Naylor et al. 2011; Iglauer et al. 2015), residual (Iglauer et al. 2011, 2016; Chaudhary et al. 2013; Krevor et al. 2015; Al-Khdheeawi et al. 2016, 2017, 2017a; Rahman et al. 2016) and dissolution trapping (Al-Khdheeawi et al. 2016, 2017, 2017a).

Rock–CO_2–water wettability studies have been conducted by several researchers. For example, Pokrovsky et al. (Pokrovsky et al. 2005) observed there was no effect of salt concentration (0.1 to 1 M NaCl) on dolomite dissolution rate for CO_2 pressures ranging from 5 to 50 atm at 25°C and pH varying between 3 to 4, e.g. the reservoir pH values were between 3-4 at reservoir conditions for CO_2-saturated ("live") brine (Schaef et al. 2004). Moreover, Pokrovsky et al. (Pokrovsky et al. 2005) observed an insignificant effect of CO_2 on the rate of dissolution of calcite, dolomite, and magnesite where the dissolution rate stays constant when CO_2 pressure was further increased. Note that the apparent activation energy for calcite dissolution at 25–100 °C is equal to 48.2 ±4.6 kJ mol^{-1} and 34 kJ mol^{-1} at pH equal to 4 (Pokrovsky et al. 2009). Therefore, CO_2 can be trapped for several hundreds of years owing to the slow dissolution kinetic triggered by the limited mixing between the CO_2 and the brine (Ballentine et al. 2001). Moreover, high temperatures (100 to 150 °C) and pressures (> 50 atm) have a week effect on dissolution rates of all carbonate minerals (Ballentine et al. 2001), which enhances carbon dioxide sequestration in deep carbonate sedimentary basins.

The contact angle between the mineral-water-CO_2 was measured to quantify the wettability of the rock substrate (Iglauer et al. 2015a, 2017). It was reported that the water contact angle (θ) increased with increasing pressure owing to the reduction of the density difference between the fluids (Al-Yaseri et al. 2016; Rahman et al 2016; Iglauer et al. 2017) and an associated increase in intermolecular interaction between CO_2 and minerals. This has been well-supported by most literature (Dietrich et al. 1991; Saraji et al. 2013; Iglauer et al. 2015a; Sarmadivaleh et al. 2015; Arif et al.

2016) and molecular dynamics simulations (Iglauer et al. 2012; Jung et al. 2012; McCaughan et al. 2013; Sedghi et al. 2014; Chen et al. 2015; Javanbakht et al. 2015).

Further, it was found that the contact angle increases with rising temperature (Yang et al. 2008; Farokhpoor et al. 2013; Iglauer et al. 2015; Sarmadivaleh et al. 2015; Al-Yaseri et al. 2016, 2016a; Roshan et al. 2016) but other researchers believe it is reduced (De Ruijter et al. 1998; Saraji et al. 2014; Arif et al. 2016). However, it was found that the contact angle is a complex function that includes temperature and many other parameters (Roshan et al. 2016).

Chapter 3 Effect of Temperature on CO_2/Brine/Dolomite Wettability: Hydrophilic vs Hydrophobic Surfaces*

Abstract

The water contact angle in a system of brine (20wt% $CaCl_2$) and CO_2 was measured on a smooth dolomite surface (RMS surface roughness 45nm) with both hydrophilic and hydrophobic behaviour as a function of pressure (0.1, 5, 10, 15, 20 MPa) and temperature (308, 323, and 343 K). The experimental results show that the contact angle of brine/CO_2 increases slightly with temperature when dolomite surface is hydrophilic but interestingly reduces when the surface is hydrophobic. The results also illustrate that the brine/CO_2 contact angles increase with increasing pressure. We interpreted the experimental observations using the concept of alteration in Van der Waals potential (substrate surface chemistry) with thermodynamics properties including pressure and temperature.

Keywords: Wettability, Dolomite, Contact angle, Carbon dioxide, Hydrophilic, Hydrophobic

*Reference: Al-Yaseri et al. (2017) *Journal of Energy and Fuel*, 31, 6329 - 6333

3.1 Introduction

CO_2 injection into carbonate reservoirs is a process for enhancing oil and gas recovery (Olenick et al. 1993; Babadagli 2006). The technique has been also suggested for CO_2 geo-sequestration (Babadagli, 2006; Izgec et al. 2008; Mohamed et al. 2011) which will be an efficient method to reduce anthropogenic CO_2 emissions to the atmosphere and thus mitigates climate change (Benson et al. 2005; Metz et al. 2005). However, it is important to understand the nature of interaction between fluid and rock in order to safely store CO_2 in the ground and assess the CO_2 ability to increase the recovery (Oomole et al. 1993; Iglauer et al. 2015, 2015a). Furthermore, the wettability of a rock–CO_2–water system is a key parameter in such process due to its impact on the three most important trapping mechanisms during the initial storage phase, i.e. structural (Naylor et al, 2011, Iglauer et al. 2015), residual (Iglauer et al. 2011; 2016, Krevor et al. 2015; Chaudhary et al. 2013; Rahman et al. 2016; Al-Khdheeawi et al. 2016, 2017, 2017a) and dissolution trapping (Al-Khdheeawi et al. 2016, 2017, 2017a).

Pokrovsky (Pokrovsky et al. 2005) observed that there was no effect of salt concentration (0.1 to 1 M NaCl) on dolomite dissolution rate for CO_2 pressures ranging from 5 to 50 atm at 25°C and pH varying between 3 to 4 e.g. the reservoir pH values are between 3-4 at reservoir conditions for CO_2-saturated ("live") brine (Schaef et al. 2004). Moreover, Pokrovsky et al. (Pokrovsky et al. 2005) observed insignificant effect of CO_2 on the rate of dissolution of calcite, dolomite and magnesite where the dissolution rate stayed constant when CO_2 pressure was further increased. Note that the apparent activation energy for calcite dissolution at 25–100 °C is equal to 48.2 ±4.6 kJ mol^{-1} and 34 kJ mol^{-1} at pH equal to 4 (Pokrovsky et al. 2009). Therefore, CO_2 can be trapped for several hundreds of years due to the slow dissolution kinetic triggered by the limited mixing between the CO_2 and the brine (Ballentine et al. 2001). Moreover, high temperatures (100 to 150 °C) and pressures (> 50 atm) have very week effect on dissolution rates of all carbonate minerals (Iglauer 2017) which enhances carbon dioxide sequestration in deep carbonate sedimentary basins.

In this context, the contact angle between the mineral-water-CO_2 was measured to quantify the wettability of the rock substrate (Iglauer et al. 2015a, 2017). It was reported that the water contact angle (θ) increases with increasing pressure due to the reduction of the density difference between the fluids (Al-Yaseri et al. 2016, Rahman et al. 2016, Iglauer 2017), and an associated increase in intermolecular interaction between CO_2 and mineral. This has been well-supported by most literature data (Dietrich et al. 1991, Saraji et al. 2013, Iglauer et al. 2015, Sarmadivaleh et al. 2015, Arif et al. 2016) and molecular dynamics simulations (Iglauer et al. 2012, Jung et al. 2012, McCaughan et al. 2013, Sedghi et al. 2014, Chen et al. 2015, Javanbakht et al. 2015).

The influence of temperature on contact angle has, however, stayed controversial with some believing that it increases with temperature; (Yang et al. 2008, Farokhpoor et al. 2013, Iglauer et al. 2015, Sarmadivaleh et al. 2015, Al-Yaseri et al. 2016, 2016a, Roshan et al. 2016), and others who argue that it reduces (De Ruijter et al. 1998, Love et al. 2005, Arif et al. 2016,). Roshan et al. (Roshan et al. 2016) showed theoretically and experimentally that the contact angle is a complex function of temperature through several parameters on electrically charged surfaces. However, a comprehensive quantitative analysis especially for weakly charged surfaces is required to give a conclusion to temperature dependency of contact angle.

Therefore, in this work the advancing and receding contact angles of brine (20 wt% $CaCl_2$)/CO_2 were measured on both, hydrophilic and hydrophobic, dolomite surfaces at different pressures (0.1, 5, 10, 15, 20 MPa) and temperatures (308, 323, and 343K). The results were analysed by extending the newly developed physical model for contact angle prediction (Al-Yaseri et al. 2016).

3.2 Experimental methodology

A dolomite sample with smooth surface (RMS roughness~110 nm measured with an atomic force microscopy instrument, model DSE 95-200, Figure 3-1) was used for the experiment. In order to measure the mineral composition of the dolomite sample, a sub-sample was first crushed in a tungsten carbide mill and the powdered sample

was mounted in an XRD sample holder and analysed using a PANalytical Empyrean II X-ray Diffractometer (45kV, 40mA; 5°-80° 2θ), equipped with a Co anode source. The patterns were analysed and quantified using SiroQuant (v.4), with minerals identified with reference to ICDD powder diffraction files, Table 3-1.

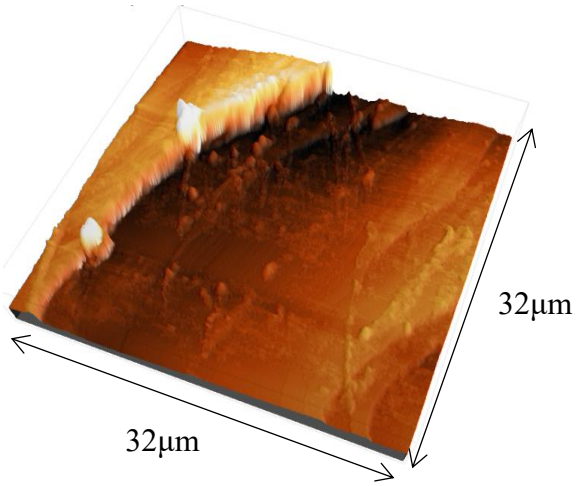

A (before)

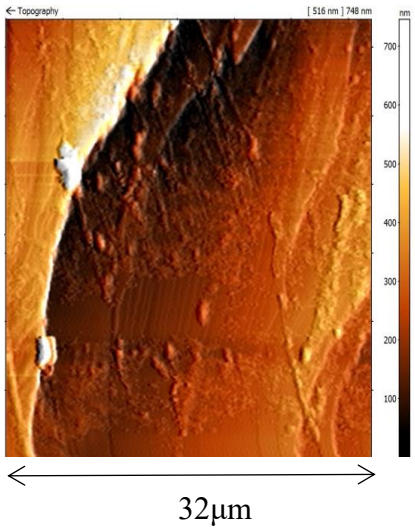

B (before)

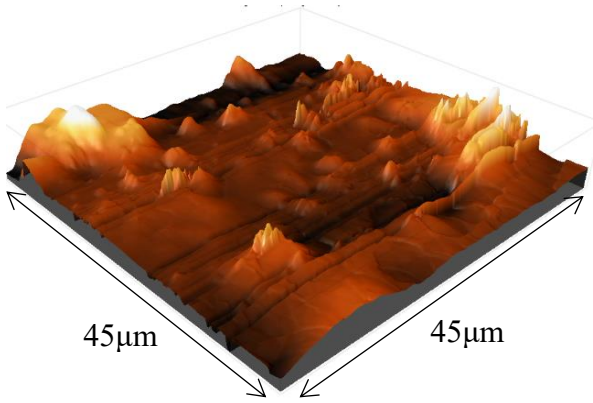

A (after)

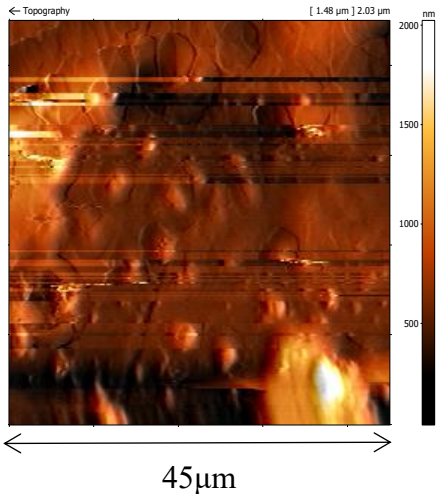

B (after)

Figure 3-1 Atomic force microscopy images of the dolomite surface used in the experiments. (a) 3D topography of the substrate; (b) deflection signal, different heights are coloured differently (black is 0 nm, white is the maximum). For interpretation of the references to colour in this figure legend, the reader is referred to the web version of this article.

Furthermore, the surface charge of the tested crushed dolomite sample suspended in brine (20 wt% $CaCl_2$) was measured (-6.24 mV) with a zeta potentiometer (Brookhaven ZetaPALS) at ambient conditions (298 K and 0.1 MPa).

Before each contact angle measurement, the dolomite (hydrophilic) sample was cleaned with acetone and DI water and then exposed to air plasma for 15 min to remove surface contaminations (Love et al. 2005, Mahadevan 2012, Iglauer et al. 2014). The substrate was then placed in a high pressure and temperature cell. The cell was pressurized with CO_2 using a high precision syringe pump (ISCO 500D; pressure accuracy of 0.1% FS) until a pre-set value was obtained. When the desired pressure was attained, a small droplet (~ 7µL) of brine (20 wt% $CaCl_2$ saturated by CO_2 using a mixing reactor; El-Maghraby et al. 2012) was dispensed onto the tilted substrate (tilting angle 12^o) and advancing and receding contact angles were measured simultaneously using a high definition video camera. This procedure was repeated for different pressures (0.1, 5, 10, 15, and 20 MPa) and temperatures (308, 323, and 343 K).

The dolomite sample surface was initially hydrophilic as seen from measured contact angles. In order to make it hydrophobic for subsequent experiments, the sample was aged in Triethoxy(octyl) (99.9 mol% purity, from Sigma–Aldrich) silane for one month at ambient conditions and then left to dry at room temperature (Grate et al. 2012), note that the hydrophobic dolomite sample was cleaned by DI water only before each measurement.

Note that the surface roughness was measured by AFM before and after each contact angle measurements to assess the surface morphology and therefore possible dissolution-precipitation (Butt et al. 2006). The result showed insignificant change on the surface roughness (from 110 nm to 180 nm) which is unlikely to affect the contact angle values (Al-Yaseri et al. 2016).

Table 3-1 Minerals identified in Dolomite sample based on XRD pattern interpretation.

Phase	Weight	Error of Fit
Dolomite ($CaMg(CO3)_2$	96.9	1.25
Talc, ($Mg_3Si_4O_{10}(OH)_2$)	3.1	1.25

3.3 Theoretical background

Young's equation (Young 1805) is often used to analyse the surface free energy of surfaces with no potential charges through contact angle measurement e.g. where the contact angle of liquid (θ) is related to the gas-solid (γ_{gs}), gas-liquid (γ_{lg}), and liquid-solid (γ_{ls}) interfacial tensions:

$$\cos\theta = \frac{(\gamma_{sg} - \gamma_{sl})}{\gamma_{\mathrm{lg}}} \quad \textbf{(1)}$$

Difficulties of measuring the gas-solid and liquid-solid interfacial tensions, however, limit the applicability of Young's equation. The sharp-kink approximation (Dietrich et al. 1991, Merath, 2008) was therefore introduced to obtain an expression for contact angle without the need of gas-solid and liquid-solid interfacial tensions (Roshan et al. 2016):

$$\cos\theta = \frac{\Delta\rho}{\gamma_{\mathrm{lg}}} I - 1 \quad \textbf{(2)}$$

Where $I = -\int_{z_{\min}}^{\infty} V(z)dz$ is the van der Waals potential integral (I) (Gatica et al. 2004, Garcia et al. 2008), and $\Delta\rho = \rho_{lf} - \rho_g$ (ρ_{lf} and ρ_g are densities of liquid film and gas respectively) (Merath, 2008).

It is evident from Eq. (2) that medium pressure influences the density difference and gas-liquid interfacial tension, however, the effect of pressure on density difference is much higher than its effect on γ_{lg} (Georgiadis et al. 2010). Increase in pressure significantly reduces $\Delta\rho$ and to some extent γ_{lg} .

The $\frac{\Delta\rho}{\gamma_{lg}}$ ratio therefore reduces with pressure thus increasing contact angles on any surfaces. In addition, the pressure effect is more significant than temperature effect on $\Delta\rho$. This is because ρ_g is a strong function of pressure and weaker function of temperature (Eq. (2)) e.g. especially for temperatures and pressures typically found in subsurface systems.

Furthermore, $\Delta\rho$, γ_{lg} and I are temperature dependent to some extent. In particular, temperature increase increases the gas-liquid interfacial tension and Δρ (especially at relatively higher pressure ≥ 5MPa) however the Δρ increment with temperature is more significant than that of γ_{lg} (Sarmadivaleh et al. 2015, Georgiadis et al. 2010). This in turn means that $\frac{\Delta\rho}{\gamma_{lg}}$ increases with increasing temperature, which should thus reduce the contact angle e.g. assuming temperature independency of the van der Waals potentials. However, a contact angle increase with temperature has been observed experimentally.

Interestingly, it has been shown that the van der Waals potentials can decrease with temperature (Pinon et al. 2016) which can in turn increase the contact angle (Eq. (2)). The van der Waals potential ($V = V_s - V_l$) in Eq. (2) describes the net preference of the adsorbate molecule for wetting the substrate instead of forming a droplet, due to intermolecular forces (Garcia et al. 2008). In the definition of V, V_s is the potential energy of the adsorbate molecule due to the substrate and V_l is the potential energy of the adsorbate molecule due to the substrate hypothetically on the same location.

Thus, the temperature influences the van der Waals potential in both, hydrophilic and hydrophobic, surfaces however the hydrophilic surfaces will be more affected by

temperature. This is because hydrophilic surfaces offer more effective van der Waals interactions between the water molecules and substrate surface that can be broken by temperature increase (Pinon et al., 2016).

3.4 Results and discussion

The advancing and receding brine contact angles measured in the presence of CO_2 on hydrophilic dolomite sample at different temperatures (308, 323 and 343 K) and pressures (0.1, 5, 10, 15 and 20 MPa) are presented in Figure 3-2, respectively. An increase in pressure significantly increased both, the advancing and receding, contacts angles; however, a temperature increase either slightly increases the contact angle or in some cases has no effect on contact angles on the hydrophilic dolomite surface. However, on the hydrophobic dolomite sample, the temperature increase reduced the contact angle (Figure 3-2), while increasing pressure still increased the contact angle. Recall from section 3 pressure significantly influences the fluid densities and reduces the density difference between the fluids (Eq. (2)). This in turn increases the contact angle considerably in both hydrophilic and hydrophobic, surfaces.

The effect of temperature, on the other hand, is different for hydrophilic and hydrophobic dolomite surfaces. This difference was discussed earlier where the ratio of $\frac{\Delta\rho}{\gamma_{lg}}$ increases with temperature and therefore θ should in fact reduce on any surface. It seems to be the case for hydrophobic surfaces where the alteration of van der Waals potentials (I) with temperature in less significant than that of hydrophilic surfaces (Pinon et al. 2006).

Temperature can however reduce the van der Waals potential on hydrophilic surfaces more significantly. This is due to the fact that the hydrophilic surfaces offer more effective van der Waals interactions between the water molecules and substrate surface and therefore more potential energy. Such effective potential energy on hydrophilic surfaces is a strong function of temperature e.g. bound rupture can occur

readily when temperature increases (Pinon et al. 2006). On hydrophobic surfaces, however such bounds are weakly present and therefore their temperature dependency is also weaker that hydrophilic surfaces.

Reduction in van der Waals potential increases the contact angle, thus two terms in Eq. (2) ($\frac{\Delta\rho}{\gamma_{lg}}$ and I) compete with each other to define the contact angle. Therefore, the decrease in contact angle by temperature is more likely to be experienced in hydrophobic surfaces than hydrophilic. That is why the contact angle measured on hydrophobic surface (Fig. 6-3) decreases significantly with temperature when compare to hydrophilic surface (Fig. 6-2).

The above-mentioned behaviour was also seen by Takei et al. (Takei et al. 1994) in the field of bio-medical science. They used different type of polymers (N-isopropylacrylamide class) to modify the substrate surface from hydrophilic to hydrophobic by changing the temperature to control the drug delivery. They observed that the contact angle of water on the substrate was quite constant below a critical temperature (when the sample was hydrophilic). As soon as the critical temperature was reached (when the sample turned hydrophobic), the contact angle reduced significantly. The hydrophilic behaviour of the surface at relatively low temperature was linked to the hydrogen bonding which was later broken (when temperature passes critical point).

(a)

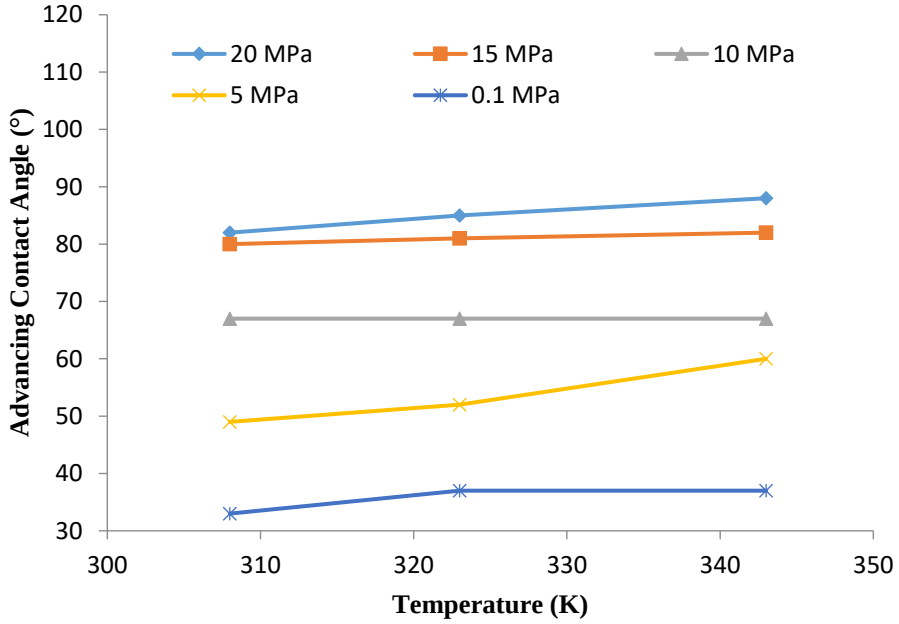

(b)

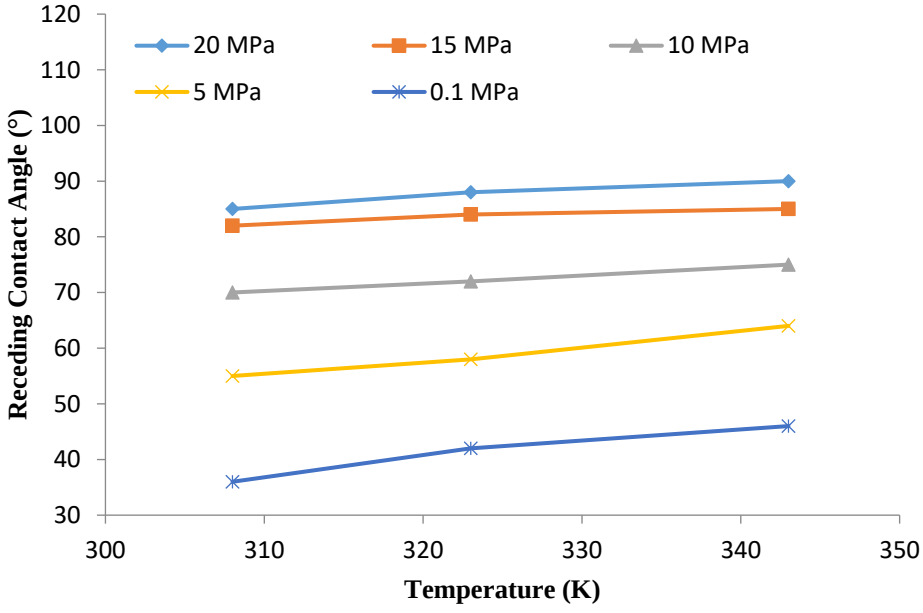

Figure 3-2 a) advancing and b) receding brine contact angles in the presence of CO_2 measured on hydrophilic dolomite at different pressures (0.1, 5, 10, 15 and 20 MPa) and temperatures (308, 323 and 343K).

(a)

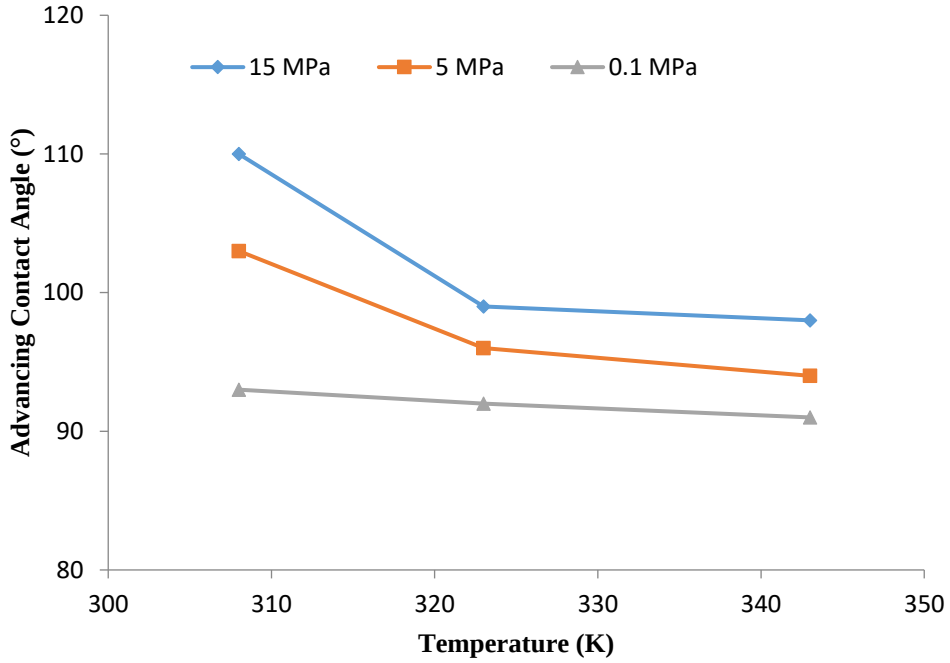

(b)

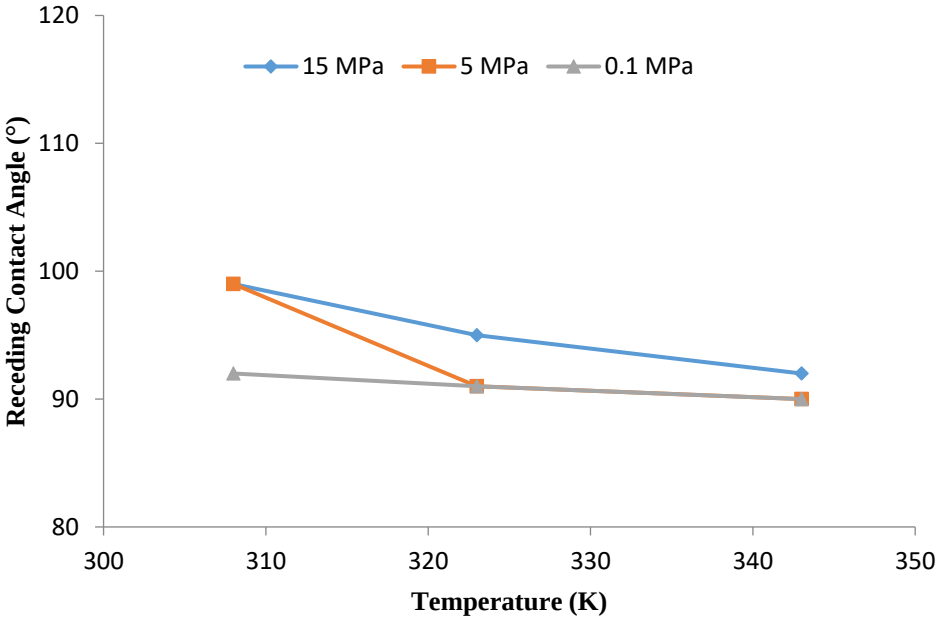

Figure 3-3 a) advancing and b) receding brine contact angles in the presence of CO_2 measured on hydrophobic dolomite at different pressures (0.1, 5 and 15 MPa) and temperatures (308, 323 and 343K).

3.5 Conclusions

In this chapter, we measured the advancing and receding contact angles of CO_2/brine system on hydrophobic and hydrophilic dolomite surfaces at different pressures and temperatures. We analysed the experimental observations with the concept of temperature-dependency of van der Waals potential and sharp-kink approximation. It was shown that pressure increases the contact angle of brine considerably regardless of surface being hydrophilic or hydrophobic. Contact angle on the other hand stayed unchanged or slightly increased on hydrophilic surfaces by increasing temperature but were reduced on hydrophobic surfaces. It was illustrated that phase-density difference, fluids interfacial tension and fluids-solid van der Waals potentials affect the contact angle of no/weakly charged surfaces when state variables such as pressure or temperature vary.

Chapter 4 Residual trapping of supercritical CO_2: direct pore-scale observation using a low-cost pressure cell for micro-computer tomography*

Abstract

We describe the design and fabrication steps of a low-cost, modular experimental cell for flooding and X-ray tomography visualization of the rock samples at reservoir conditions (confining pressure up to 45 MPa, pore fluid pressure up to 20 MPa, and temperature up to 80°C). The main body of the cell is made from Polyether ether ketone (PEEK) tube. The cell can be easily machined and assembled in house from off-the-shelf components at a low cost. Modular design allows adopting the cell to a wide range of X-ray visualization experiments. To demonstrate the capabilities of the equipment we are presenting how the residual CO_2 phase spreads in the rock as a function of thermo-physical conditions, namely, for ambient condition CO_2 gas, near-critical CO_2 gas, liquid CO_2, and supercritical CO_2.

Keywords: CO_2, Rocks, Micro CT, Pressure cell

*Reference: Lebedev et al. (2017) in *Journal of Energy Procedia*, 114, 4967 – 4974

4.1 Introduction

Injection of CO_2 into the subsurface is one of the known methods to mitigate greenhouse gas emissions (Lackner 2003, Metz et al. 2005, Orr 2009). The buoyant CO_2 is contained in the subsurface by structural, residual, dissolution and mineral trapping mechanisms. Quantitative knowledge of the residual trapping capacity of the reservoir is thus crucial for storage site selection. This residual saturation depends on porosity, initial CO_2 saturation, pore morphology and wettability, or in other words on reservoir properties at the microscopic level; note that the macroscopic residual saturation also depends on sweep efficiency and gravity. Therefore, it is of crucial importance to understanding the major factors, which determine residual trapping efficiency. Micro-CT tomography technique is a powerful tool to understand such factors at micro-level.

It is standard practice in micro-CT to image rocks at ambient conditions (i.e. at room pressure and temperature) (Madonna et al. 2013, Shulakova et al. 2013). However, reservoir rocks are buried at such depth that they experience high stresses and temperatures. The thermodynamic properties of the fluids inside the reservoir are pressure and temperature dependent. Therefore, transport properties are also temperature and pressure dependent. Moreover, it is well established that elastic rock properties of rocks are strongly affected by stress and or fluid distribution. Thus, in order to acquire realistic pore network structures and fluid distributions (including but not limited to residual saturation), and to reliably estimate transport and elastic properties from micro images, rocks have to be imaged at reservoir pressure and temperature conditions. At this moment, cells for micro-CT are custom made (Iglauer et al. 2011, Fusseis et al. 2014) and thus are expensive.

We thus have developed suit of X-ray transparent pressure and temperature (P-T) cells capable of holding from 5 mm to 38.5 mm diameter samples. To demonstrate capabilities of the equipment, in this paper we report how the residual CO_2 saturation depends on the thermodynamical conditions of the CO_2 (which changes from gas to liquid, near-supercritical and supercritical), in order to link CO_2 saturation and fluid distribution to acoustic properties of the samples.

4.2 Pressure cells for microCT

We have designed and fabricated two X-ray transparent pressure – temperature cell: both cells are utilized for visualization of the process inside the reservoir samples during flooding. The first cell is prepared for the simultaneous acoustic measurements and CT imaging at moderate resolution (40 um) of the 38.5 mm (1.5") in diameter samples; the second one is applied for micro-CT imaging of smaller samples (5mm in diameter) at sub-micrometer resolution. Cell for large samples is shown in Figure 4-1(a), this cell has been described in detail previously (Lopes et al. 2014, Lebedev et al. 2014).

Figure 4-1 (b) shows the cell for high-resolution imaging. This cell can be easily fabricated and assembled from off-the-shelf components at a low cost. Modular design allows adaptation of the cell to a wide range of X-ray experiments. The main body of the pressure cell is made from a 21-mm-diameter, 300-mm-long PEEK (Polyether ether ketone) rod supplied by RS components. An 8 mm in diameter hole to accommodate the sample inside was drilled in the laboratories' workshop using a lathe. All other parts of the cell have been assembled from the standard Swagelok fittings. Both ends of the cell have the same assembly. Stainless steel, ¾" nuts with ferrule are swaged on both ends of the PEEK tube. The ¾" to ¼" unions are connected to both ends of the PEEK rod. The ¼" tees unions fittings are using for confining pressure supply and getting through of two 1/8" stainless steel fluid lines inside the cell. The cell is fixed on the rigid holder that can be easily connected to a stage inside micro-computed tomography (μCT). A 5-mm-diameter sample was jacketed in the rubber sleeve and was connected to the fluid lines using custom made plastic plates. Some steps of the fabrication and assembly and testing of the cell are shown in Figure 4-2.

The arrangement of the cell inside X-ray micro-CT (3D X-ray Microscope VersaXRM 500 (XRadia-Zeiss) is shown in the Figure 4-3. X-Y-Z micropositioning stage of the X-ray micro-CT is able to hold up to 10 kg weight; the weight of the developed cells is not exceed kg, thus the pressure cell with can be fixed to X-Y-Z stage without compromising performance of the scanner. All hydraulic and fluid lines of the cell are connected to equipment by flexible PEEK 1/8" tubes (Sigma-

Aldrich). Such flexible tubes allow the rotation of the cell from -180° to +180° during the imaging. Confining pressure to a sample is applied by a set of syringe pumps (Teledyne-Isco 260 and 500 series). Depending on the requirements of the experiment, the heating and cooling of the sample inside the cell can be done by using continuous circulating of the pressurized confining fluid. A small flexible electrical heater attached to the low part of the cell (not shown in the Figures) can be used to boost the heating process. Injection of the fluids into the sample is performed using two syringe pumps (Teledyne-Isco 100 and 260 series). All pumps are placed in an outside X-ray micro-CT. All pumps and connecting tubes are maintained at a given temperature within the range -15°C +80°C by circulating of liquid antifreeze.

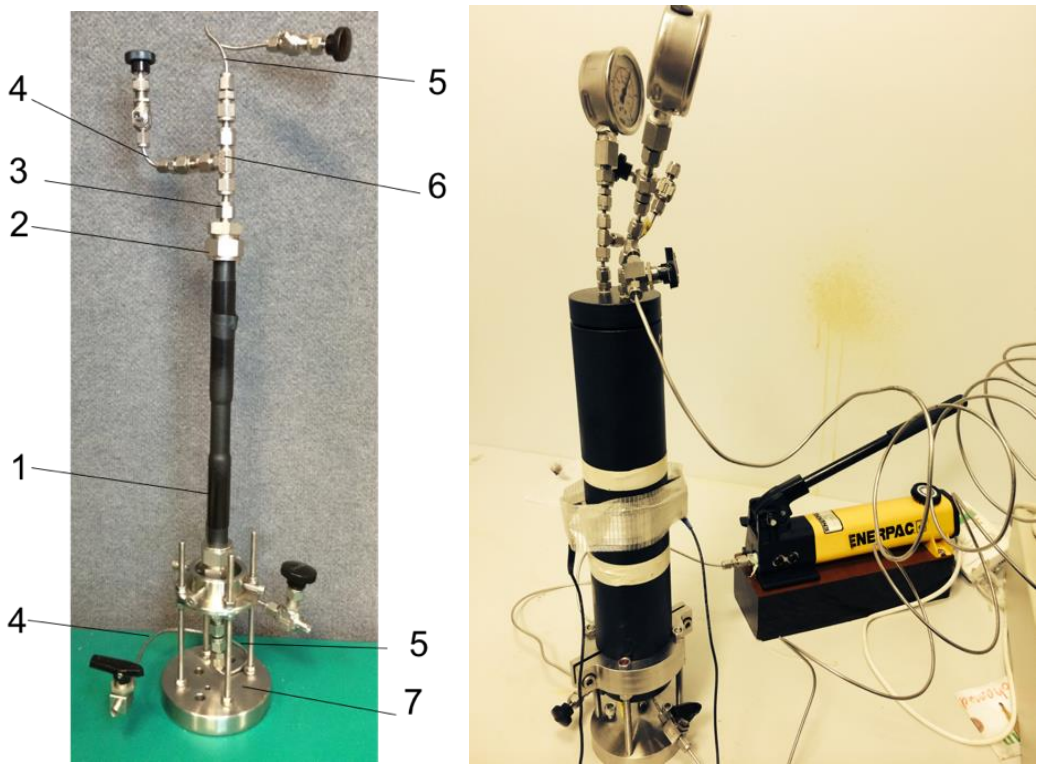

(a) **(b)**

Figure 4-1 Pressure-Temperature cells for CT: a) pressure cell for 5 mm diameter samples; b) pressure cell for 38.5 mm diameter samples. 1) PEEK pipe; 2) Stainless steel, ¾" nuts with ferrule; 3) ¾" to ¼" unions; 4) confining pressure line 1/8"; 5) pore pressure/ flooding line; 6) ¼" tees union; 7) stage to be fixed to X-Y-Z stage of the micro-CT.

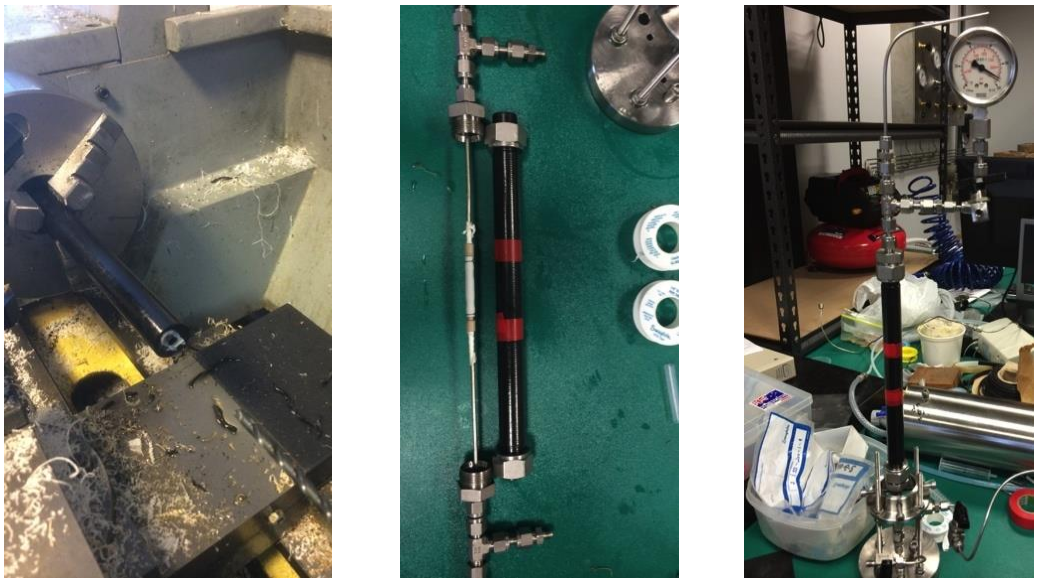

(a) **(b)** **(c)**

Figure 4-2 (a) Fabrication of the PEEK tube in the lab; (b) cell assembly: sample inside the white rubber sleeve is connected to flooding lines; (c) hydraulic test outside the micro-CT (confining pressure is 33 MPa, zero pore pressure).

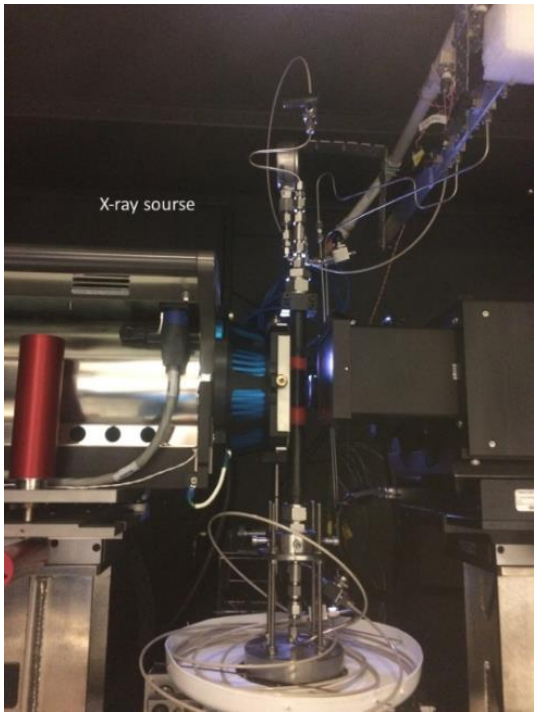

Figure 4-3 Pressure - Temperature cell inside micro-CY. X-Ray source in on the left, X-Ray objective (detector) is on the right.

4.3 Demonstration experiments

The cylindrical sample has been drilled from the bigger block, the sample is trimmed to size to accommodate inside a rubber sleeve inside the cell. After pressure test outside, the cell is placed inside micro-CT and the test image is performed. The cell and all hydraulic systems inside and outside the micro-CT are heated to designated temperature and controlled within 0.5C accuracy.

Monitoring and control of fluid injection inside the sample are performed between high-resolution imaging. Such real time in situ flooding visualization technique allows to estimate the amount of pore volumes (PV) injected inside the sample more precisely. Figure 4-4 shows the sequence of X-ray radiographs, i.e. one plane projection, of the Bentheimer sandstone sample inside the cell acquired at 20 MPa of confining pressure. Radiograph (a) is taken for the dry sample. On the radiograph (b) it can be observed that brine (doped with ten presents of sodium iodate) is entering the sample from the bottom and coming out the sample from the top. The last image (c) is the image after liquid CO_2 injection at 10 MPa injection pressure.

At each stage of the experiment, 3D imaging of the sample is performing at X-Ray energy ranged from 40kV to 80kV. Minimum time to acquire one 3D image is about 1.5h. During the acquisition, the injection valve is closed thus no fluid is injecting into the sample. However, the backpressure is maintained by a production pump. Figure 4-5 shows 2D images (sliced from 3D) of the dry, brine saturated and after liquid CO_2 flooding Bentheimer sandstone acquired at confining pressure of 20 MPa, pore pressure of 10 MPa, and temperature of 28°C with a nominal voxels size resolution of $(3.4348\ \mu m)^3$.

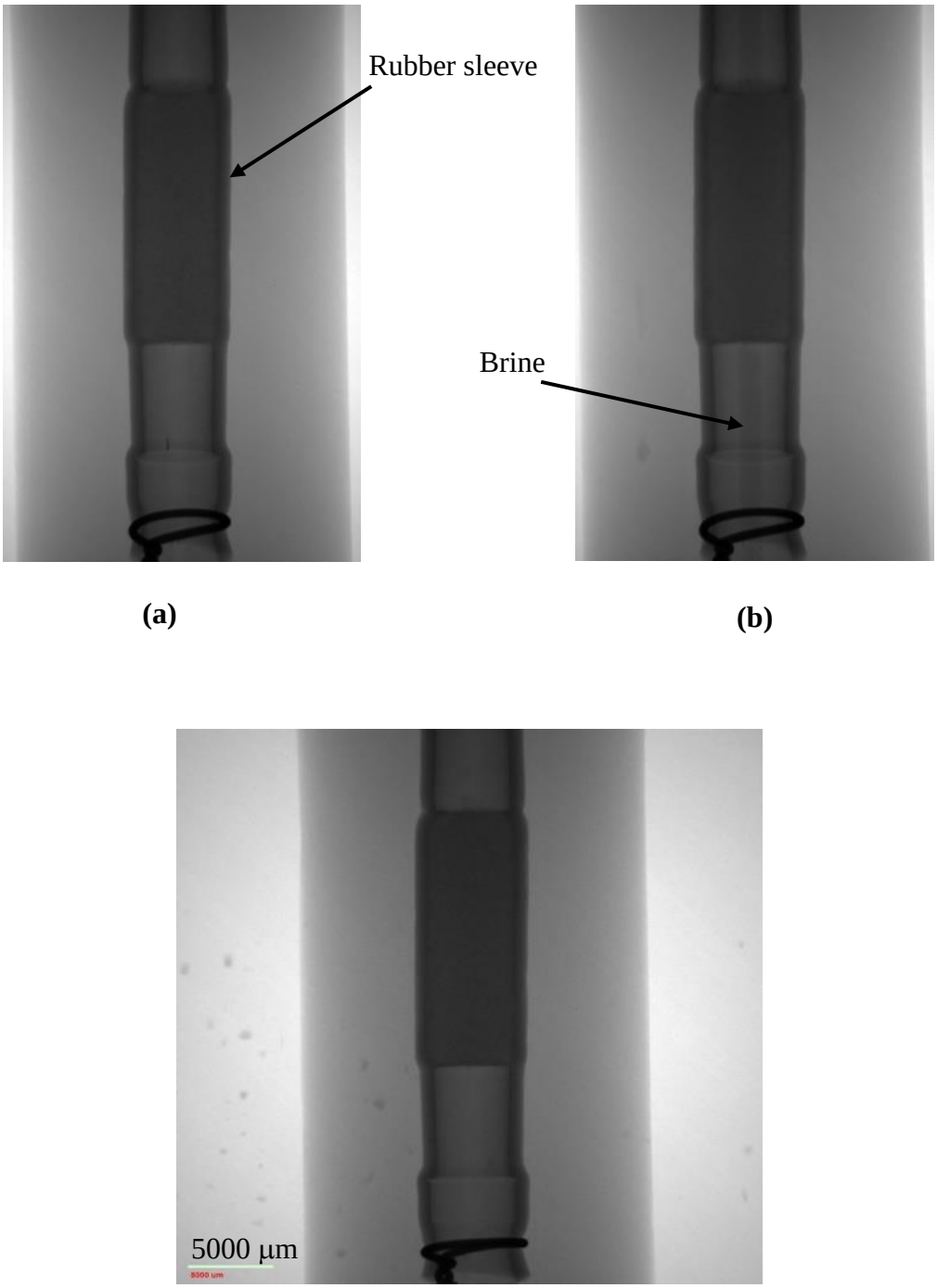

Figure 4-4 Time lapse of X-ray radiographs of the sample inside the cell at 20 MPa confining pressure: (a) dry sample; (b) brine injection; (c) after CO_2 injection. Low resolution image using 0.4x objective.

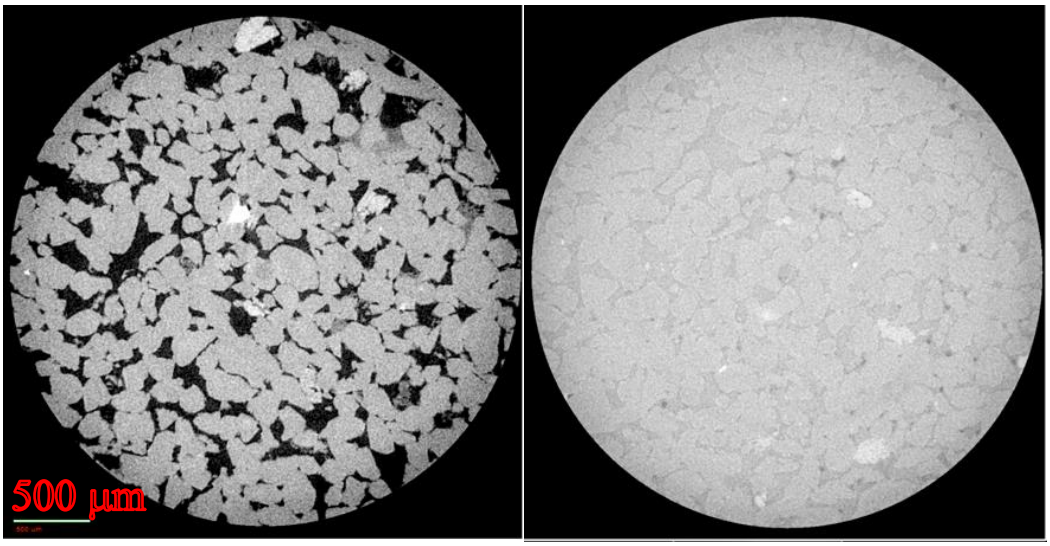

(a) **(b)**

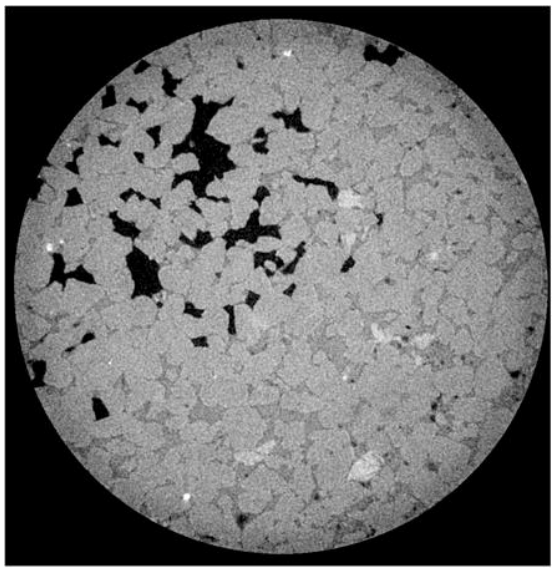

(c)

Figure 4-5 Tomographic images in the flooding experiment. (a) dry sample; (b) 10%NaI-doped brine saturated sample; (c) after flooding with liquid CO_2. The direction of CO_2 injection is perpendicular to the paper plane. X-ray energy is 80kV, the distance between X-Ray source and the sample is 20 mm, the distance between the sample and 4x objective is 20 mm; pixel size is 3.4348 micrometer. Confining pressure is 20 MPa, pore pressure is 10 MPa, the temperature is 28°C. Note that the images (b) and (c) are corresponding to the same area of the sample.

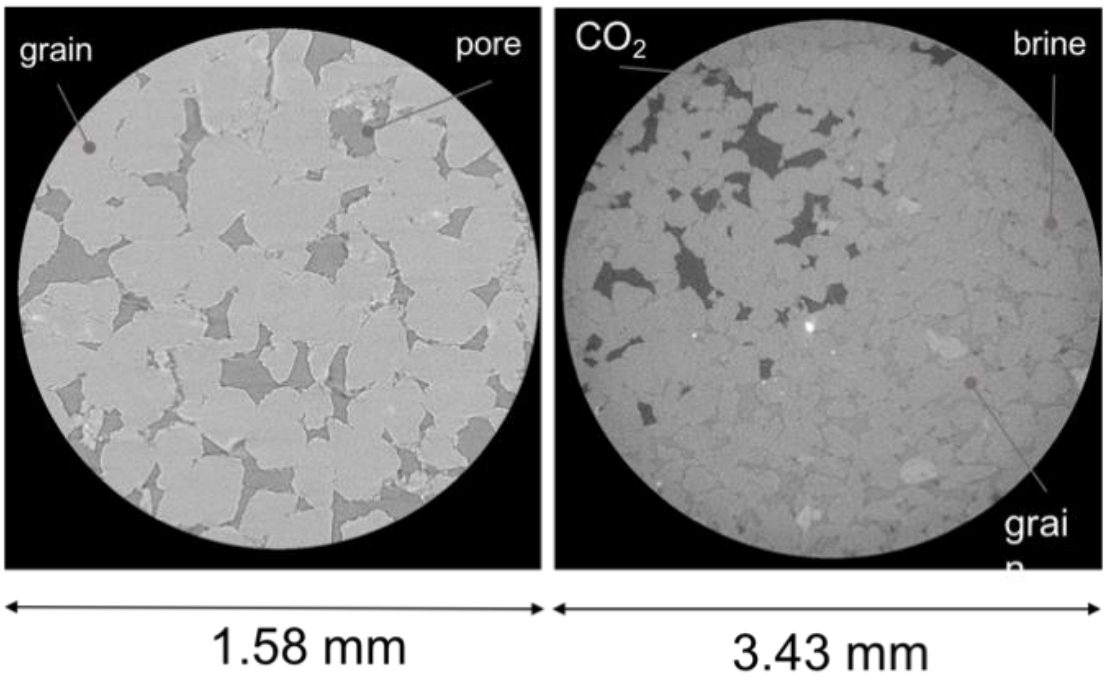
grain
pore
CO_2
brine
grai
1.58 mm
3.43 mm

(a) **(b)**

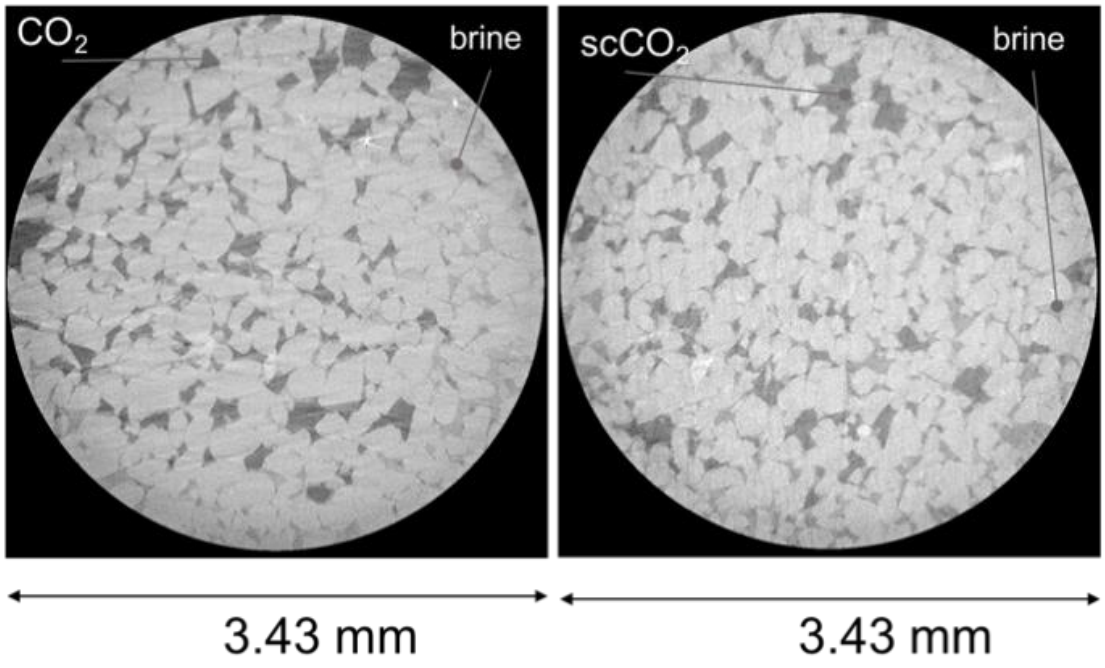
CO_2
brine
$scCO_2$
brine
3.43 mm
3.43 mm

(c) **(d)**

Figure 4-6 Influence of Pressure, Temperature and Fluid on the image quality. Bernheimer sandstone, gas permeability 1880mD. X-Ray energy is 60kV, the distance between X-Ray source and the sample is 19 mm, the distance between the sample and 4x objective is 19 mm; pixel size is 3.4348 micrometer. Number of scans (radiographs) is 4001: (a) Dry sample, Pconf=30 MPa, T=28°C; (b) after liquid CO_2 injection into brine saturated sample, Pconf=25 MPa, Ping=10 MPa, T=28°C; (c) after "near critical" CO_2 injection into brine saturated sample Pconf=15 MPa, Ping=7 MPa, T=42°C; (d) after supercritical-CO_2 injection into brine sa turated sample P_{conf}=15 MPa, Ping=10 MPa, T=42°C.

By increasing the pressure and especially temperature during the experiment the quality of raw images can decrease. Such slight degradation in quality caused mainly by the sample drift induced by a circulating high pressure and temperature confining fluid. Figure 4-6 shows how raw image quality changes when pressure and temperature increases.

4.4 Conclusion

The simple experimental cells that allow micro tomographic visualization of fluids inside rocks under elevated pressure was presented. The modular cell design allows hassle-free maintenance and easily modifications of the cell. The cell can be used for visualisation of multiphase fluids distribution inside porous media.

Using developed cell, we investigated how the residual CO_2 phase spreads in the rock as a function of thermo-physical conditions (for ambient condition CO_2 gas, liquid CO_2, near-critical CO_2 gas, and supercritical CO_2); and how residual CO_2 is dissolved by under saturated formation brine (dissolution trapping). We found that CO_2 spread is relatively homogeneous throughout the core plugs for all conditions; however, less scCO_2 was trapped at higher pressures, which is possible due to the lower water-wettability of sandstone at high pressures. We conclude that μCT is a very powerful tool for non-destructive visualisation of microstructure as well as pore-scale fluid distribution inside rocks samples. So far, the micro-CT cell has been successfully used in the following experiments pressure research (Saenger et al. 2016, Rahman et al. 2016, Zhang et al. 2016, 2016a, 2016b).

Chapter 5 Residual Trapping of Supercritical CO_2 in Oil-wet Sandstone*

Abstract

Residual trapping, a key CO_2 geo-storage mechanism during the first decades of a sequestration project, immobilizes micrometre sized CO_2 bubbles in the pore network of the rock. This mechanism has been proven to work in clean sandstones and carbonates; however, this mechanism has not been proven for the economically most important storage sites into which CO_2 will be initially injected at industrial scale, namely oil reservoirs. The key difference is that oil reservoirs are typically oil-wet or intermediate-wet, and it is clear that associated pore-scale capillary forces are different. And this difference in capillary forces clearly reduces the capillary trapping capacity (residual trapping) as we demonstrate here. For an oil-wet rock (water contact angle $\theta = 130°$) residual CO_2 saturation $S_{CO2,r}$ ($\approx 8\%$) was approximately halved when compared to a strongly water-wet rock ($\theta = 0°$; $S_{CO2,r} \approx 15\%$). Consequently, residual trapping is less efficient in oil-wet reservoirs.

Keywords: CO_2 geo-sequestration; Residual trapping; Storage capacity; Wettability; Oil-wet; Oil reservoir

*Reference: Rahman et al. (2016) in *Journal of Colloid and Interface Science*, 469, 63-68

5.1 Introduction

Carbon geo-sequestration has been identified as a feasible technology to mitigate global warming (Lackner 2003, Metz et al. 2005, Orr 2009). Technically, CO_2 is captured from large emitters (e.g. coal-fired power plants), and injected deep underground into geological formations for storage. However, although CO_2 is in a dense supercritical state at reservoir conditions (below 800m depth), it migrates upwards as it has a lower density than the resident formation brine. One key mechanism, which prevents the CO_2 from leaking back to the surface is residual trapping, where the CO_2 plume is split into many micrometre sized bubbles which are immobilized by capillary forces in the pore network of the rock (Suekane et al. 2006, Sukena et al. 2008, Pentland et al. 2011, Iglauer et al. 2011a, Krevor et al. 2012). Pore-scale residual trapping has been proven to work in clean sandstone (Iglauer et al. 2011a) and carbonate (Andrew et al. 2013, 2014). However, this mechanism has not been proven for oil-wet rock, despite its key importance as initial industrial scale CO_2 storage projects are very likely to occur in oil reservoirs (Firoozabadi et al. 2010); and these oil reservoirs are typically oil-wet (Cantucci et al 2009). The significance of oil reservoirs for carbon storage is high, as sequestration can be directly combined with CO_2 driven enhanced oil recovery (Cuiec 1991, Emberley et al. 2005, Lake 2010); furthermore, depleted oil reservoirs already have required infrastructure in place (Cook 2014), and they are typically well characterised in terms of seismic surveys, which significantly aids (reservoir scale) CO_2 flow monitoring (Gurevich et al. 2014).

We thus imaged initial and residual CO_2 in an oil-wet rock at typical storage conditions with an x-ray micro-computed tomograph (μCT), and we demonstrate that the residual trapping capacity is significantly reduced in oil-wet rock at (high pressure) storage conditions.

5.2 Experimental Procedure

5.2.1 Simulating Subsurface Condition

A sandstone oil reservoir at a depth of approximately 1000m was simulated (10MPa pore pressure, 318K temperature). For this, a clean homogeneous sandstone (Bentheimer) was selected to represent storage rock. Small core plugs (5mm diameter and 10mm length) were drilled and used for the experiments. Porosity was 22%, permeability 1800mD, and the rock consisted of 99wt% quartz, 0.7wt% kaolinite, and 0.3wt% rutile.

This rock was completely water-wet at ambient conditions (0° water contact angle in air), note that at higher pressures quartz is less water-wet (Chiquet et al. 2007, Broseta et al. 2012, Al-Yaseri et al. 2015). To mimic an oil reservoir the wettability of the rock was altered by immersing the plug into silane (Dodecyltriethoxysilane, 99.9mol% purity, from Sigma-Aldrich) under vacuum (so that the plug was fully saturated with the silane) and ageing the plug for 4 weeks at ambient conditions (Al-Anssari et al. 2016). This process rendered the plug strongly oil-wet (130° water contact angle at ambient conditions in air).

5.2.2 Imaging scCO_2 at the pore-scale with μCT

The oil-wet core plug was mounted into a high pressure μCT cell (Iglauer et al. 2011a), vacuumed and fully saturated with doped "dead" brine (7wt% NaI in deionized water; note that NaI is required for CT contrast). Subsequently 15 MPa confining pressure was applied, and pore pressure was raised to 10MPa. All flow lines and fluids were isothermally heated to 318K. These conditions approximately correspond to a storage depth of 1000m, see above. The dead brine was then displaced with >40 pore volumes (PV) of "live" brine (live brine is brine thermodynamically equilibrated with CO_2; (El-Maghraby et al. 2012)). Then 40PV of supercritical (sc) CO_2 were injected at a flow rate of 0.1 mL/min, which corresponded to a capillary number of 6×10^{-8}, and the core plug was imaged in 3D at a resolution of $(3.4\mu m)^3$ with an Xradia VersaXRM μCT instrument. Finally, live brine (40PV) was injected at a flow rate of 0.1mL/min, which corresponded to a capillary number of 1.7×10^{-6}, and the sample was μCT imaged again. This

experiment was repeated again, and the results were reproducible. The μCT images were filtered with a 3D non-local means algorithm (Buades et al. 2005) and segmented with a watershed algorithm (Schlüter et al. 2014). Petrophysical properties were then measured on the images, see below. For comparison, the same experiment was conducted again with a water-wet Bentheimer plug (0° water contact angle, see above).

5.3 Results and Discussion

5.3.1 Visualization, cluster morphologies and initial & residual CO_2 Saturations

Initial and residual CO_2 saturations of the oil-wet and water-wet plugs are visualized in Figure 5-1. Initial CO_2 saturations ($S_{CO2,i}$) were approximately the same (~50%), but the residual saturation ($S_{CO2,r}$) in the oil-wet plug was significantly lower (≈8 %) than in the water-wet plug ($S_{CO2,r} \approx 15\%$), Table 5-1. Precisely, the $S_{CO2,r}$ measured for the water-wet plug was 14.9%, consistent with independent measurements (Sukena et al. 2008, Pentland et al. 2011, Iglauer et al. 2011a, Andrew et al. 2013, Krevor et al. 2015, Akbarabadi et al. 2013); note that $S_{CO2,r}$ varies to some degree as it is also a function of porosity (Iglauer et al. 2011b) and pore body-pore throat aspect ratio (Wardlaw et al. 1988, Pentland et al. 2012); and CO_2 was located mainly in larger pores, although in some cases it also spread into relatively small pores. This indicates weakly water-wet conditions, consistent with 2D micromodel (Chalbaud et al 2010, Kim et al. 2012) and contact angle (Chiquet et al. 2007, Broseta et al. 2012, Farokhpoor et al. 2013, Saraji et al 2013, 2014, Kaveh et al 2014, Al-Yaseri et al. 2015, 2015a, Iglauer et al. 2015a, 2015b, Sarmadivaleh et al. 2015) measurements.

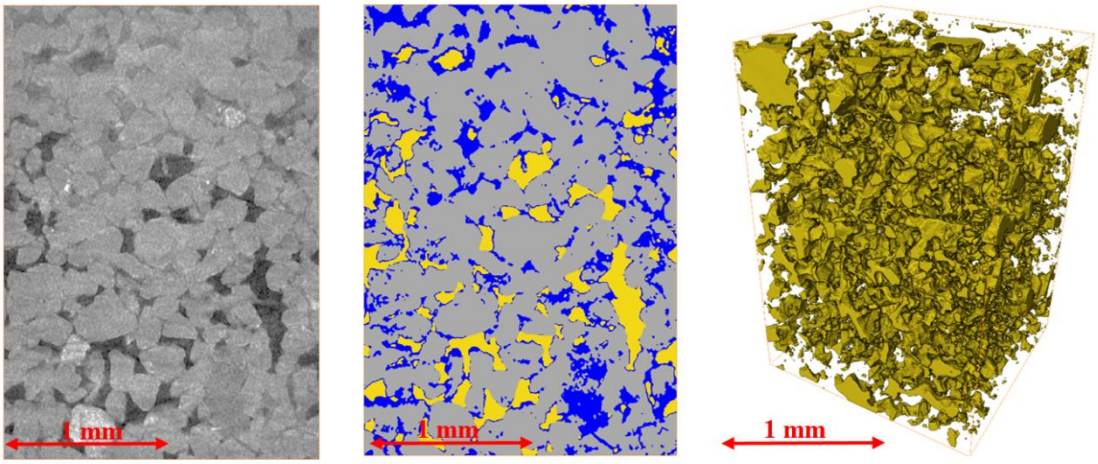

(a) (b) (c)

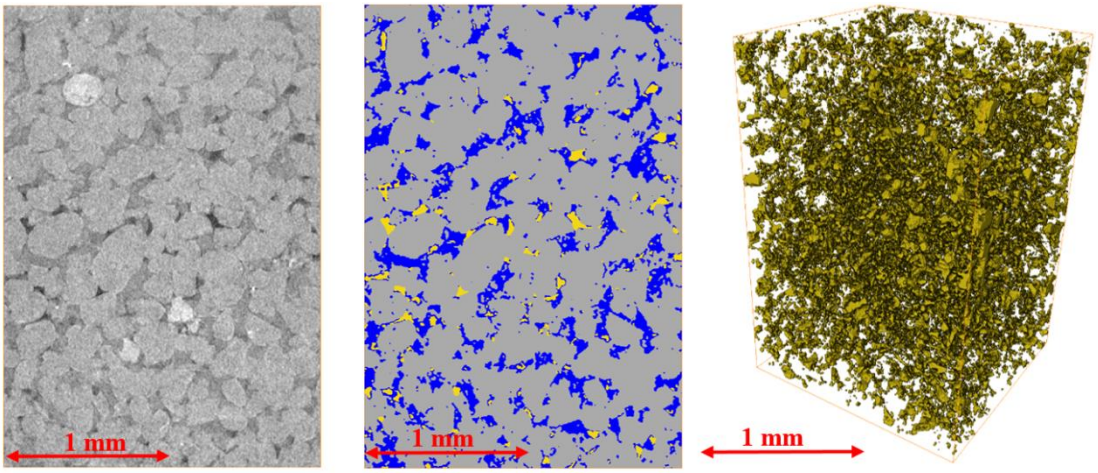

(d) (e) (f)

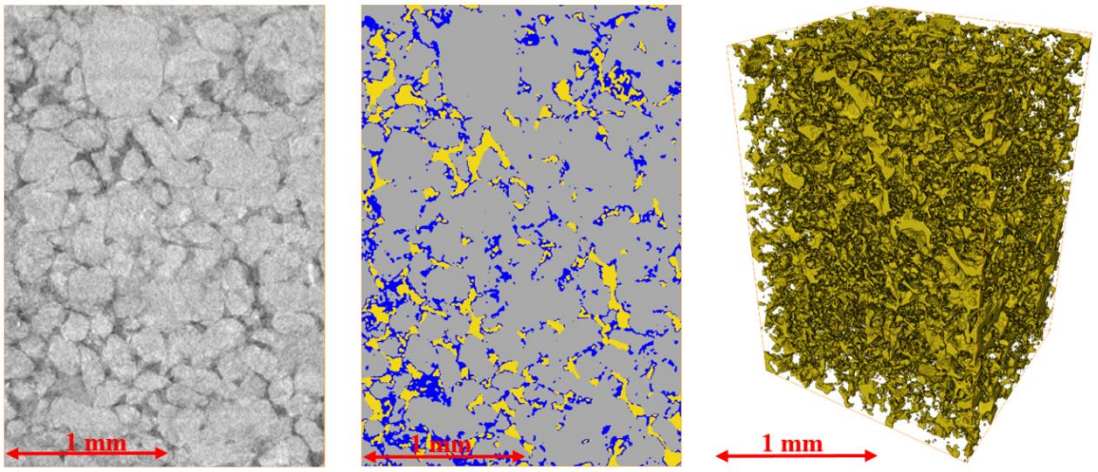

(g) (h) (i)

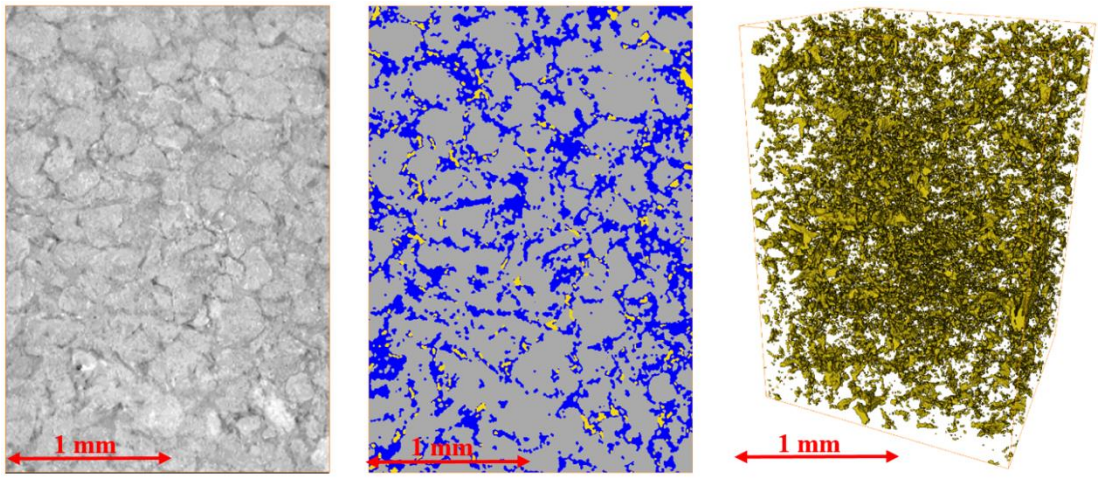

Figure 5-1 μCT image of Bentheimer sandstone at 10MPa pore pressure and 318K: (a) water-wet initial CO_2 saturation, raw image; (b) water-wet initial CO_2 saturation, segmented image; (c) CO_2 clusters in 3D for the water-wet initial CO_2 saturation, a volume of $3mm^3$ is shown; (d) water-wet residual CO_2 saturation, raw image; (e) water-wet residual CO_2 saturation, segmented image; (f) CO_2 clusters in 3D for the water-wet residual CO_2 saturation, a volume of $3mm^3$ is shown; (g) oil-wet initial CO_2 saturation, raw image; (h) oil-wet initial CO_2 saturation, segmented image; (i) CO_2 clusters in 3D for the oil-wet initial CO_2 saturation, a volume of $3mm^3$ is shown; (j) oil-wet residual CO_2 saturation, raw image; (k) oil-wet residual CO_2 saturation, segmented image; (l) CO_2 clusters in 3D for the oil-wet residual CO_2 saturation, a volume of $3mm^3$ is shown. CO_2 is black/dark grey, brine is grey and sandstone is light grey; in the segmented images CO_2 is yellow, brine is blue and rock is grey.

Table 5-1 Initial and residual CO_2 saturations in water-wet and oil-wet Bentheimer sandstone at 318K and 10MPa pore pressure.

Wettability state	**Contact angle [°][a]**	**Initial CO_2 saturation [%]**	**Residual CO_2 saturation [%]**
Water-wet	0	50.6	14.9
Oil-wet	130	49.2	8.7

[a]water contact angle in air at ambient conditions.

The fact that $S_{CO2,r}$ was significantly lower in the oil-wet plug (8.7%, i.e. ~40% less CO_2 was trapped in this scenario) is consistent with measurements in an oil-wet plastic bead pack [40], where a substantial reduction of residual scCO_2 was observed when compared to a water-wet analogue. Furthermore, CO_2 was frequently located in smaller pores and adjacent to rock surfaces, which indicates intermediate- or CO_2-wet behaviour. Such wetting behaviour was also observed in 2D micromodels (Chalbaud et al. 2010) and contact angle measurements (Dickson et al. 2006, Yang et al. 2007, 2008, Espinoza et al. 2010, Ameri et al. 2013).

The morphology of the CO_2 clusters in the water-wet plug was also different than in the oil-wet plug (Figure 5-2): while the CO_2 clusters in case of the initial CO_2 saturation state in the water-wet plug were bulky and essentially mimicked the pore space geometry, the corresponding residual CO_2 clusters thinned out considerably and had a somewhat fractal-like shape. Compare this with observations for an oil-water system in a completely water-wet sandstone ((Iglauer et al. 2010); which is known to be strongly water-wet, also at reservoir conditions (Xie et al. 1998)); here the initial and residual clusters mimicked the pore geometry. We conclude that the more fractal-like shape for the residual CO_2 clusters is caused by a shift towards weakly water-wet conditions (CO_2-brine-quartz is weakly water-wet at reservoir conditions, (e.g. (Al-Yaseri et al. 2015)). The initial CO_2 clusters in the oil-wet plug were already thinner, more “skeleton-like”, than their water-wet counterparts, and the associated residual CO_2 clusters were flat and sheet-like (Figure 5-2d). This is somewhat similar to what has been observed for an oil-water system in an intermediate-wet sandstone (Iglauer at al. 2013), where sheet-like residual oil clusters were observed. This indicates that the oil-wet plug showed intermediate-wet or CO_2-wet behaviour, consistent with 2D micromodel and contact angle measurements, see above.

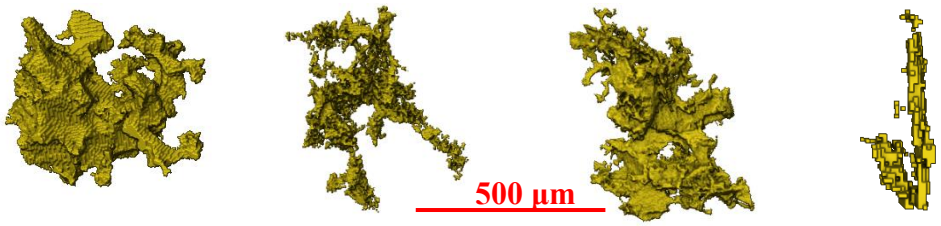

Figure 5-2 Morphologies and volumes of the largest initial and residual CO_2 clusters in Bentheimer sandstone at 318K and 10MPa pore pressure: (a) water-wet initial CO_2 saturation (volume = 27.7 x 106 µm3), (b) water-wet residual CO_2 saturation (volume = 5.39 x 106 µm3), (c) oil-wet initial CO_2 saturation (volume = 18.4 x 106 µm3), (d) oil-wet residual CO_2 saturation (volume = 3.03 x 106 µm3).

5.3.2 CO_2 cluster statistics

5.3.2.1 CO_2 cluster size distributions

CO_2 cluster size distributions were analysed for all scenarios (oil-wet, water-wet, residual, initial), they are plotted in Figure 5-3. As in other experiments of this type (Iglauer et al. 2011a, Iglauer et al. 2010, 2012, 2013, Andrew et al. 2013, 2014, Georgiadis et al. 2013, Geistlinger et al. 2014, 2015) power-law correlations were observed ($N \propto V^{-\tau}$, where N is the count number of clusters of size V, and τ is a fitting exponent), Table 5-2.

Table 5-2 Statistical parameters associated with the initial and residual CO_2 clusters for oil-wet and water-wet sandstone (Bentheimer, 318K, 10MPa pore pressure).

Plug state		**τ**	**p**
Water-wet	Initial CO_2	1	0.79
	Residual CO_2	1.6	0.85
Oil-wet	Initial CO_2	1	0.83
	Residual CO_2	1.9	0.85

This essentially means that, for each scenario, a large number of small clusters was observed, and only few large clusters. As expected the largest CO_2 clusters at initial CO_2 saturation state (Vmax = 28 x 10^{-6} μm^3 for the water-wet rock and Vmax = 18 x 10^{-6} μm^3 for the oil-wet rock) were significantly reduced by waterflooding (Vmax = 5 x 10^{-6} μm^3 for the water-wet rock and Vmax = 3 x 10^{-6} μm^3 for the oil-wet rock). Furthermore, the largest clusters always spanned almost the entire observed volume, which may imply that waterflooding (especially in oil-wet reservoirs) reduces the efficiency of structural trapping as the height of the CO_2 plume may not be affected while the CO_2 saturation in the bulk rock is reduced.

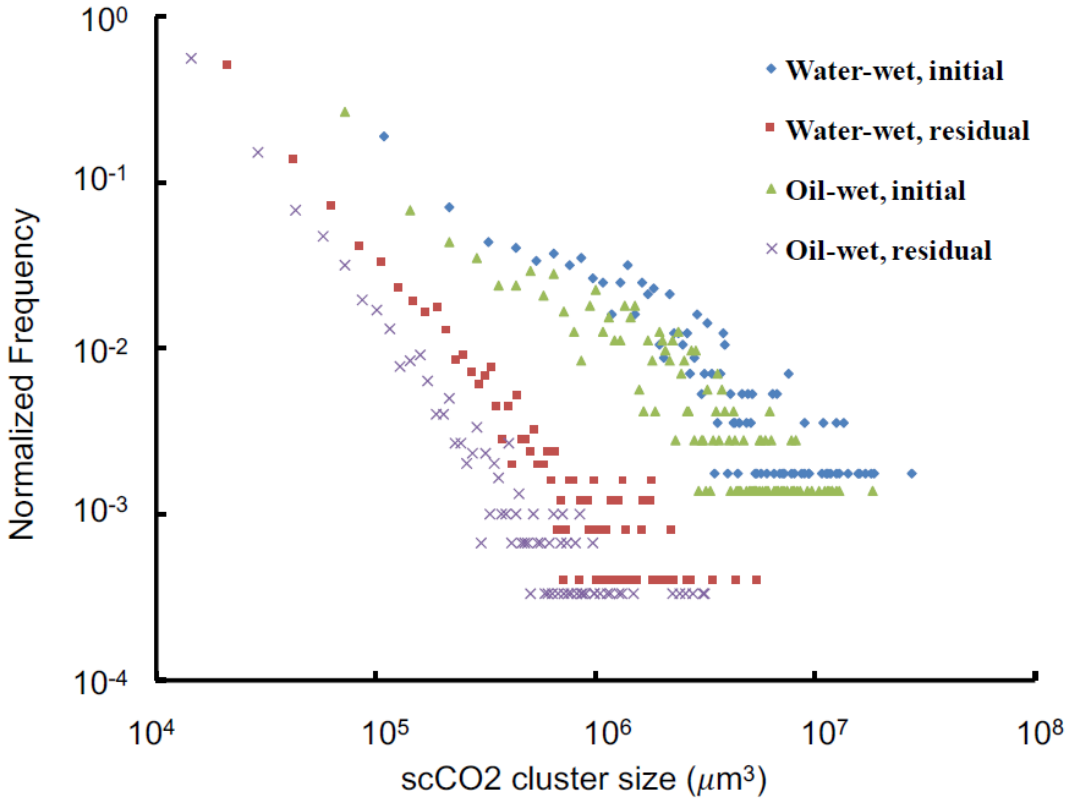

Figure 5-3 Initial and residual CO_2 droplet size distributions measured in water-wet and oil-wet Bentheimer sandstone at 318K and 10MPa pore pressure.

With respect to the scaling exponentτ; τ was significantly increased by waterflooding; this effect is caused by snap-off of many small CO_2 droplets (Roof 1970). Interestingly, τ increased more in the oil-wet plug, an effect which must be caused by the wettability (as all other parameters were constant, see methods section

above). Mechanistically, CO_2 can enter small pores in the oil-wet plug (due to the lower capillary entry pressure constraint (Oren et al. 1992); as oil-wet surfaces are more CO_2-wet, cp. review paper by (Iglauer et al. 2015a)), and these CO_2 volumes in the smaller pore channels may also snap-off, leading to additional small clusters (= larger τ).

5.3.2.2 CO_2-water interfacial areas

Subsequently, surface areas A for each CO_2 cluster were measured and plotted against their volumes V, see Figure 5-4. From the graph, again a power-law relation is evident ($A \sim V^{-p}$); and as with all other measurements of this kind (Karpyn et al. 2010, Pentland et al. 2012, Iglauer et al. 2013), p was always ~0.8.

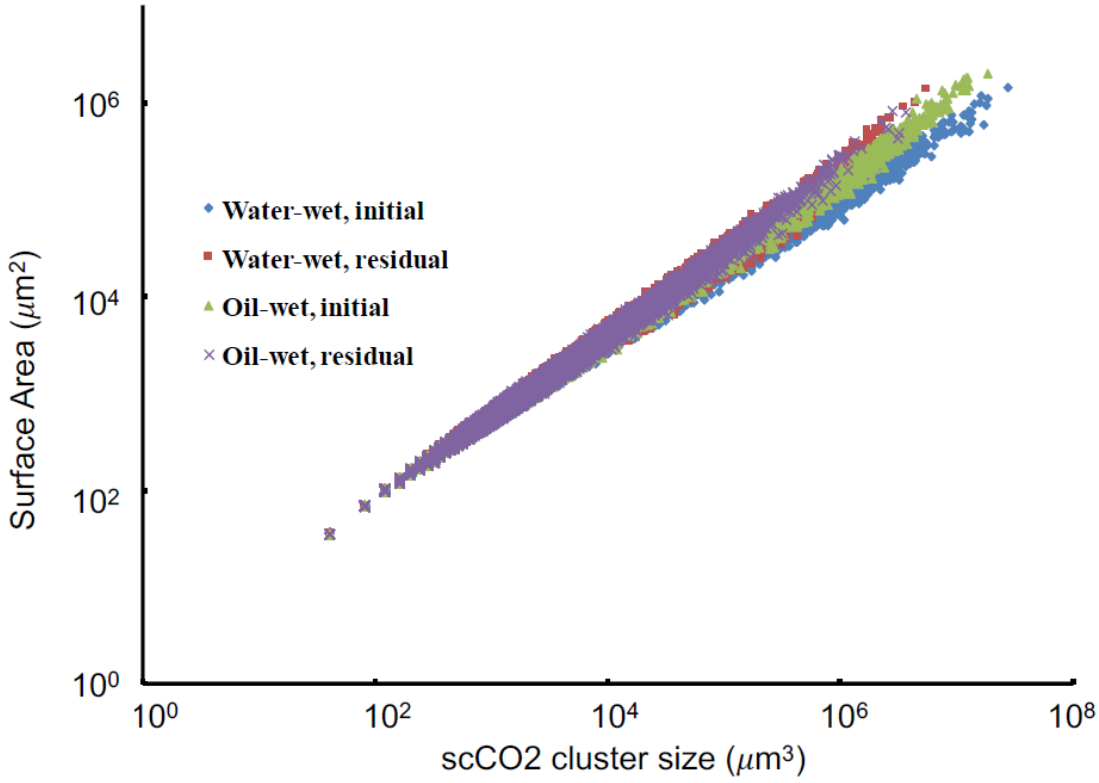

Figure 5-4 CO_2 droplet surface areas plotted against their volumes for various conditions, at 318K and 10MPa pore pressure.

In this context, it is interesting to note that the power-law exponents measured (τ and p) are significantly lower than predicted by percolation theory (which predicts τ = 2.189 and p ≈1; (Stauffer 1979, Lorenz 1998)). We conclude that simple percolation models will not deliver accurate and reliable predictions, as already evident in Georgiadis et al.'s work (Georgiadis et al. 2013).

5.3.2.3 Capillary pressure distributions

Finally, we measured curvatures (C) of each cluster, and calculated associated capillary pressures (p_c) for each CO_2 bubble and water droplet ($p_c = \gamma C$; Figure 5-5) assuming a water-CO_2 interfacial tension γ of 40mN/m (Li et al. 2012, Arif et al. 2016).

The capillary pressure distributions were roughly bell-tower shaped, and always showed a narrow and high peak around zero capillary pressure, consistent with data reported for oil-water systems (Armstrong et al. 2012). Nominally the capillary pressures ranged from ~-0.4 MPa to + 0.3MPa in case of CO_2, and from -0.6MPa to +0.6MPa in case of water (the water distributions were slightly stretched to the left, Figure 5-5b).

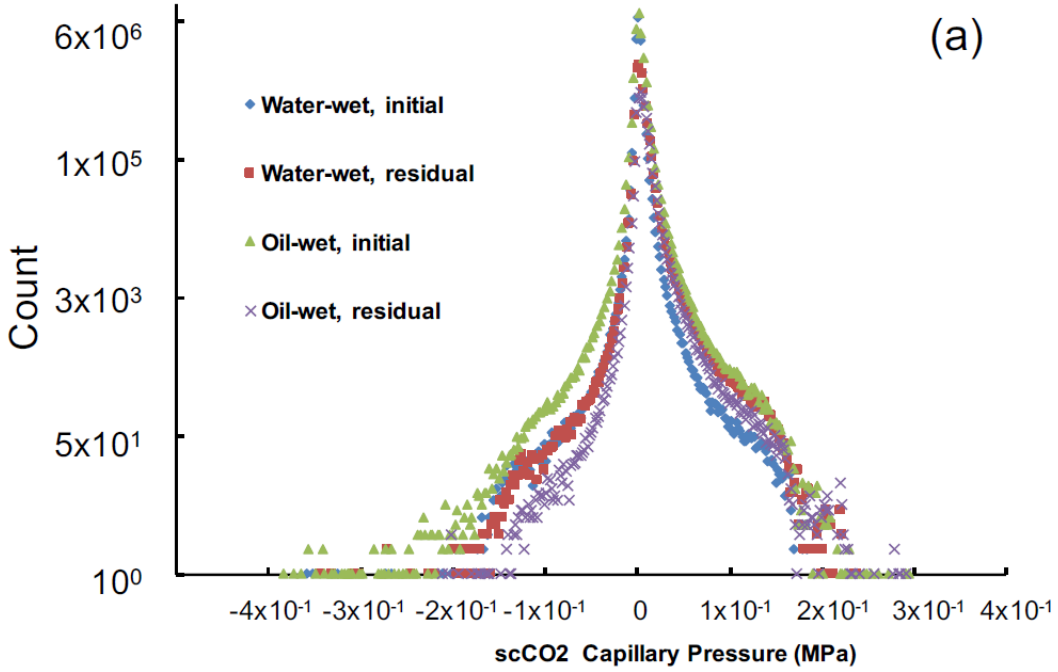

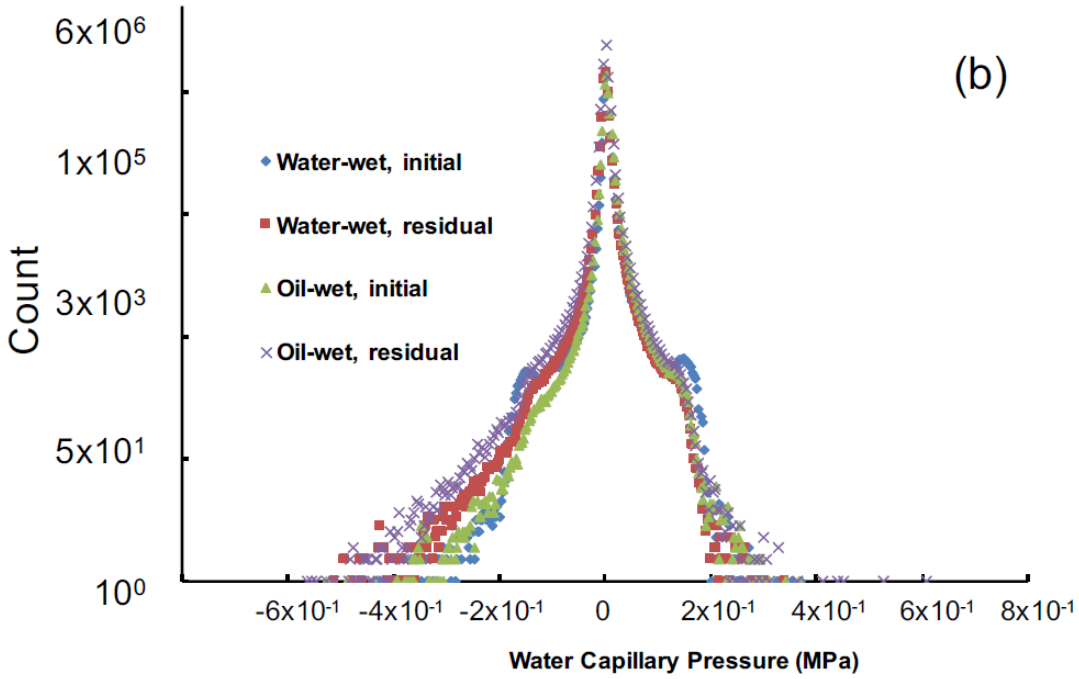

Figure 5-5 CO_2 (a) and water (b) droplet capillary pressures measured in water-wet and oil-wet Bentheimer sandstone at 318K and 10MPa pore pressure.

5.4 Conclusions and Implications

We demonstrated that residual CO_2 saturations ($S_{CO2,r}$) in oil-wet sandstone are dramatically lower than in equivalent water-wet sandstone ($S_{CO2,r}$ = 8.7% versus 14.9%). This is consistent with data reported for a plastic bead pack (Chaudhary et al. 2013), and indicates that oil-wet rock is intermediate-wet or CO_2-wet at reservoir conditions; a phenomenon which was also observed in independent contact angle measurements (Dickson et al. 2006, Yang et al. 2007, 2008, Espinoza et al. 2010, Ameri et al. 2013). This shift in CO_2-wettability also significantly influenced CO_2 cluster morphologies and residual cluster size distributions: flatter and more sheet-like clusters and more small CO_2 bubbles were observed in the oil-wet sample.

We conclude that, importantly, residual trapping is less efficient in oil reservoirs than in deep saline aquifers.

Chapter 6 Influence of wettability on residual gas trapping and enhanced oil recovery in three-phase flow: a pore-scale analysis using micro-computed tomography*

Abstract

We imaged an intermediate-wet sandstone in 3D at high resolution $(1\text{-}3.4\mu m)^3$ with an x-ray micro-computed tomograph at various saturation states. Initially the core was at connate water saturation and contained a large amount of oil (94%), which was produced by a waterflood (recovery factor R_f = 52% OOIP) or a direct gas flood (R_f = 66% OOIP). Subsequent water and/or gas flooding (WAG process) resulted in significant incremental oil recovery (R_f = 71% OOIP), while a substantial amount of gas could be stored (~50%) – significantly more than in an analogue water-wet plug. The oil and gas cluster size distributions were measured and followed power-law correlations $N \propto V^{-\tau}$ (where N is the frequency with which clusters of volume V are counted) with decay exponents τ between 0.7 and 1.7. Furthermore, the cluster volume V plotted against cluster surface area A also correlated with a power-law $A \propto V^p$, and p was always $\approx$ 0.75. The measured τ and p values are significantly smaller than predicted by percolation theory (which predicts $p \approx 1$ and $\tau = 2.189$); which raises increasing doubts about the applicability of simple percolation models. In addition, we measured curvatures and capillary pressures of the oil and gas bubbles in-situ, and analysed the detailed pore scale fluid configurations. The complex variations in fluid curvatures, capillary pressures and the fluid-fluid or fluid-fluid-fluid pore scale configurations (exact spatial locations also in relation to each other and the rock surface) are the origin of the well-known complexity of three-phase flow through rock.

*Reference: Iglauer et al. (2016) in Journal of Society of Petroleum Engineers, SPE 179727

6.1 Introduction

Three-phase flow through porous media is an important topic in the oil and gas industry as it occurs in gas-assisted enhanced oil recovery (EOR) processes, and carbon capture and storage (CCS), when CO_2 is injected into oil reservoirs for storage and incremental oil recovery (Blunt et al. 1993, IPCC 2005); furthermore, three-phase flow also occurs in soils contaminated by organic solvents (Sleep and McClure 2001). In this context, a significant amount of work has been completed to study such three-phase flow at the reservoir scale (e.g. compare Qi et al. 2009, Moortgat et al. 2011, Beygi et al. 2013) and the mesoscale (centimetre scale; e.g. Oak et al. 1990, Egermann et al. 2000, Caubit et al. 2004, Al-Mansoori et al. 2009, Amaechi et al. 2014). However, the detailed pore-scale (micrometre scale) fluid dynamics are poorly understood despite the fact that pore-scale flow determines the overall reservoir-scale (kilometre scale) flow, in addition to other larger scale mechanisms, e.g. reservoir heterogeneity or gravity segregation (Bear, 1988). It is therefore vital to deepen our understanding in this area to aid the development of better CCS and EOR schemes and to improve clean-up technologies for contaminated soils.

Such pore-scale three-phase flow has previously been studied theoretically (e.g. Van Dijke et al. 2011; Piri and Blunt 2004, 2005a,b; Al-Dhahli et al. 2012) or experimentally using 2D micromodels (e.g. Oren 1992, Oren and Pincewzski 1995, Dong et al. 1995, Keller et al. 1997); both approaches rely on strongly simplified pore morphologies. It is, however, well established that the pore space morphology has a significant impact on the related fluid dynamics (Dullien 1979); in addition, it is clear that 3D flow characteristics cannot be fully captured by 2D models (e.g. the percolation threshold is significantly lower in 3D, Stauffer 1979). Only recently, with the advent of micro-computed tomography (μCT), three-phase flow through porous media can be studied in 3D at the pore-scale of realistic geological porous media (compare the recent reviews by Blunt et al. (2013), Wildenschild and Sheppard (2013) and Cnudde and Boone (2013)), which is most relevant for industrial applications.

In this work, we extend our previous investigation of three-phase pore-scale flow in water-wet sandstone (Iglauer et al. 2013) to include intermediate-wettability. This wettability effect is of particular importance in sandstone and carbonate oil reservoirs as these are frequently intermediate-wet or even oil-wet (Cuiec 1991). Specifically, wettability has a strong impact on petrophysical parameters (Anderson 1987) including residual saturations (Morrow 1990, Tanino and Blunt 2013), relative permeabilities (McCaffery and Bennion 1974), capillary pressures (Morrow 1976, Anderson 1987), fluid topologies (Iglauer et al. 2012), and CO_2 storage capacities (Iglauer et al. 2015). We demonstrate that there is a large variation in fluid configurations, fluid-fluid curvatures and capillary pressures, which leads to the well-known complexity of three-phase flow (e.g. cp, Oren et al. 1992).

6.2 Experimental Methodology

We selected a clean homogenous water-wet outcrop sandstone (Clashach, from Elgin in Scotland), and from a larger block we drilled a small cylindrical plug (5mm diameter, 9mm length). The sandstone had a porosity of 10%, Table 6-2, and a brine permeability of 9.6 x 10^{-14} m^2 (Iglauer et al. 2012); its chemical composition was measured via XRD: 96wt% quartz, 2wt% K-feldspar, 1wt% calcite, 1wt% ankerite and illite traces. The plug was mounted in a flow cell, and its wettability was altered with North Sea crude oil using a procedure described previously (Iglauer et al. 2012) to intermediate-wet (Amott-Harvey index = -0.1, Amott oil index = -0.1, and Amott water index = 0; which is slightly oil-wet). The aged plug (now mounted in a flow cell) was then imaged with a micro-computed tomograph (Xradia Versa-XRM-500) at a resolution of $(3.4\ \mu m)^3$. Note that an inner cylindrical volume of the plug was imaged with a diameter of 3.4mm to achieve good resolution (i.e. not the whole 5mm-diameter plug). The same resolution was used throughout the whole work flow for each μCT scan except for a few high-resolution scans $(\sim 1\ \mu m)^3$ with which we investigated the detailed fluid configurations in the pore space. The aged plug was vacuumed for 60 min (to ensure no air was trapped in the pore space) and deaired brine was injected for 5 min under vacuum followed by injection of ~1000 pore volumes (PV) of oil at a capillary number (= $\mu q/\gamma$, where q is the Darcy flow rate, μ is the viscosity of the injected phase and γ is the interfacial tension) of 3.54 x 10^{-4} to

achieve connate water saturation S_{wc}. The brine was a 10wt% solution of potassium iodide (KI) in deionized water, the KI is required to achieve sufficient x-ray contrast between the fluids. The oil used was 1-bromododecane (purity ≥ 99mol%, from Sigma Aldrich), again to enable CT contrast. The plug then essentially represented an oil reservoir ("connate water saturation", with no gas present), and we acquired a μCT image of the plug in this state. Following our previous study line (Iglauer et al. 2013), we then distinguished two cases to study residual gas and oil topologies and distributions: the "waterflood" scheme resembles the process typically used in the petroleum industry, where oil reservoirs are waterflooded to enhance oil recovery (Lake 1990), and subsequently gas flooded for further improving oil recovery (e.g. Blunt et al. 1993) and/or gas storage (e.g. CO_2 storage, cp. e.g. Iglauer et al. 2011a, Pentland et al. 2012, Iglauer et al. 2013), i.e. a WAG flood. The second flow scheme "gasflood" uses an alternative process sequence, which has been shown to be significantly more efficient in terms of oil recovery and gas storage in a water-wet sandstone (Iglauer et al. 2013).

6.2.1 Waterflood

25 PV of brine were injected at a capillary number of 7.4×10^{-7} into the plug at connate water saturation to establish residual oil saturation (S_{or}); subsequently, approximately 50 PV of N_2 gas were injected at S_{or} at a pressure drop of 20000 Pa over a 9mm plug length (0.05 mL/min flow rate for 6 minutes), which approximately corresponded to a capillary number of 0.01, so that an initial gas saturation state ($S_{gi,bg}$) was established. This was followed by another brine flood (using the same capillary number as above, $\sim 7.4 \times 10^{-7}$) to measure residual oil and gas saturations and configurations ($S_{gr,bgb}$ state).

6.2.2 Gasflood

N_2 gas was directly injected into the plug at connate water saturation (S_{wc}) using the same conditions as above to establish the initial gas saturation, $S_{gi,g}$. This was followed by brine injection (same conditions as above) to establish residual gas saturation, $S_{gr,gb}$.

All plug states were μCT imaged; and all experiments were conducted at ambient laboratory conditions (295K and 0.1MPa). Note that the plugs were always positioned horizontally during the floods. Bond numbers were estimated to be $\approx 10^{-4}$ for the liquid-gas and the oil-brine system; we therefore do not expect the residual clusters/residual saturations to be influenced by buoyancy forces (Morrow et al. 1988).

We note that the oil used was non-spreading with a spreading coefficient S (= γ_{gw} - γ_{ow} - γ_{go}, where γ_{gw} is the gas-brine interfacial tension, γ_{ow} is the oil-brine interfacial tension and γ_{go} is the gas-oil interfacial tension, cp. Table 6-1) of -11.05 mN/m; and it is clear that the algebraic sign of S has a profound influence on the fluid dynamics and statics (Blunt et al. 1995, Oren and Pinczewski 1995).

Table 6-1 Interfacial tensions of the fluids used.

Fluid-fluid system	**Interfacial tension [mN/m]**
water/1-bromododecane*	γ_{ow} = 52.09
water/nitrogen**	γ_{gw} = 72
1-bromododecane/nitrogen***	γ_{go} = 30.96

*measured at 295K (Ortiz-Arango and Kantzas 2009).

**measured at 293.15K and 0.101 MPa (Lide 2007).

***surface tension of 1-bromododecane.

6.3 Results and Discussion

Figure 6-1 shows a set of 2D slices through the rock and pore space filled with the various fluids at different saturation stages: connate water saturation (S_{wc}), residual oil saturation (S_{or}), the two initial gas saturations ($S_{gi,g}$ and $S_{gi,bg}$), and the two residual gas saturations ($S_{gr,gb}$ and $S_{gr,bgb}$). The slices display a greyscale map, where each greyscale corresponds to a specific relative radiodensity of a volume element, and this greyscale can be assigned to a certain material (i.e. rock, oil, gas or water),

Golab et al. (2013). The gas has the lowest relative radiodensity and it is thus black, while oil (because it is brominated) has the highest relative radiodensity: it is white. The brine and the solid grains have a relative radiodensity in between, they are both grey; the brine being slightly darker than the grains. On the left side greyscale image slices were shown, which were filtered with a non-local means filter, Buades et al. (2005), and segmented with a watershed algorithm (Schlüter et al. 2014; right side). The detailed pore-scale fluid configurations can be observed at this resolution (~1-3 μm), this is discussed further below; moreover, the 3D topology of the oil and gas phases can be visualized (Figure 6-2) and analysed.

Porosities, and oil, water and gas saturations were subsequently measured on the segmented μCT images (Table 6-2). The oil recovery factor R_f is also shown in Table 6-2, it has been calculated based on the initial oil in place ($R_f = (S_{o,wc}-S_o)/S_{o,wc}$ with S_o = actual oil saturation, $S_{o,wc}$ = oil saturation at S_{wc}). Initially the oil saturation at S_{wc} was quite high, because a high capillary pressure was applied; consequently, a relatively high residual oil saturation was obtained after waterflooding as a high initial oil saturation leads to a high residual saturation (e.g. compare Pentland et al. 2010, 2011, Iglauer et al. 2011b, Gittins et al. 2010).

Gas injection directly into the plug at connate water saturation or into the plug at residual oil saturation both produced significant amounts of incremental oil, consistent with literature results (e.g. Dumoré and Schols 1974, Egermann et al. 2000, Al-Mansoori et al. 2009, Amaechi et al. 2014). The final waterflood again produced a significant amount of additional oil. In the intermediate-wet plug, oil recovery efficiencies for both flood sequences were similar ("waterflood": R_f = 70.8% OOIP; "gasflood": R_f = 71.1% OOIP). Compare this with recovery factors in an analogue water-wet plug ("waterflood": R_f = 68.9% OOIP; "gasflood": R_f = 77.1% OOIP), here the gas flood was significantly more efficient, cp. Table 6-2.

We furthermore observed that the residual gas saturation was similar in both flooding processes in the intermediate-wet plug, while in the analogue water-wet plug, direct gas flooding led to higher residual gas saturations, Table 6-2. In the context of CO_2 storage, it is of key relevance to estimate how much CO_2 can be stored: for residual trapping, this can be accomplished with the capillary trapping capacity C_{trap}, which

quantifies how much gas can be stored in a unit rock bulk volume (Iglauer et al. 2011b), C_{trap} is defined as the product of rock porosity and residual gas saturation (= ϕS_{gr}). Interestingly C_{trap} is much higher for the intermediate-wet plug; this is contrary to what has been observed in two-phase systems, where residual gas saturation is lower in intermediate-wet systems (cp. Iglauer et al. 2011a with Chaudhary et al. 2013).

Table 6-2 Porosites, oil S_o, water S_w, and gas saturations S_g measured on the μCT images (percentages shown). *water-wet condition (taken from Iglauer et al. 2013). R_f is the oil recovery factor, C_{trap} is the capillary trapping capacity.

Saturation state	**Porosity**	**S_o**	**S_g**	**S_w**	**C_{trap}**	**R_f [OOIP]**
S_{wc}	9.3	94.3	0	5.7	---	0
S_{or}	10.4	45.3	0	27.8	---	52.0
$S_{gi,g}$	11.6	32.2	48.8	19.0	4.88	65.8
$S_{gi,bg}$	9.8	35.0	56.8	8.2	5.68	62.9
$S_{gr,gb}$	10.1	27.2	54.6	18.2	5.46	71.2
$S_{gr,bgb}$	10.5	27.5	50.0	22.5	5.00	70.8
$S_{gr,gb}^*$	11.6	21.6	20.6	57.8	2.06	77.1
$S_{gr,bgb}^*$	10.7	29.3	5.3	65.4	0.53	68.9

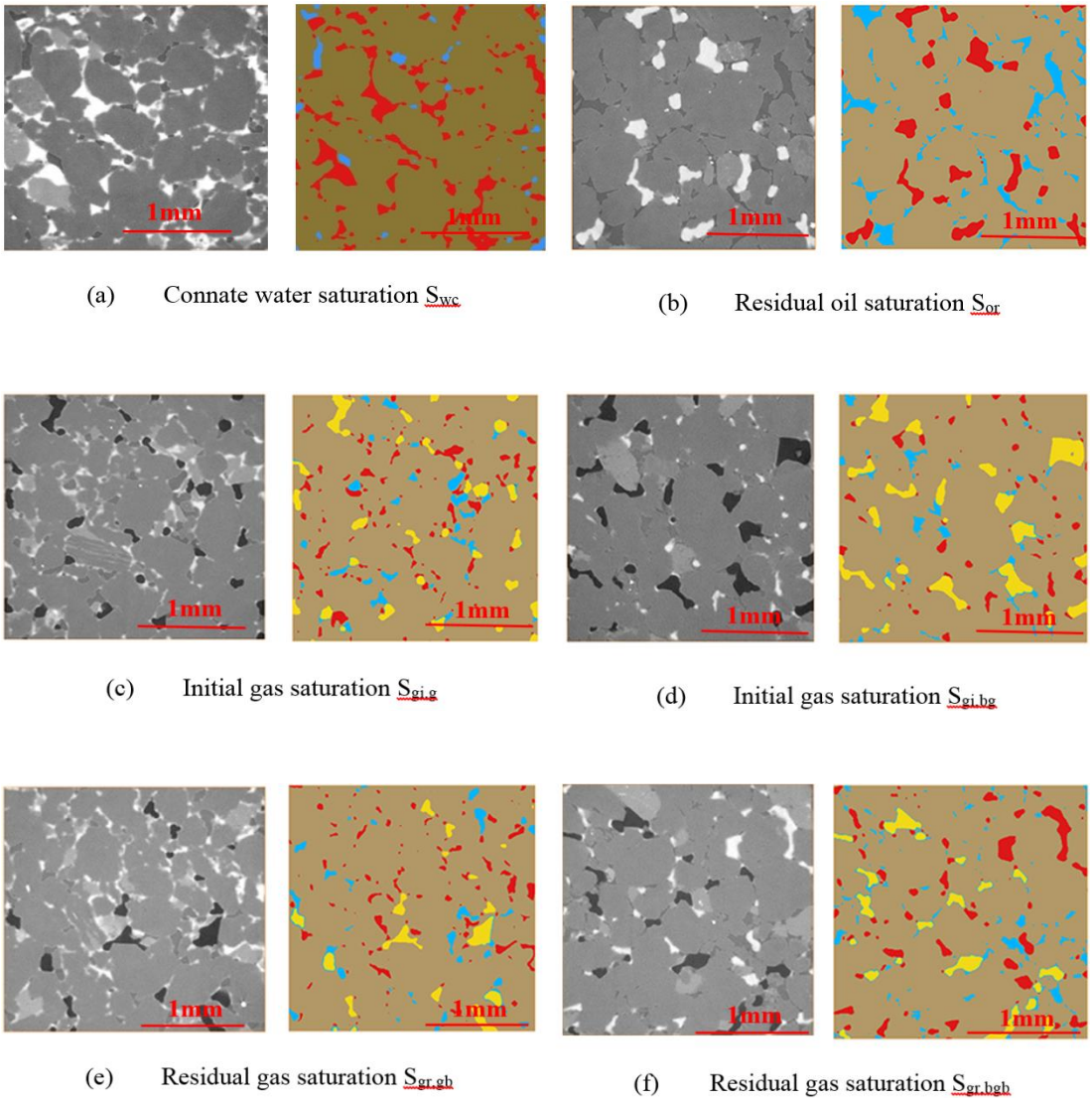

Figure 6-1 2D slices through the rock and various fluids at different saturation states. (a) connate water saturation S_{wc}; (b) residual oil saturation S_{or}; (c) initial gas saturation $S_{gi,g}$; (d) initial gas saturation $S_{gi,bg}$; (e) residual gas saturation $S_{gr,gb}$; (f) residual gas saturation $S_{gr,bgb}$. Left: greyscale images; right: segmented images. In the raw images, oil is white, gas is black, brine dark grey, and sandstone is light grey. Oil is red, brine blue, gas yellow and rock is brown in the segmented images.

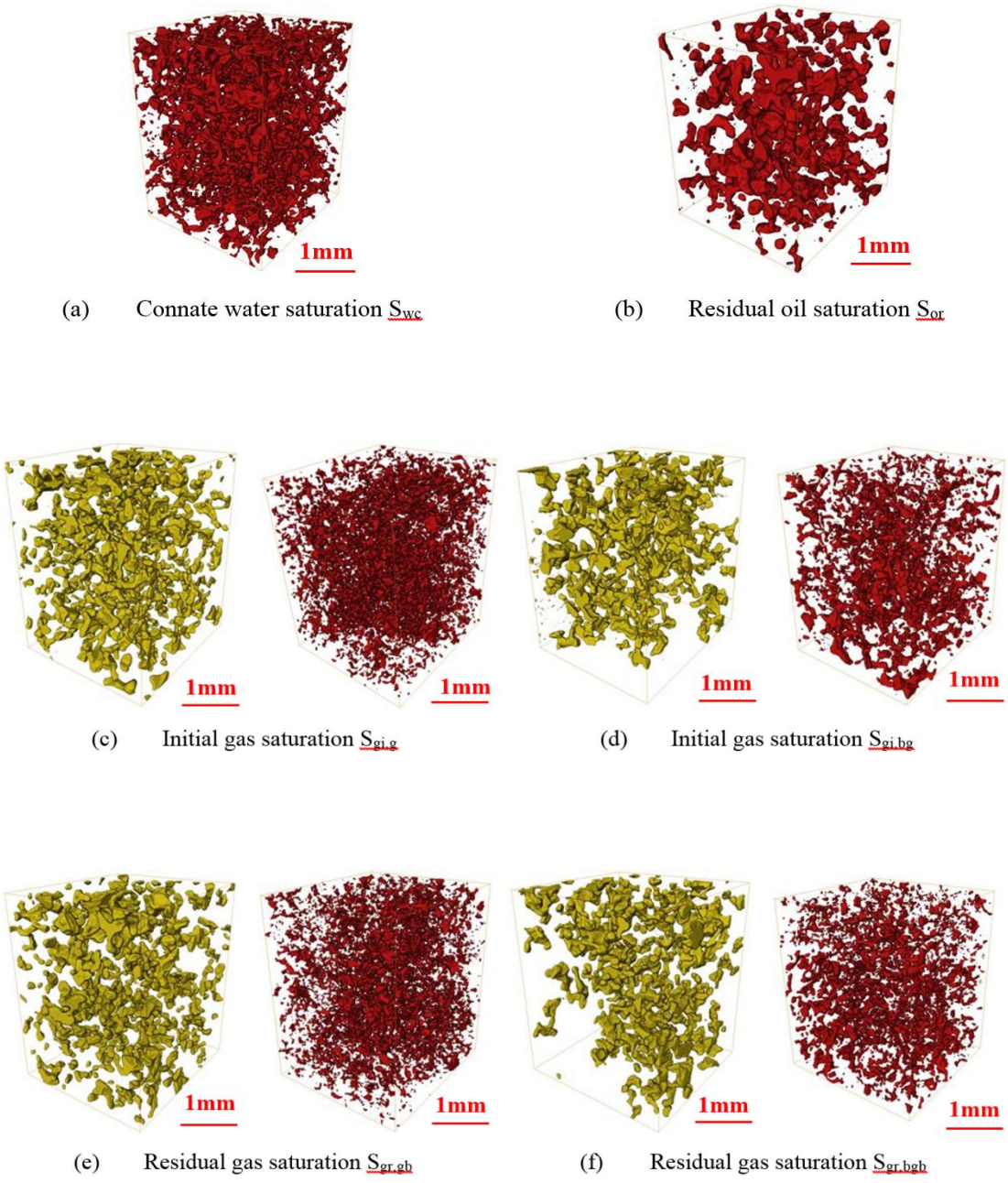

Figure 6-2 3D topology of the gas (yellow), oil (red) phases at various saturation states. All volumes shown are ~12mm^3.

Figure 6-2 clearly demonstrates that the oil saturation decreases substantially during the initial waterflood (from the S_{wc} to the S_{or}), and S_o is further reduced in the tertiary production steps. The oil is uniformly distributed but split into many separate clusters; see below for a more detailed analysis. Moreover, it is apparent from the images that the gas saturation S_g did not change significantly, and the gas was also distributed in many individual clusters.

6.3.1 Qualitative analysis Pore-scale fluid configurations

The wettability state of the sandstone influenced oil distribution and fluid topology in the pores as expected and measured previously in two-phase oil-water systems (Kumar et al. 2009, 2012, Iglauer et al. 2012).

6.3.1.1 Waterflood

The oil saturation was high at S_{wc}, because of the high applied capillary pressure during primary drainage. However, many small and some large water volume elements were still present in the pore network of the rock; the curvature of these ganglia varied quasi randomly from convex to concave throughout the plug, apparently depending on the wettability state of the directly adjacent pore surfaces; this is discussed further below. Moreover, oil and water were both present in the smallest pores, which indicates intermediate wettability as expected and consistent with the independent Amott index measurement (see above).

The waterflood was very efficient and about half of the oil was produced (S_o decreased from 94.3% at S_{wc} to 45.3% at S_{or}, Table 6-2); in addition, a significant amount of oil was displaced from the smaller pores, which again indicated intermediate-wet conditions. At S_{or}, oil was located mainly in medium-sized and larger pores, although some oil still resided in smaller pores. Compare this with a water-wet plug: here all residual oil is located in large pores as disconnected bubbles (Iglauer et al. 2010). We infer that oil was partially mobilized into oil banks during production, consistent with mesoscopic observations (e.g. Egermann et al. 2000, Gittins et al. 2010).

A similar situation was observed at the $S_{gr,bgb}$ state where oil had been displaced from small pores to a large extend (but not fully), and was trapped in medium-sized pores, probably by snap-off events (Roof 1970). We note that oil layer flow (cp. for instance Table 6-3 below) may contribute to further oil recovery, but at a slow rate, because of the low relative permeability of these layers (caused by their thin cross-sectional area) (e.g. Oren et al. 1992, and Blunt et al. 1995). In this context one clear limitation of the μCT technique needs to be mentioned: thin layers (thickness of a

few to a few hundred nanometres) cannot be observed, although they play a significant role in terms of wettability effects and associated fluid dynamics (e.g. Hirasaki 1991, Blunt et al. 1995, Tokunaga and Wan 2013).

In summary, the oil phase was often touching the rock surface (i.e. oil-wet behaviour), but in many cases oil drops were also located in pore centres, an indication of water-wet behaviour – this adds up to an intermediate-wet state. In contrast, oil is always sandwiched between the gas and water phases in water-wet rock, cp. Figure 6-3 (Iglauer et al. 2013).

6.3.1.2 Gas Injection

More oil accumulated in medium-sized and larger pores in the $S_{gi,bg}$ state than in the $S_{gi,g}$ state (due to the additional waterflooding step), while more oil was present in small pores in the $S_{gi,g}$ state. These configurations somewhat reflect the oil distributions prior to gas flooding. However, in both sequences - more ($S_{gr,gb}$) or much more ($S_{gr,gb}$ state) - oil was present in smaller pores in the intermediate-wet plug than in the analogue water-wet plug, Figure 6-3, where oil was mainly localized in larger pores.

In both flood sequences, however, gas entered the largest pores, and was typically located in their centres (in both, the intermediate-wet and the water-wet plugs; this is expected as gas is the most non-wetting phase in both cases, Oren and Pinzcewski (1995) Consequently, the gas bubbles were frequently larger than the oil clusters, cp. Figures 6-2. In addition, the gas clusters adopted a range of morphologies: from quasi-spherical to ganglia-like; their specific morphologies were determined by pore connectivity, pore geometry, rock wettability and capillary pressure p_c (Youssef et al. 2010, Iglauer et al. 2012, Berg et al. 2013).

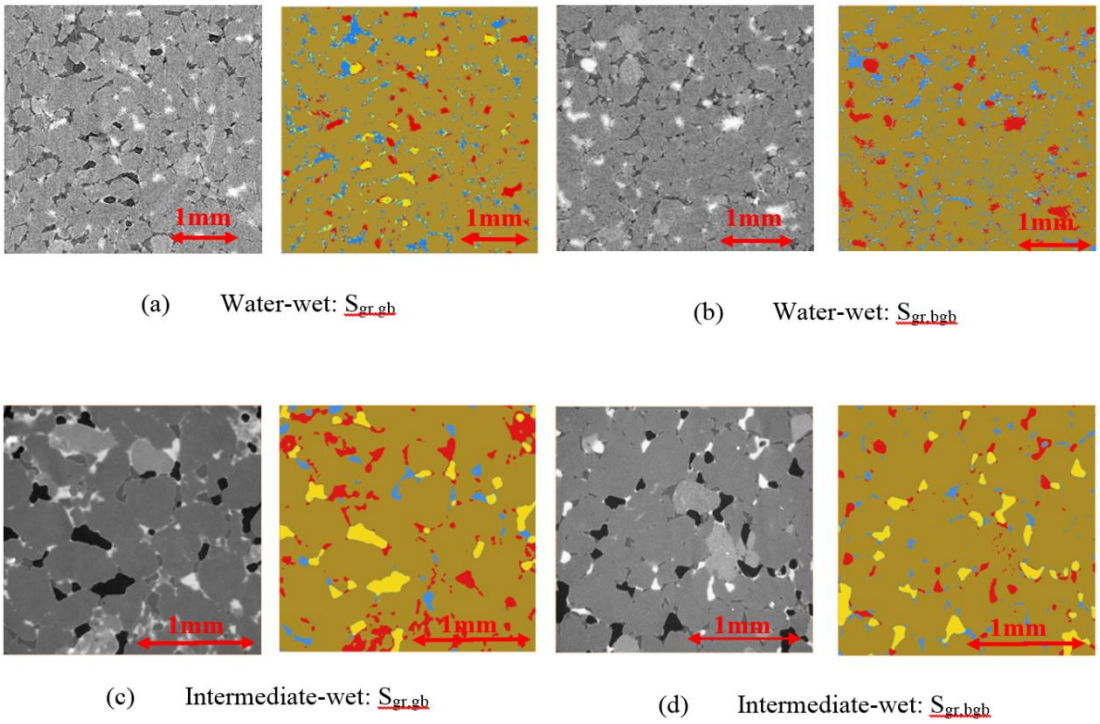

Figure 6-3 Comparison of oil and gas phase configurations at the two residual gas saturation states ($S_{gr,gb}$ and $S_{gr,bgb}$) in water-wet (top) and intermediate-wet (bottom) Clashach sandstone. Note that the plugs were drilled from the same block. The water-wet plug images were acquired with monochromatic light at a nominal resolution of $(9\mu m)^3$ (Iglauer et al. 2013); the intermediate-wet plug images are those discussed in this script, their resolution is $(3.4\mu m)^3$.

Figure 6-4 shows slices through high resolution µCT images for some selected areas for both residual gas saturation states; the pore-scale configuration of the different fluid phases can be quite clearly seen. Most configurations observed were previously identified theoretically (Zhou and Blunt 1998, Piri and Blunt 2004), and we can provide experimental verification for these here; in addition, µCT imaging enables a detailed analysis and new subcategories were found (Table 6-3). Furthermore, analysis of the interplay between the pore morphology and surface-free energies (oil-wet or water-wet) and how that affects the exact fluid configurations can be explored. The images demonstrate that these settings are more complicated than current models, which are based on strongly simplified pore geometries and wettability alteration concepts (typically it is assumed that the surface which contacted crude oil changed towards oil-wet, cp. e.g. Piri and Blunt 2004), however,

surfactant molecules can diffuse through the water and adsorb onto the rock surface, which would then also alter the wettability of the surface without direct contact (Buckley et al. 1998). Interestingly the fluid-fluid curvature can be observed (cp. Table 6-3); such curvatures are rather important as they determine pore-scale fluid dynamics (e.g. Jettestuen et al. 2013). These effects are analysed in more detail in the statistics section below.

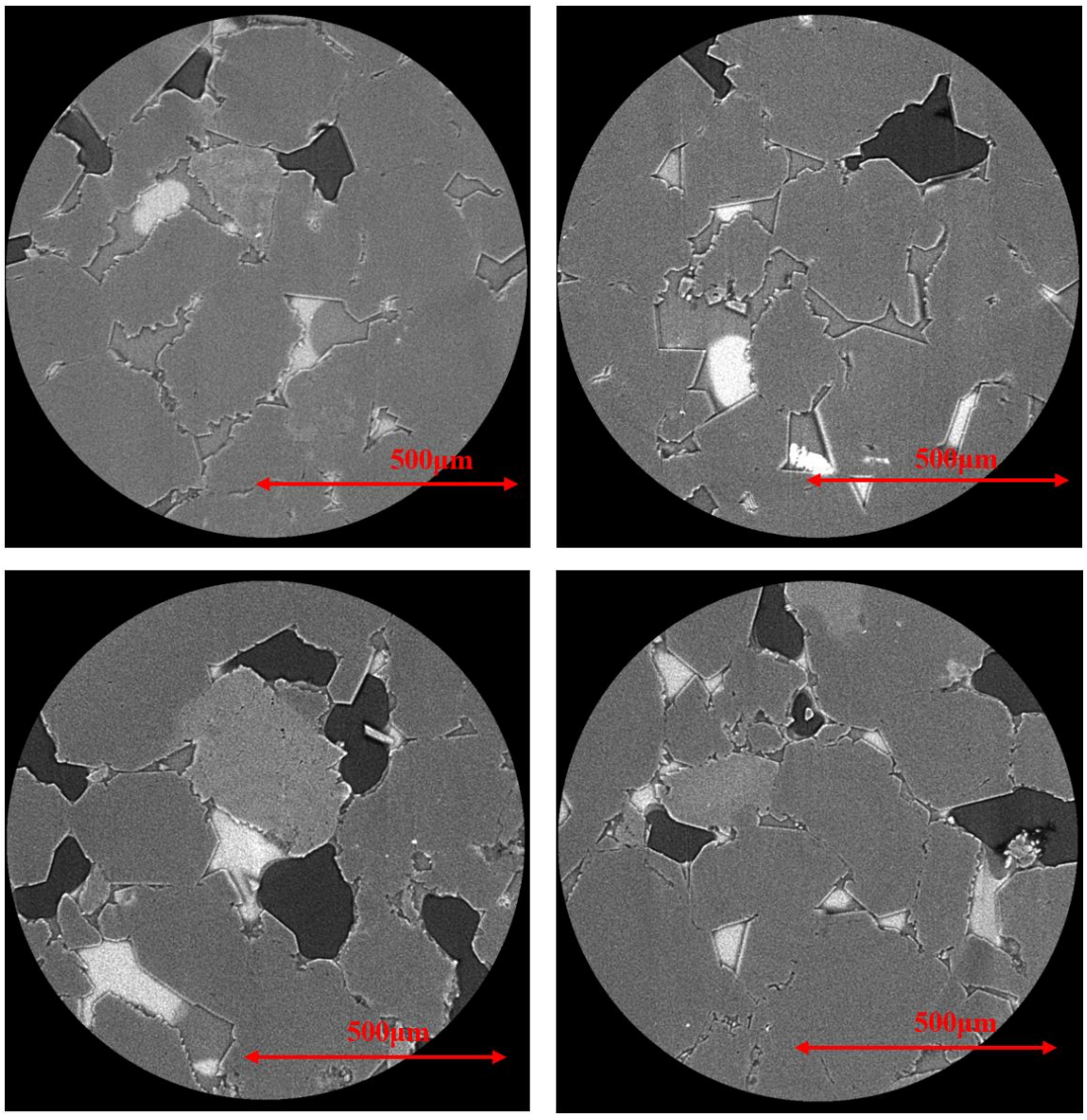

Figure 6-4 Selected high resolution 2D slices through the plug at residual gas saturation; top: $S_{gr,gb}$, $(1.00\mu m)^3$ resolution; bottom: $S_{gr,bgb}$, $(1.07\mu m)^3$ resolution. Gas is black, oil white, brine dark grey and rock light grey. For classification consult Table 6-3.

Table 6-3 Pore-corner fluid configurations identified in the μCT images of the intermediate-wet plug.

Pore configuration			Pore Image at $(1\mu m)^3$ Resolution
Symbol	**State**	**Category**	
	Water (1 phase)	W	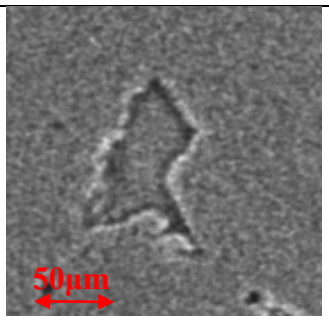
	Oil (1 phase)	O	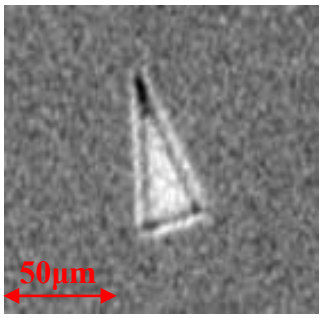
	Oil in water (2 phase)	WO	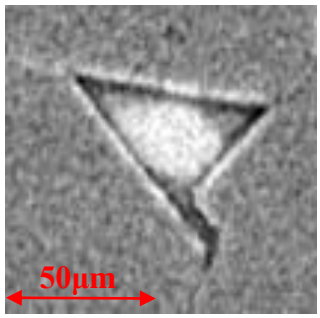
	Gas in water (2 phase)	WG	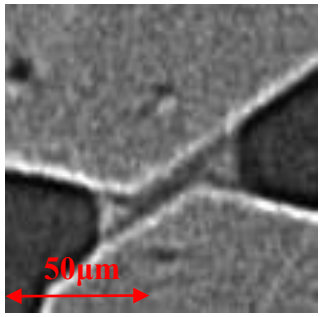

	Gas in oil (2 phase)	OG	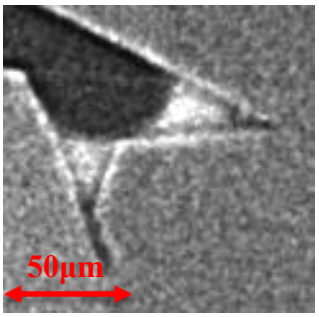
	Gas in oil in water (2 phase)	WOG	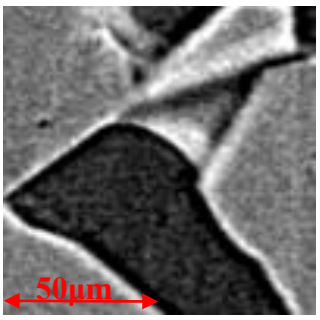
	Gas in water in oil (3 phase)	OWG	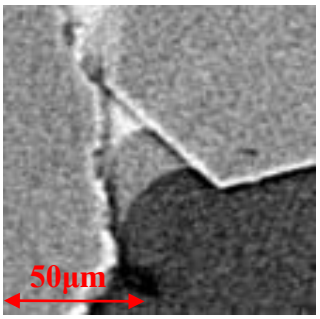
	Water and oil wet	f-WO	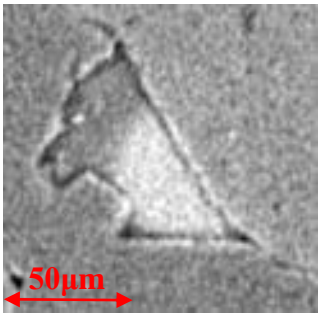
	Oil and water: oil curvature = convex	f-WOcx	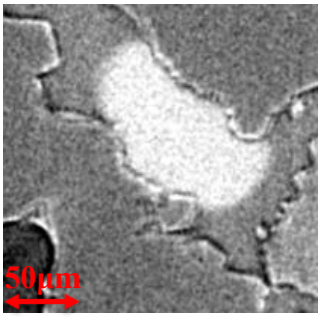

	Oil and water: oil curvature = concave	f-WOcv	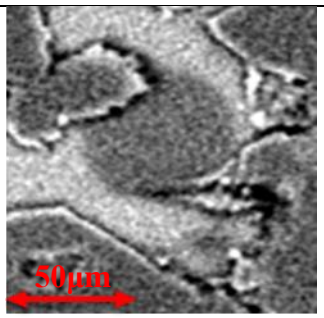
	Oil droplet attached to rock surface in water	f-WOd	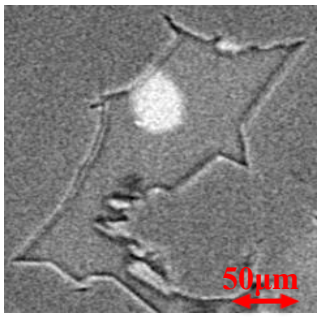
	Water and oil wet with gas in center	f-GWO	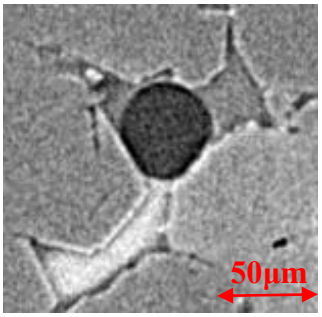

The fluid configurations listed in Table 6-3 include pores filled with a single fluid, two fluids or three fluids, and categories for several fractionally-wetted pores. The precise fluid configuration in these fractionally-wetted pores is a consequence of the distribution of oil-wet rock surfaces, for instance gas can be surrounded by oil on one side and brine on another; oil can be located in a pore corner while the remaining pore space is filled with water; or a water drop can stretch from one pore surface to the opposite side (between two isolated water-wet surfaces), surrounded by a concave oil volume, which fills most of the remaining pore space. Furthermore, small water droplets can reside in water-wet locations within a pore.

An interesting phenomenon is that some pores contain convex oil drops which stretch from one oil-wet rock surface to the opposite (oil-wet) side, while others show concave oil drops. This is a clear indication of variation in oil contact angles within the same plug, which again reflects the intermediate-wet character of the

sandstone. Individual oil drops attached to one pore wall side only, and water layers sandwiched between gas and oil in pore corners were also observed: both an indication of partially oil-wet rock walls.

In summary, the large variability in terms of pore-scale fluid configurations adds to the high complexity of three-phase flow (and static distributions) in intermediate-wet rock, and the associated difficulty in predicting such flow with confidence, not only at hectometre reservoir-scale, but already at the micrometre pore-scale. In the next section, these physical phenomena were quantitatively analysed.

6.3.2 Quantitative analysis - Cluster statistics

6.3.2.1 Cluster interfacial areas

The relationships between oil and gas cluster volumes V and their surface areas A are plotted in Figures 6-5 and 6-6. The relations can be very well described using a power-law correlation $V \propto A^p$, where p is around ~0.75 for all saturation states, Table 6-4. This is essentially the same value as measured for oil and gas clusters in a water-wet sandstone (Iglauer et al. 2013), and in two-phase flow for residual oil or supercritical CO_2 clusters (Iglauer et all. 2010, 2011, Pentland et al, 2012). We thus hypothesize that $p \sim 0.75$ may be a universal constant, at least for relatively homogeneous sandstones and water-wet to intermediate-wet conditions.

We also note that p is significantly lower than the value predicted by percolation theory (which predicts $p \approx 1$, Stauffer 1979), and this has important implications for mass transfer processes as the real oil-water or gas-water interfacial area is significantly smaller than expected, and associated kinetics (e.g. CO_2 dissolution trapping as a method to dispose CO_2, Hirai et al. 1997, Suekane et al. 2006, Iglauer 2011), are much slower than anticipated.

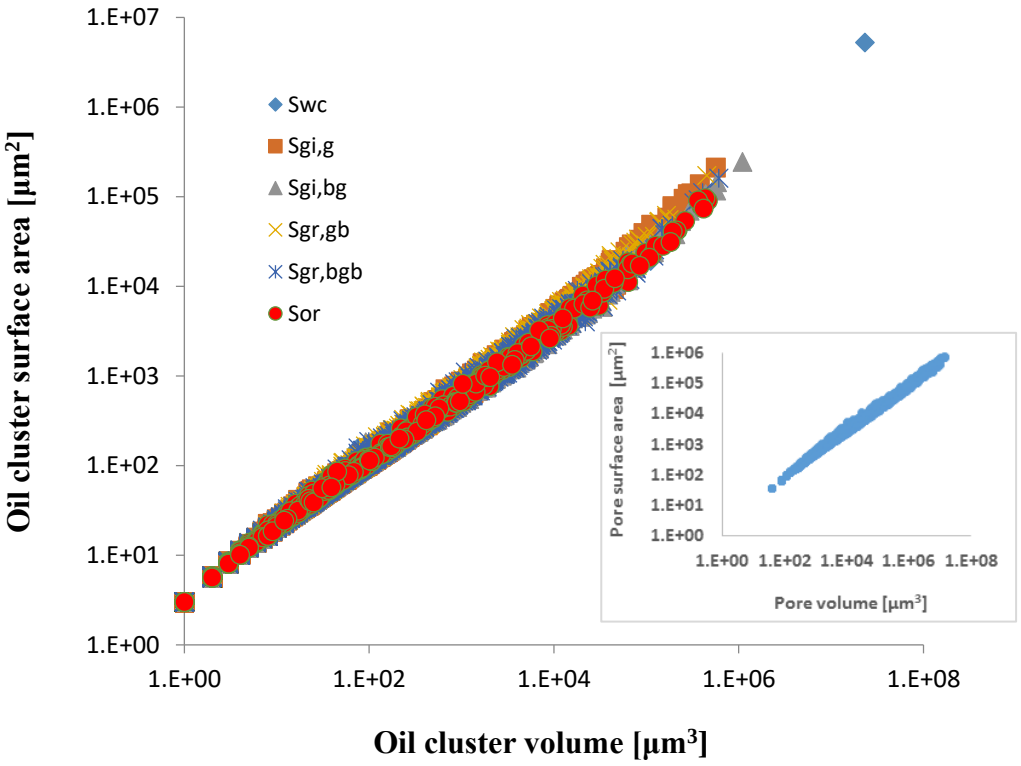

Figure 6-5 Surface area versus cluster volume for each oil cluster and production step.

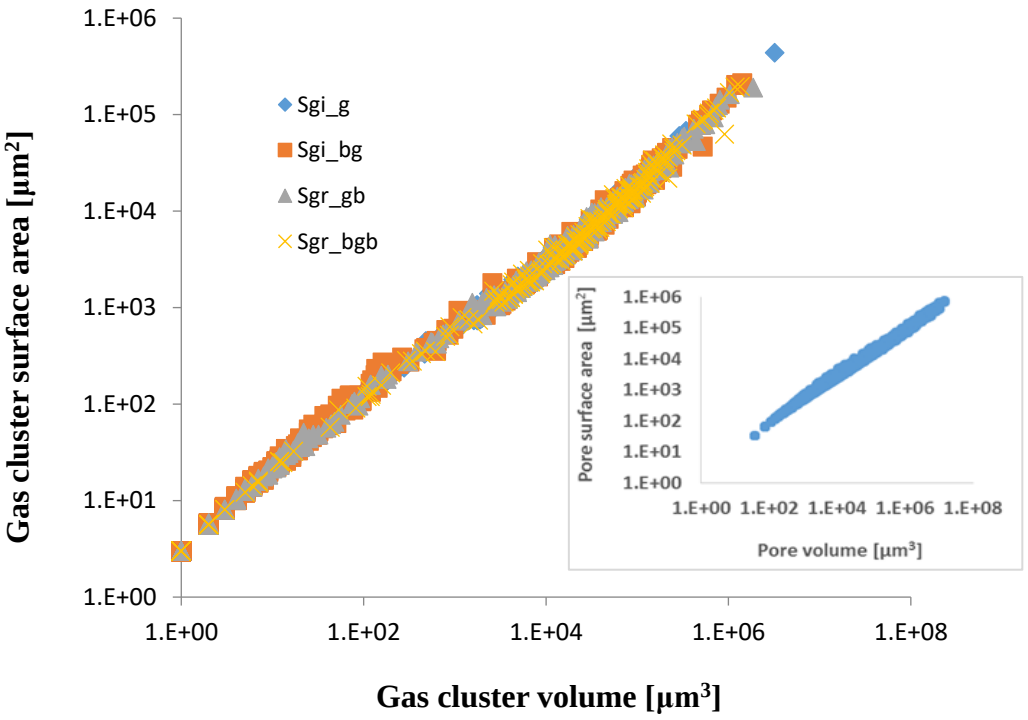

Figure 6-6 Surface area versus cluster volume for each gas cluster and production step.

Table 6-4 Oil and gas cluster statistics: cluster size distribution exponents τ and interfacial area exponents p for intermediate-wet and water-wet sandstone. *Reassessed value: data taken from Iglauer et al. (2014). **Reassessed value: data taken from Iglauer et al. (2013).***Taken from Iglauer et al. (2013).#4Taken from Pentland et al. (2012).

Saturation state	Intermediate wet		Water-wet		Intermediate wet		Water-wet	
	τ, oil	τ, gas	τ, oil	τ, gas	p, oil	p, gas	p, oil	p, gas
S_{wc}	0.70	---			0.752	---		
S_{or}	0.80	---	0.68*		0.754	---	0.749#4	
$S_{gi,bog}$	0.72	0.75			0.765	0.740		
$S_{gi,bobg}$	1.05	0.95			0.754	0.744		
$S_{gr,bogb}$	0.67	1.00	0.9**	0.7**	0.766	0.741	0.729***	0.730***
$S_{gr,bobgb}$	1.00	1.30	1.7**	1.15**	0.756	0.749	0.728***	0.777***

6.3.2.2 Cluster size distributions

Figures 6-7 and 6-8 display the oil and gas cluster size distributions. These distributions can be best fitted with a power-law $N \propto V^{-\tau}$, where N is the frequency with which a cluster of size V is counted in the rock pore space, and τ is a fitting exponent. The best fitting equations are tabulated in Table 6-5. We note that the τ values we obtained (0.7 – 1.7, cp. Table 6-4) are significantly lower than the values estimated previously for two-phase (Iglauer et al. 2010, 2011, 2012, Pentland et al. 2012, Georgiadis et al., 2013) and a three-phase flow scenario (Iglauer et al. 2013). This discrepancy is caused by the statistical methods used previously (Iglauer and Wülling 2015); precisely, previously the methodology suggested by Dias and Wilkinson (1986) was applied, however, this method is biased as it is limited to finding $\tau \geq 2$. We thus used a direct least square fit instead where we qualitatively weighted the points with high counts (i.e. small clusters) more heavily than the points with lower counts, (i.e. larger clusters); this approach is justified as there are only very few large clusters counted, which is caused by the finite size of the observed domain, and the count number for large clusters has thus a lower statistical confidence (cp. Iglauer and Wülling 2015 for a detailed discussion).

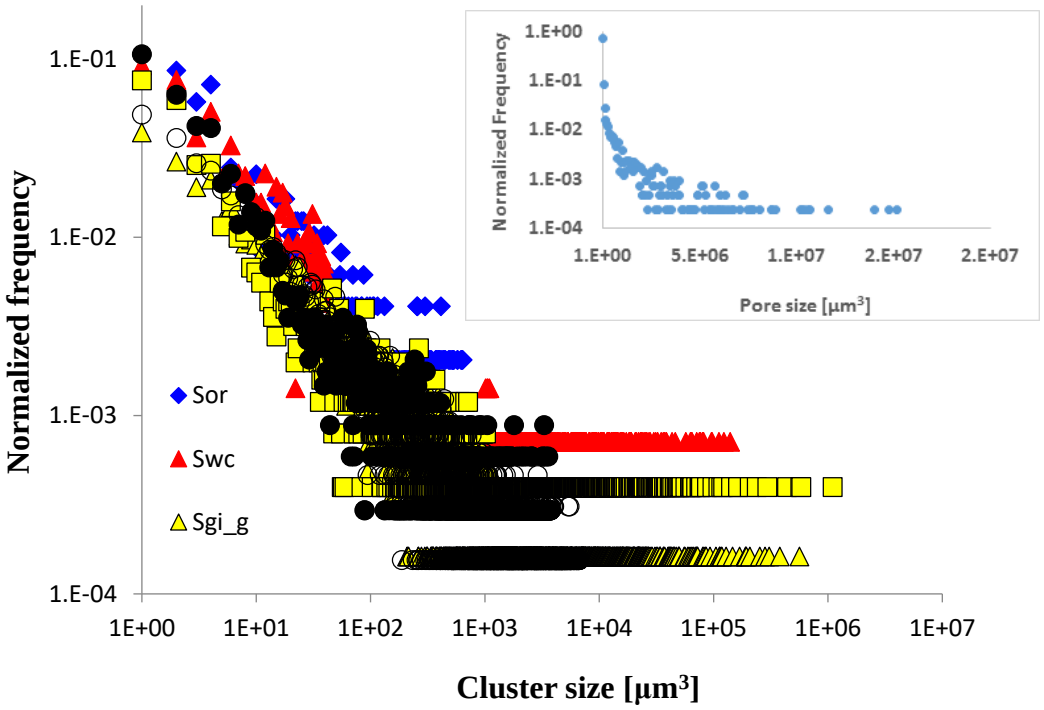

Figure 6-7 Oil cluster size distribution for each saturation state.

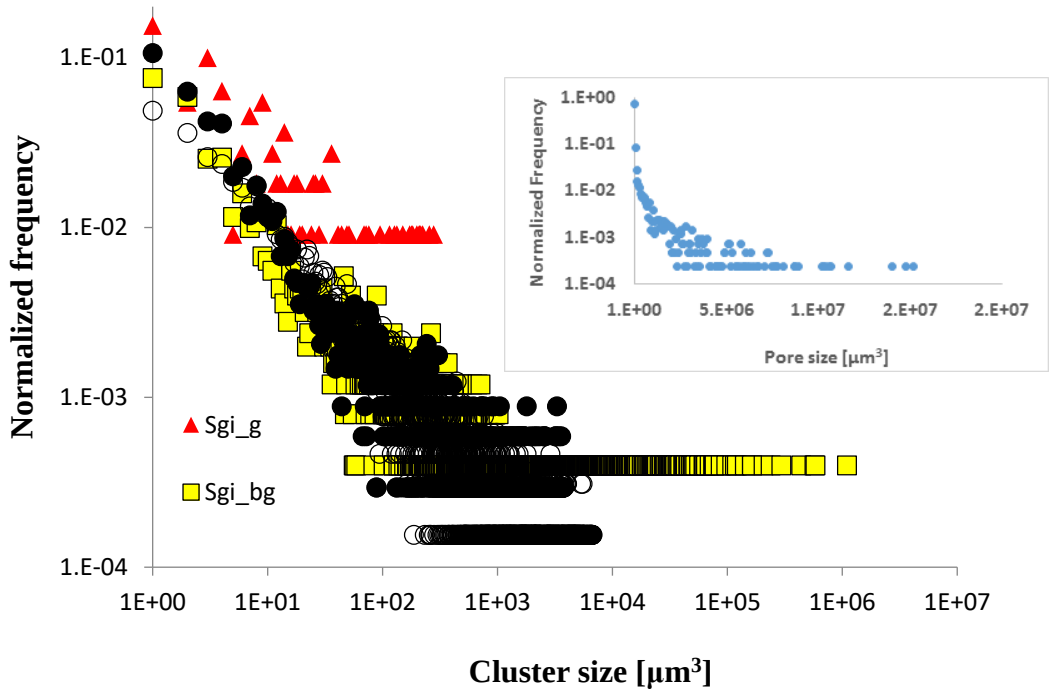

Figure 6-8 Gas cluster size distribution for each saturation state.

Table 6-5 Best least square fitting equations for the measured oil and gas cluster size distributions in water-wet and intermediate-wet sandstone. *Data taken from Iglauer et al. (2014). **Data taken from Iglauer et al. (2013).

Saturation state	Fitting equation			
	Oil (intermediate-wet)	gas (intermediate-wet)	oil (water-wet)	gas (water-wet)
S_{wc}	$0.09s^{-0.70}$	---		
S_{or}	$0.11s^{-0.80}$	---	$0.083s^{-0.68*}$	
$S_{gi,bog}$	$0.043s^{-0.72}$	$0.16s^{-0.75}$		
$S_{gi,bobg}$	$0.08s^{-1.05}$	$0.22s^{-0.95}$		
$S_{gr,bogb}$	$0.05s^{-0.67}$	$0.22s^{-1.00}$	$0.16s^{-0.9**}$	$0.136s^{-0.7**}$
$S_{gr,bobgb}$	$0.11s^{-1.00}$	$0.38s^{-1.30}$	$0.45s^{-1.7**}$	$0.304s^{-1.15**}$

It is clear that the cluster size distribution curves for the presented cases fall rapidly and there are many more smaller clusters than larger clusters, however, the decay is much smaller than predicted by percolation theory (which predicts $\tau = 2.189$, Lorenz and Ziff 1998). The cluster size distributions again have an important impact on mass transfer processes as they influence interfacial areas, see discussion above and also Figures 6-6 and 6-7, but also re-mobilization of larger drops (which is easier to accomplish, Herring et al. (2013)). The τ values are similar for all saturation states (τ is between ~0.7 to 1), except for oil ($\tau = 1.7$) and gas ($\tau = 1.15$) in the water-wet plug and gas ($\tau = 1.3$) in the intermediate-wet plug. The reason for this may be an increased number of snap-off events as gas is always non-wetting and oil is intermediate-wet in a water-wet plug.

6.3.3 Interface curvatures and capillary pressures

6.3.3.1 Interface curvatures

The curvatures (C) of all gas and oil bubbles was measured on smoothed surfaces generated from the segmented images (Armstrong et al. 2012, 2014), Figures 6-9 and 10. For all saturations states the oil curvature distribution was generally quite narrow and always peaked at zero (Figure 6-9) with the exception of S_{wc}, where highly negative curvatures (down to ~ -40/μm) were measured, although count numbers were very low. This reflects the intermediate-wet character of the rock (Amott-Harvey index = -0.1, see above). Waterflooding strongly narrowed the distribution and C ranged from ~ -5 to +5. Gas and secondary water injection created a tail on the positive side, C increased to up to ~20. These distributions are approximately consistent with those observed for a two-phase oil-water system (Armstrong et al. 2012).

The gas curvature distributions showed a similar behaviour, they also peaked at zero, but a slightly lower symmetry and no tail on the positive curvature side was observed (Figure 6-10).

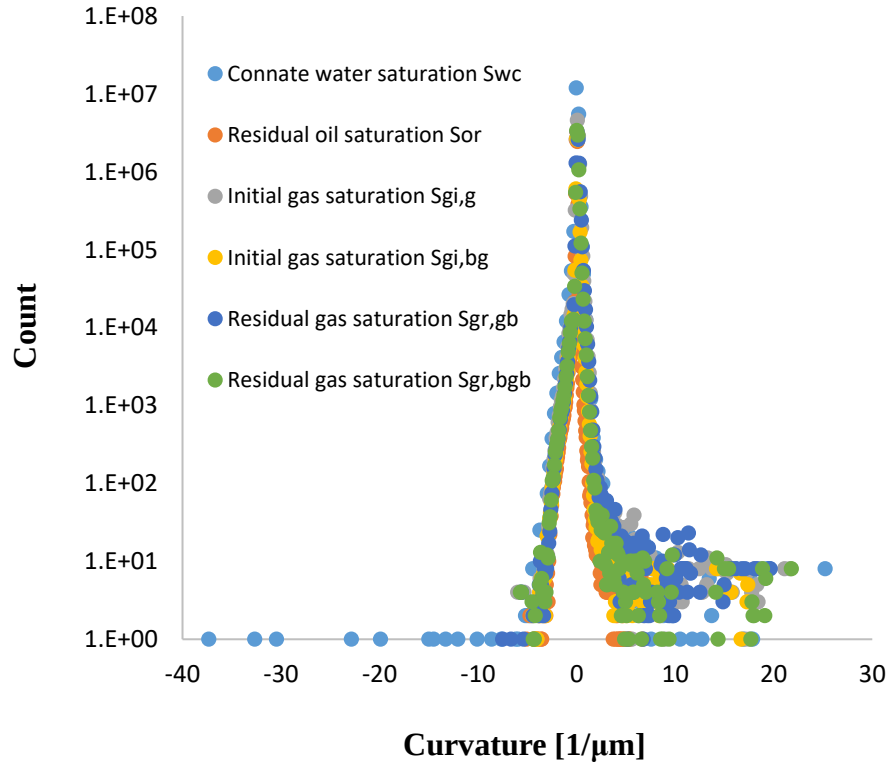

Figure 6-9 Oil curvature distribution at various saturation states.

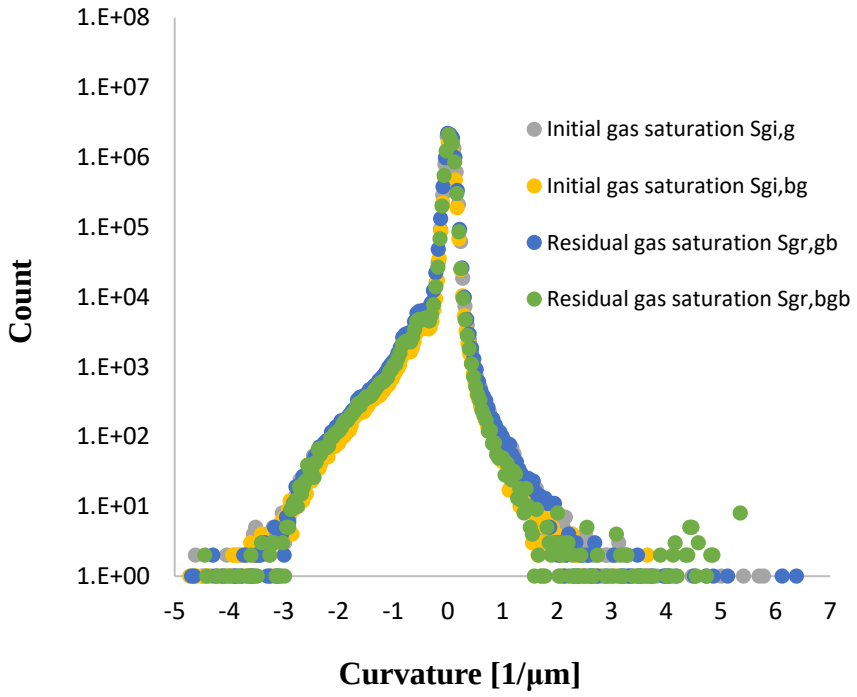

Figure 6-10 Gas curvature distribution at various saturation states.

6.3.3.2 Capillary pressures

The curvatures were then converted into capillary pressures (P_c) using the Young-Laplace equation:

$$P_c = 2\gamma C$$

The resulting capillary pressure distributions of course reflect the curvature distributions, Figures 6-11 and 6-12. Overall remarkably low P_c values were measured at S_{wc} (~ -13 MPa), although count numbers were rare. P_c values for oil were also quite high at the upper end of the tail (after gas and/or secondary waterflood), up to ~ 7-10 MPa. This is evidence that intermolecular forces can be very significant at the pore-scale. P_c values were generally lower for gas, although the shape of the curve is similar. The lower numbers were probably due to gas always being the non-wetting phase. We conclude that μCT is a suitable technique to measure capillary pressures and associated curvatures of individual phase ganglia in-situ.

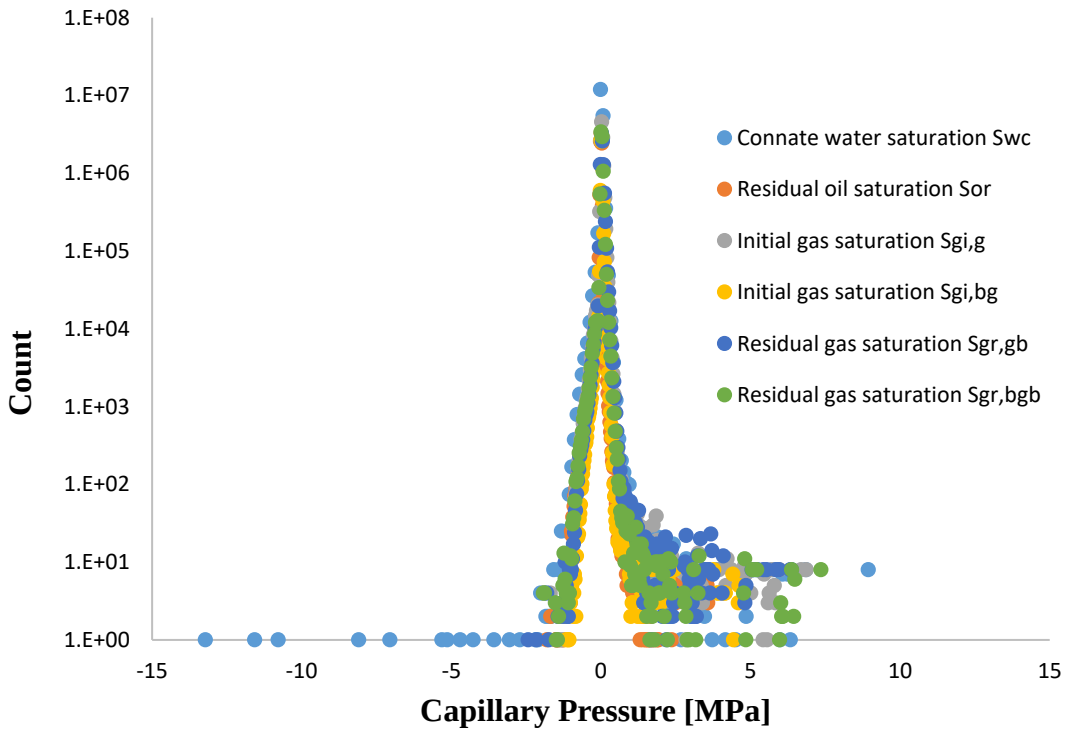

Figure 6-11 Distribution of capillary pressures for oil at various saturation states.

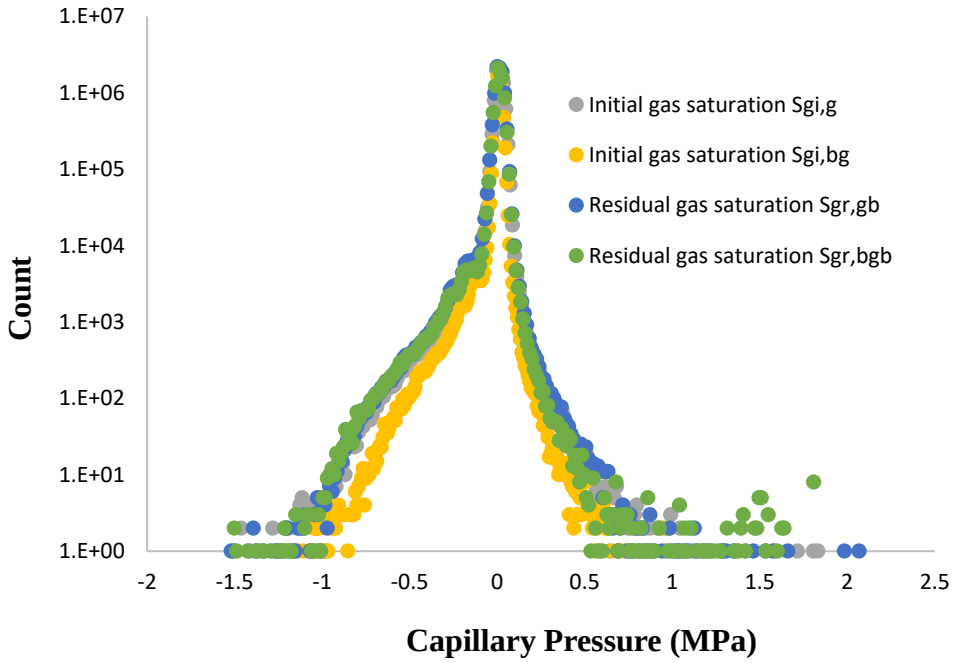

Figure 6-12 Distribution of capillary pressures for gas at various saturation states.

6.4. Conclusions

We imaged two gas-flood assisted enhanced oil recovery processes in an intermediate-wet sandstone at a high resolution of $(3.4\mu m)^3$ in 3D with an x-ray micro-computed tomograph. Waterflooding an intermediate-wet oil reservoir proved to be quite efficient ($R_f \approx 52\%$), although direct gas flooding was even more efficient ($R_f \approx 66\%$). Significant incremental oil could be produced by alternating gas-water flooding ($R_f \approx 71\%$). A large amount of gas (~50% saturation) could be stored via both processes contrary to what was measured in water-wet sandstone, where ~20% gas could be stored by direct gas flooding and only ~5% was stored when the rock was waterflooded prior to gas injection, Iglauer et al. (2013).

The capillary trapping capacity is thus significantly higher in intermediate-wet rock. The gas and oil cluster size distributions followed power-law relations $N \propto V^{-\tau}$ (where N is the frequency with which clusters of volume V are counted; and the decay exponent τ ranged between 0.7 and 1.7; note that percolation theory predicts a significantly higher τ (= 2.189), Lorenz and Ziff 1998). The cluster volume V – cluster surface area A also correlated with a power-law $A \propto V^p$, and p was always ≈

0.75, which is a) significantly smaller than the p predicted by percolation theory (which predicts $p \approx 1$, Stauffer 1979), and b) all values for p measured so far in rocks (Pentland et al. 2012, Iglauer et al. 2013) were ≈ 0.75 for all cases considered.

The fact that significantly lower τ and p values were measured than predicted by percolation theory raises increasing doubt about the applicability of simple percolation models. Furthermore, the curvatures of the oil and gas bubbles were measured and thus the capillary pressure distributions could be determined. The curvatures peaked at zero curvature, consistent with previous measurements in two-phase flow (Armstrong et al. 2012). However, the shapes of the curvature distributions stretched more to positive values in case of oil, and more to negative curvatures in case of gas. These shapes are reflected in the capillary pressure distributions; however, a nominally higher-pressure range was measured for the oil bubbles (from ~ -13MPa to +9MPa for oil versus -1.5MPa to +2.1MPa for gas). Importantly, the detailed pore-scale fluid configurations could be examined at highest scanning resolution ~1 μm^3; many configurations previously predicted theoretically (Piri and Blunt 2004; Al-Dhahli et al. 2012) or observed in 2D micromodels (Oren and Pincewski 1995) could be verified, and additional, new configurations could be identified; all configurations were categorized in a table.

In conclusion, there is a large variety of possible fluid configurations, fluid curvatures and capillary pressures, and this variety is the origin of the well-known complexity of three-phase flow through intermediate-wet rock.

Chapter 7 Conclusion and Future Work

7.1 Conclusion

Sequestration of carbon dioxide in geological formations is the most direct carbon management strategy for reducing anthropogenic CO_2 in the long term. Further, it has been recognised that residual trapping mechanisms are an effective approach for CO_2 geo-sequestration projects because they immobilise micrometre-sized CO_2 bubbles in the pore network of the rock and increase the safety of the storage sites as they inhibit the upward migration of CO_2. In this study, this mechanism was applied to (oil-wet) oil reservoirs because they are the most important and have been observed for the first time here.

In this thesis, the wettability of CO_2/brine system was measured on hydrophobic and hydrophilic dolomite surfaces at different pressures and temperatures. The experimental observations with the concept of temperature-dependency of van der Waals potential and sharp-kink approximation has been analysed here. It was shown that as pressure increases, the dolomite becomes more CO_2-wet, regardless of the surface being hydrophilic or hydrophobic. The wettability of dolomite, on the other hand, remained unchanged or became slightly more CO_2-wet on hydrophilic surfaces by increasing temperature but was reduced on hydrophobic surfaces. It was illustrated that phase-density difference, fluid interfacial tension, and fluid-solid van der Waals potentials, affect the contact angle (wettability) of no/weakly charged surfaces when state variables, such as pressure and temperature, vary.

Furthermore, intermediate-wet sandstone was imaged in 3D at high resolution (1-3.4μm)^3 with x-ray micro-computed tomography at various saturation states. Initially, the core was at connate water saturation and contained a large amount of oil (94%), which was produced by a waterflood (recovery factor R_f = 52% OOIP) or a direct gas flood (R_f = 66% OOIP). Subsequent water and/or gas flooding (WAG process) resulted in significant incremental oil recovery (R_f = 71% OOIP) while a

substantial amount of gas could be stored (~50%)—significantly more than in an analogue water-wet plug. The oil and gas cluster size distributions were measured and followed power-law correlations $N \propto V^{-\tau}$ (where N is the frequency with which clusters of volume V are counted) with decay exponents τ between 0.7 and 1.7. Further, the cluster volume V plotted against cluster surface area A also correlated with a power-law $A \propto V^{p}$, and p was always ≈ 0.75. The measured τ and p values are significantly smaller than predicted by percolation theory (which predicts $p \approx 1$ and $\tau = 2.189$); which raises increasing doubts about the applicability of simple percolation models. In addition, curvatures and capillary pressures of the oil and gas bubbles in-situ were measured and the detailed pore-scale fluid configurations analysed. The complex variations in fluid curvatures, capillary pressures, and the fluid-fluid or fluid-fluid-fluid pore scale configurations (exact spatial locations also in relation to each other and the rock surface) are the origin of the well-known complexity of three-phase flow through rock.

In addition, it was found that the residual CO_2 saturations ($S_{CO2,r}$) in oil-wet sandstone are dramatically lower than in equivalent water-wet sandstone ($S_{CO2,r}$ = 8.7% versus 14.9%). This is consistent with data reported for a plastic bead pack (Chaudhary et al. 2013) and indicates that oil-wet rock is intermediate-wet or CO_2-wet at reservoir conditions—a phenomenon that was also observed in independent contact-angle measurements (Dickson et al. 2006; Yang et al. 2007, 2008; Espinoza et al. 2010; Ameri et al. 2013;). This shift in CO_2-wettability also significantly influenced CO_2 cluster morphologies and residual cluster size distributions. Flatter and more sheet-like clusters and more small CO_2 bubbles were observed in the oil-wet sample. Therefore, it has been concluded that, importantly, residual trapping is less efficient in oil reservoirs than in deep saline aquifers.

Moreover, the simple experimental cells that allow micro-tomographic visualization of fluids inside rocks under elevated pressure were presented. The modular cell design allows hassle-free maintenance and easy cell modifications. The cell can be used for visualising multiphase fluid distribution inside porous media. Using developed cells, it was investigated how the residual CO_2 phase spreads in the rock as a function of thermo-physical conditions (for ambient condition CO_2 gas, liquid

CO_2, near-critical CO_2 gas, and supercritical CO_2) and how residual CO_2 is dissolved by under-saturated formation brine (dissolution trapping). It was also found that CO_2 spread is relatively homogeneous throughout the core plugs for all conditions. However, less $scCO_2$ was trapped at higher pressures, which is possible owing to the lower water-wettability of sandstone at high pressures.

7.2 Future Work

While this work has a wide discussion of issues associated with pore-scale investigation in porous media concerning CO_2 geo-sequestration, there are certain other related issues that need to be addressed.

- There is a serious lack of experiments and studies in a three-phase (oil-water-CO_2) system, where oil and water are always present in subsurface formation (meanwhile, the CO_2 is injected for disposal at the pore-scale (micrometre-scale)). Furthermore, determining the whole (hectometre-scale) reservoir behaviour (pressure, temperature, and physical properties) (Bear 1972; Sahimi 2011; Blunt 2013) is even more complicated. This generates a high uncertainty in storage capacity and containment security predictions and, thus, project risk.

- Wettability plays an important role in the underground geological storage of carbon dioxide as the fluid flow and distribution mechanism within the porous medium is controlled by this phenomenon. It is documented that the CO_2 pressure, temperature, brine composition, and minerals type have significant effects on wettability. Despite past research carried out on the subject, the factors controlling the wettability variation for CO_2/water/minerals, particularly the effect of pores of the porous substrate on the contact angle at different pressure, temperature, and salinity and the physical processes, involved are not yet fully understood.

- The contact angle measurement of pure clay minerals (kaolinite, montmorillonite, and illite with CO_2/brine, nitrogen/brine and nitrogen/oil (decane)) at different pressures and temperatures was not systematically studied. Although it was well recognized the temperature, pressure, and salinity have significant effects on contact angel. However, they could considerably differ in subsurface formation. Moreover, it is important to study specifically the wettability in clay minerals, as the materials are also critical to oil recovery in clay-bearing reservoirs and the capacity of capillary seals, and is still not fully understood.

References

Akbarabadi, M., and M. Piri (2013) Relative permeability hysteresis and capillary trapping characteristics of supercritical CO_2/brine systems: An experimental study at reservoir conditions, Advances in Water Resources., 52, 190–206.

Al-Anssari, S., Barifcani, A., Wang, S., Lebedev, M., and S. Iglauer (2016) Wettability alteration of oil-wet carbonate by silica nanofluid, Journal of Colloid and Interface Science, 461, 435-442.

Al-Dhahli, A., Geiger, S., Van Dijke, M.I.J. (2012) Three-phase pore-network modelling for reservoirs with arbitrary wettability. SPE Journal. 18, 285-295.

Al-Khdheeawi, E., Vaille, S., Barifcani, A., Sarmadivaleh, M., Iglauer, S. 2017. Influence of CO_2 injection well type on CO_2 plume behavior and the capacity of different trapping mechanisms in different rock wettability conditions. Journal of Natural Gas Science and Engineering, in press.

Al-Khdheeawi, E.A., Vialle, S., Barifcani, A., Sarmadivaleh, M. and Iglauer, S., 2017. Impact of reservoir wettability and heterogeneity on CO_2-plume migration and trapping capacity. International Journal of Greenhouse Gas Control, 58, pp.142-158.

Al-Khdheeawi, E.A., Vialle, S., Barifcani, A., Sarmadivaleh, M. and Iglauer, S., 2016. Influence of CO_2-wettability on CO_2 migration and trapping capacity in deep saline aquifers. Greenhouse Gases: Science and Technology.

Al-Mansoori, SK, Iglauer, S, Pentland, CH, Blunt, MJ. (2009). An experimental study of three-phase trapping in sand packs. Advances in Water Resources. 32, 1535-1542.

Al-Mansoori, SK, Iglauer, S, Pentland, CH, Blunt, MJ. (2009). An experimental study of three-phase trapping in sand packs. Advances in Water Resources. 32, 1535-1542.

Al-Yaseri, A. Z., Lebedev, M., Barifcani, A., S. Iglauer (2015) Receding and advancing CO_2-brine-quartz contact angles as a function of pressure, temperature, surface roughness, salt type and salinity, J. Chem. Thermodynamics, S0021-9614(15)00255-4, doi:10.1016/j.jct.2015.07.031.

Al-Yaseri, A. Z., Sarmadivaleh, M., Saeedi, A., Lebedev, M., Barifcani, A., S. Iglauer (2015a) N_2+CO_2+NaCl brine interfacial tensions and contact angles on quartz at CO_2 storage site conditions in the Gippsland basin, Victoria/Australia, Journal of Petroleum Science and Engineering, S0920-4105(15)00027-3, doi: 10.1016/j.petrol.2015.01.026.

Al-Yaseri, A.Z., Lebedev, M., Barifcani, A. and Iglauer, S., 2016. Receding and advancing (CO_2+ brine+ quartz) contact angles as a function of pressure, temperature, surface roughness, salt type and salinity. The Journal of Chemical Thermodynamics, 93, pp.416-423.

Al-Yaseri, A.Z., Roshan, H., Lebedev, M., Barifcani, A. and Iglauer, S., 2016a. Dependence of quartz wettability on fluid density. Geophysical Research Letters, 43(8), pp.3771-3776.

Amaechi, B., Iglauer, S, Pentland, CH, Bijeljic, B., Blunt, MJ. (2014) Three-phase measurements of oil and gas trapping in sand packs. Transport in Porous Media. 103, 421-436.

Amaechi, B., Iglauer, S, Pentland, CH, Bijeljic, B., Blunt, MJ. (2014) Three-phase measurements of oil and gas trapping in sand packs. Transport in Porous Media. 103, 421-436.

Ameri, A., Kaveh, N. S., Rudolph, E. S. J., Wolf, K. H., Farajzadeh, R., and J. Bruining, (2013) Investigation on interfacial interactions among crude oil–brine–sandstone rock–CO_2 by contact angle measurements. Energy & Fuels, 27(2), 1015-1025.

Amott, E., Observations relating to the wettability of porous rock, Trans. AIME. 1959. 216: p. 156–162.

Anderson, W. G. (1987). Wettability Literature Survey- Part 1: Rock/Oil/Brine interactions, and the effects of core handling on wettability. Journal of Petroleum Technology. 38, 10, 1125–1149.

Anderson, W. G. (1987). Wettability Literature Survey- Part 2: Wettability Measurement. Journal of Petroleum Technology. 38, 11, 1246–1262.

Anderson, W. G. (1987). Wettability Literature Survey- Part 3: The Effects of Wettability on Electrical Properties of Porous Media. Journal of Petroleum Technology. 38, 12, 1371–1378.

Anderson, W. G. (1987). Wettability Literature Survey- Part 4: The Effects of Wettability on Capillary Pressure. Journal of Petroleum Technology. 39, 10, 1283–1300.

Anderson, W. G. (1987). Wettability Literature Survey- Part 5: The Effects of Wettability on Relative Permeability. Journal of Petroleum Technology. 39, 11, 1453–1468.

Anderson, W. G. (1987). Wettability Literature Survey- Part 6: The Effects of Wettability on Waterflooding. Journal of Petroleum Technology. 39, 12, 1605–1622.

Anderson, W., Wettability Literature Survey- Part 2: Wettability Measurement. Journal of Petroleum Technology, 1986. 38(11): p. 1246-1262.

Anderson, W., Wettability Literature Survey- Part 2: Wettability Measurement. Journal of Petroleum Technology, 1986. 38(11): p. 1246-1262.

Anderson, W., Wettability Literature Survey-Part 6: Effects of Wettability on Waterflooding Journal of Petroleum Technology, 1987. 39(12): p. 1605-1622.

Anderson, W.G., Wettability Literature Survey- Part 1: Rock/Oil/Brine Interactions and the Effects of Core Handling on Wettability Journal of Petroleum Technology, 1986. 38(10): p. 1125-1144.

Anderson, W.G., Wettability Literature Survey- Part 4: Effects of Wettability on Capillary Pressure Journal of Petroleum Technology, 1987. 39(10): p. 1283- 1300.

Anderson, W.G., Wettability Literature Survey Part 5: The Effects of Wettability on Relative Permeability Journal of Petroleum Technology, 1987. 39(11): p. 1453-1468.

Anderson, W.G., Wettability Literature Survey-Part 3: The Effects of Wettability on the Electrical Properties of Porous Media Journal of Petroleum Technology, 1986. 38(12): p. 1371-1378.

Andrew, M., Bijeljic, B., and M.J. Blunt (2013) Pore-scale imaging of geological carbon dioxide storage under in situ conditions; Geophysical Research Letters 40 (15), 3915-3918, doi: 10.1002/grl.50771.

Andrew, M., Bijeljic, B., and M.J. Blunt (2014) Pore-scale imaging of trapped supercritical carbon dioxide in sandstones and carbonates, International Journal of Greenhouse Gas Control 22, 1-14.

Andrew, M., Bijeljic, B., and M.J. Blunt., 2015. Reservoir Condition Pore-scale Imaging of Multiple Fluid Phases Using X-ray Microtomography, Journal of Visualized experiments. (96), 52440.

Arif, M., Al-Yaseri, A.Z., Barifcani, A., Lebedev, M. and Iglauer, S., 2016. Impact of pressure and temperature on CO_2–brine–mica contact angles and CO_2–brine interfacial tension: Implications for carbon geo-sequestration. Journal of Colloid and Interface Science, 462, pp.208-215.

Armstrong R. T., Georgiadis A., Ott H., Klemin D., Berg S. (2014) Critical capillary number: Desaturation studied with fast X-ray computed microtomography. Geophysical Research Letters, 41, 1, 55–60.

Armstrong, R. T., M. L. Porter., D. Wildenschild. (2012). Linking porescale interfacial curvature to column-scale capillary pressure. Advances in Water Resources. 46, 55–62.

Armstrong, R.T., Porter, M.L., and D. Wildenschild (2012) Linking pore scale interfacial curvature to column-scale capillary pressure, Advances in Water Resources, 46, 55–62.

Arns, C, H., Bauget, F., Limaye, A., Sakellariou, A., Senden, J, T., Sheppard, P, A., Sok, M, R., Pinczewski, V, W., Bakke, S., Berge, I, L., Oren, E, P., and Knackstedt, A, M., 2005. Pore-Scale Characterization of Carbonates Using X-Ray Microtomography. Journal of SPE. 10(4): p. 475-484.

Babadagli, T., 2006. Optimization of CO_2 injection for sequestration/enhanced oil recovery and current status in Canada. In Advances in the Geological Storage of Carbon Dioxide (pp. 261-270). Springer Netherlands.

Babadagli, T., 2006. Optimization of CO_2 injection for sequestration/enhanced oil recovery and current status in Canada. In Advances in the Geological Storage of Carbon Dioxide (pp. 261-270). Springer Netherlands.

Bachu, S., Gunter, W. D., and Perkins, E.H., 1994, Aquifer disposal of CO2: hydrodynamic and mineral trapping, Energy Convers. Mgmt., V. 35, p. 269-279.

Bakke, S. and P.E. Øren, 3-D pore-scale modeling of sandstones and flow simulations in the pore networks. Journal of SPE, 1997. 2: p. 136-149.

Ballentine, C.J., Schoell, M., Coleman, D. and Cain, B.A., 2001. 300-Myr-old magmatic CO_2 in natural gas reservoirs of the west Texas Permian basin. Nature, 409(6818), pp.327-331.

Bear, J. (1988). Dynamics of fluids in porous media / Jacob Bear. New York: New York: Dover.

Benson, M, S., Bennaceur, k., Cook, P., Davison, J., de Coninck, Farhat, K., Ramirez, A., Simbeck, D., Surles, T., Verma, P., Wright, I., 2012. Global Energy Assessment. Chapter 13. Carbon Capture and Storage, Cambridge University Press.

Benson, S. and Cook, P., 2005. Intergovernmental Panel on Climate Change, Special Report on Carbon Dioxide Capture and Storage: Underground Geological Storage. Chapter, 5, p.196r276.

Berg, S., et al. (2013), Real-time 3D imaging of Haines jumps in porous media flow, Proc. Natl. Acad. Sci. U.S.A., doi:10.1073/pnas.1221373110.

Beygi, M.R., Delshad, M., Pudugramam, V.S., Pope, G.A., Wheeler, M.F. (2013) Novel three-phase compositional relative permeability and three-phase hysteresis models. Proc SPE Western Regional & AAPG Pacific Section Meeting, Monterey, California, USA, SPE 165324.

Blunt, M., Bijeljic, B., Dong, H., Gharbi, O., Iglauer, S., Mostaghimi, P., Paluszny, A., Pentland, CH. 2013. "Pore-scale imaging and modelling", Advances in Water Resources, Vol. 51,197-216.

Blunt, M.J., Fayers, F.J., Orr, F.M. (1993) Carbon dioxide in enhanced oil recovery. Energy Conversion and Management. 34, 9-11, 1197-1204.

Blunt, M.J., Zhou, D., Fenwick, D. (1995) Three-phase flow and gravity drainage in porous media. Transport in Porous Media. 20, 77-103

BP Statistical Review of World Energy. June 2014. Key world crude oil.bp.com/statisticalreview.

Broseta, D., Tonnet, N., Shah, V. (2012) Are rocks still water-wet in the presence of dense CO_2 or H_2S?, Geofluids, 12, 280-294.

Buades, A., Coll, B., and J.M. Morel (2005) A non-local algorithm for image denoising, Proc. Computer Vision and Pattern Recognition, 2, 60-65.

Buckley, J.S., Liu, Y., and S. Monsterleet (1998) Mechanisms of wetting alteration by crude oils, SPE Journal, 54-61.

Burnside, N., & Naylor, M. (2011) Evaluation of CO_2 storage actuarial risk: defining an evidence base. DEVEX, 12th May, School of Geoscience, University of Edinburgh, Aberdeen.

Butt, H.J., Graf, K. and Kappl, M., 2006. Physics and chemistry of interfaces. John Wiley & Sons.

Cantucci, B., Montegrossi, G., Vaselli, O., Tassi, F., Quattrocchi, F., and Perkins, E.H. (2009) Geochemical modelling of CO_2 storage in deep reservoirs: The Weyburn Project (Canada) case study, Chemical Geology, 265, 181-197.

Caubit, C, Bertin, H, Hamon, G. (2004) Three-phase flow in porous media: wettability effect on residual saturations during gravity drainage and tertiary waterflood. Proc SPE An Tech Conf 2004, SPE 90099.

Chalbaud, C., Robin, M., Lombard, J.-M., Bertin, H., and P. Egermann (2010) Brine/CO_2 interfacial properties and effects on CO_2 storage in deep saline aquifers, Oil & Gas Science and Technology, 65(4), 541-555.

Chaudhary, K., Bayani Cardenas, M., Wolfe, W.W., Maisano, J.A., Ketcham, R.A., and P.C. Bennett (2013) Pore-scale trapping of supercritical CO_2 role of grain wettability and shape, Geophysical Research Letters, 40, 15, 3878-3882, doi: 10.1002/grl.50658.

Chaudhary, K., M. Bayani Cardenas, W. W. Wolfe, J. A. Maisano, R. A. Ketcham, and P. C. Bennett (2013) Pore-scale trapping of supercritical CO_2 and the role of grain wettability and shape, Geophysical Research Letters, 40, 1-5.

Chaudhary, K.T., Rizvi, Z.H., Bhatti, K.A., Ali, J. and Yupapin, P.P., 2013. Multiwalled carbon nanotube synthesis using arc discharge with hydrocarbon as feedstock. Journal of Nanomaterials, 2013, p.145.

Chen, C., Wan, J., Li, W. and Song, Y., 2015. Water contact angles on quartz surfaces under supercritical CO_2 sequestration conditions: Experimental and molecular dynamics simulation studies. International Journal of Greenhouse Gas Control, 42, pp.655-665.

Chiquet, P., Broseta, D. and S. Thibeau (2007) Wettability alteration of caprock minerals by carbon dioxide, Geofluids, 7, 112–122.

Clarkson, C. R., & Bustin, R. M. (2000). Binary gas adsorption/desorption isotherms: effect of moisture and coal composition upon carbon dioxide selectivity over methane. International Journal of Coal Geology, 42(4), 241-271.

Cook, P.J (Ed) (2014) Geologically Storing Carbon: Learning from the Otway Project Experience. CSIRO Publishing, Melbourne. IBSN 9781486302321.

Cuiec, L.E (1991) Evaluation of reservoir wettability and its effect on oil recovery. In: Interfacial Phenomena in Petroleum Recovery (ed.: N.R. Morrow). New York: Marcel Dekker.

De Ruijter, M., Kölsch, P., Voué, M., De Coninck, J. and Rabe, J.P., 1998. Effect of temperature on the dynamic contact angle. Colloids and Surfaces A: Physicochemical and Engineering Aspects, 144(1), pp.235-243.

Dias, M.M., Wilkinson, D., 1986. Percolation with trapping. J. Phys. A: Math Gen. 19, 3131 – 3146.

Dickson, J.L., Gupta, G., Horozov, T.S., Binks, B.P. and K.P. Johnston, K.P. (2006) Wetting Phenomena at the CO_2/Water/Glass Interface, Langmuir, 22(5), 2161-2170.

Dietrich, S. and Napiórkowski, M., 1991. Analytic results for wetting transitions in the presence of van der Waals tails. Physical Review A, 43(4), p.1861.

Dong, H., Blunt, M.J. (2009) Pore-network extraction from micro-computerized tomography images. Physical Review E. 80, 036307.

Dong, M, Dullien, FAL, Chatzis, I. (1995) Imbibition of oil in film form over water present in edges of capillaries with an angular cross section. J Colloid Interf Sci. 172, 21-36.

Dumoré, JM, Schols, RS. (1974) Drainage capillary-pressure functions and the influence of connate water. SPE J. 437-444.

Egermann, P, Vizika, O, Dallet, L, Requin, C, Sonier, F. (2000) Hysteresis in three-phase flow: experiments, modelling and reservoir simulations. Proc SPE Euro Petrol Conf 2000, SPE 65127.

El-Maghraby, R., Pentland, C.H., Iglauer, S., and M.J. Blunt (2012) A fast method to equilibrate carbon dioxide with brine at high pressure and elevated temperature including solubility measurements, Journal of Supercritical Fluids, 62, 55-59.

Emberley S., Hutcheon, I., Shevalier, M., Durocher, K., Mayer, B., Gunter W.D., Perkins E.H. (2005) Monitoring of fluid-rock interaction and CO_2 storage through

produced fluid sampling at the Weyburn CO_2-injection enhanced oil recovery site, Saskatchewan, Applied Geochemistry, 20, 1131-1157.

Ennis-King, J. and Paterson, L., 2002, January. Engineering aspects of geological sequestration of carbon dioxide. In SPE Asia Pacific Oil and Gas Conference and Exhibition. Society of Petroleum Engineers.

Espinoza, D.N., and J.C. Santamarina (2010) W ater-CO_2-mineral systems: Interfacial tension, contact angle, and diffusion – Implications to CO_2 geological storage, Water Resour Res, 46, 7, W0753, doi:10.1029/2009WR008634.

Farokhpoor, R., Bjørkvik, B.J., Lindeberg, E. and Torsæter, O., 2013. Wettability behaviour of CO_2 at storage conditions. International Journal of Greenhouse Gas Control, 12, pp.18-25.

Firoozabadi, A., and P. Cheng (2010) Prospects for subsurface CO_2 sequestration, AIChE Journal, 56(6), 1398-1405.

Fusseis, F., Steeb, H., Xiao, X., Zhu, W., Butler, I., Elphicka, S., Mader , U. A low-cost X-ray-transparent experimental cell for synchrotron-based X-ray microtomography studies under geological reservoir conditions. Journal of Synchrotron Radiation 2014; 21: 251-253.

Garcia, R., Osborne, K. and Subashi, E., 2008. Validity of the “sharp-kink approximation” for water and other fluids. The Journal of Physical Chemistry B, 112(27), pp.8114-8119.

Gatica, S.M., Johnson, J.K., Zhao, X.C. and Cole, M.W., 2004. Wetting transition of water on graphite and other surfaces. The Journal of Physical Chemistry B, 108(31), pp.11704-11708.

Geistlinger H, Mohammadian S, Schlu¨ ter S, Vogel HJ (2014) Quantification of capi llary trapping of gasclusters using X- ray microtomography. Water Resource Research, 50, 4514–29.

Geistlinger, H., Mohammadian, S. (2015) Capillary trapping mechanism in strongly water-wet systems: comparison between experiment and percolation theory, Advances in Water Resources, 79, 35-50.

Georgiadis, A., Berg, S., Makurat, A., Maitland, G, Ott, H. (2013) Pore-scale micro-computed tomography imaging: non-wetting-phase cluster-size distribution during drainage and imbibition, Physical Review E, 88, 033002.

Georgiadis, A., Maitland, G., Trusler, J.M. and Bismarck, A., 2010. Interfacial tension measurements of the (H_2O+ CO_2) system at elevated pressures and temperatures†. Journal of Chemical & Engineering Data, 55(10), pp.4168-4175.

Georgiadis, A., S. Berg, G. Maitland, and H. Ott (2013), Pore-scale microcomputed-tomography imaging: Nonwetting-phase cluster-size distribution during drainage and imbibition, Phys. Rev. E, 88(3), 033,002–033,011.

Gilfillan, S. M., Lollar, B. S., Holland, G., Blagburn, D., Stevens, S., Schoell, M., and Ballentine, C. J. (2009). Solubility trapping in formation water as dominant CO_2 sink in natural gas fields. Nature, 458(7238), 614-618.

Giraldo, J., Benjumea, P., Lopera, S., Cortés, F. B., & Ruiz, M. A. (2013). Wettability alteration of sandstone cores by alumina-based nanofluids. Energy & Fuels, 27(7), 3659-3665.

Golab, A., Romeyn, R., Averdunk, H., Knackstedt, M., Senden, T.J. (2013). 3D characterisation of potential CO_2 reservoir and seal rocks, Australian Journal of Earth Sciences, 2013, 60, 111-123.

Grate, J.W., Dehoff, K.J., Warner, M.G., Pittman, J.W., Wietsma, T.W., Zhang, C. and Oostrom, M., 2012. Correlation of oil–water and air–water contact angles of diverse silanized surfaces and relationship to fluid interfacial tensions. Langmuir, 28(18), pp.7182-7188.

Gurevich, B., Pevzner, R., Urosevic, M., Kepic, A., Shulakova, V., Caspari, E., Lebedev, M (2014) “2D and 3D seismic investigations for Stages 1 and 2C.” In Geologically Storing Carbon: Learning from the Otway Project

Experience. Editor: Cook P.J. CSIRO Publishing, Melbourne. 155-196, IBSN 9781486302321.

Herring, A.L., Harper, E.J., Andersson, L., Sheppard, A., Bay, B.K., Wildenschild, D. (2013). 3D characterisation of potential CO_2 reservoir and seal rocks, Australian Journal of Earth Sciences, 2013, 60, 111-123.

Herring, A.L., Harper, E.J., Andersson, L., Sheppard, A., Bay, B.K., Wildenschild, D. (2013) Effect of fluid topology on residual nonwetting phase trapping: implications for geologic CO_2 sequestration, Advances in Water Resources, 62, 47-58.

Hesse, A, M., Orr, M, F., Tchelepi, A, H., 2008. Gravity currents with residual trapping, Journal of Fluid Mechanics. 611, pp. 35-60

Hirai, S., Okazaki, K., Yazawa, H., Ito, H., Tabe, Y., Hijikata, K. (1997). Measurement of CO_2 diffusion coefficient and application of LIF in pressurized water, Energy, 22, 2-3,363-367.

Hirasaki, G. and Zhang, D.L., 2004. Surface chemistry of oil recovery from fractured, oil-wet, carbonate formations. SPE Journal, 9(02), pp.151-162.

Hirasaki, G.J. (1991) Thermodynamics of thin films and three-phase contact regions. In: Interfacial Phenomena in Petroleum Recovery (ed.: N.R. Morrow). New York: Marcel Dekker.

Hui, M.H. and M.J. Blunt, Effects of wettability on three-phase flow in porous media. Journal of Physical Chemistry, 2000. 104(16): p. 3833–3845.

Iglauer, S. 2012. Carbon capture and storage with a focus on capillary trapping as a mechanism to store carbon dioxide in geological porous media. In: Mewes D, Cheng L, editors. Advances in multiphase flow and heat transfer. Bussum: Bentham Science Publishers. p. 135–50.

Iglauer, S. 2017. CO_2-water-rock wettability: variability, influencing factors and implications for CO_2 geo-storage. Accounts of Chemical Research, doi: 10.1021/acs.accounts.6b00602.

Iglauer, S. and Wülling, W., 2016. The scaling exponent of residual nonwetting phase cluster size distributions in porous media. Geophysical Research Letters, 43(21).

Iglauer, S., A. Paluszny, and M. Blunt (2013) Simultaneous oil recovery and residual gas storage: a pore-level analysis using in-situ x-ray micro-tomography. Fuel. 1, 1-11.

Iglauer, S., A. Paluszny, C. H. Pentland, and M. J. Blunt (2011a) Residual CO_2 imaged with X-ray micro-tomography, Geophysical Research Letters, 38, 21, L21403, doi: 10.1029/2011GL049680.

Iglauer, S., Al-Yaseri, A.Z., Rezaee, R. and Lebedev, M., 2015. CO_2 wettability of caprocks: Implications for structural storage capacity and containment security. Geophysical Research Letters, 42(21), pp.9279-9284.

Iglauer, S., C.H. Pentland, and A. Busch (2015a) CO_2-wettability of seal and reservoir rocks and the implications for carbon geo-sequestration, Water Resources Research, 51, 1, 729-774, WR015553, doi: 10.1002/wrcr.21095.

Iglauer, S., M. A. Fernø, P. Shearing, and M. J. Blunt (2012) Comparison of residual oil cluster size distribution, morphology and saturation in oil-wet and water-wet sandstone, Journal of Colloid and Interface Science, 375, 1, 187–192.

Iglauer, S., Mathew, M.S. and Bresme, F., 2012. Molecular dynamics computations of brine–CO_2 interfacial tensions and brine–CO_2–quartz contact angles and their effects on structural and residual trapping mechanisms in carbon geo-sequestration. Journal of Colloid and Interface Science, 386(1), pp.405-414.

Iglauer, S., Mathew, M.S. and Bresme, F., 2012. Molecular dynamics computations of brine–CO_2 interfacial tensions and brine–CO_2–quartz contact angles and their effects on structural and residual trapping mechanisms in carbon geo-sequestration. Journal of colloid and interface science, 386(1), pp.405-414.

Iglauer, S., Paluszny, A. and Blunt, M.J., 2013. Simultaneous oil recovery and residual gas storage: A pore-level analysis using in situ X-ray micro-tomography. Fuel, 103, pp.905-914.

Iglauer, S., Paluszny, A., Pentland, C.H. and Blunt, M.J., 2011. Residual CO_2 imaged with X-ray micro-tomography. Geophysical Research Letters, 38(L21403).

Iglauer, S., Pentland, C.H. and Busch, A., 2015a. CO_2 wettability of seal and reservoir rocks and the implications for carbon geo-sequestration. Water Resources Research, 51(1), pp.729-774.

Iglauer, S., Rahman, T., Sarmadivaleh, M., Al-Hinai, A., Fernø, M.A. and Lebedev, M., 2016. Influence of Wettability on Residual Gas Trapping and Enhanced Oil Recovery in Three-Phase Flow: A Pore-Scale Analysis by Use of Microcomputed Tomography. SPE Journal.

Iglauer, S., S. Favretto, G. Spinelli, G. Schena, and M. J. Blunt (2010) X-ray tomography measurements of power-law cluster size distributions for the nonwetting phase in sandstones, Physical Review E, 82, 056315.

Iglauer, S., Salamah, A., Sarmadivaleh, M., Liu, K. and Phan, C., 2014. Contamination of silica surfaces: impact on water–CO_2–quartz and glass contact angle measurements. International Journal of Greenhouse Gas Control, 22, pp.325-328.

Iglauer, S., Wu, Y., Shuler, PJ., Tang, Y., Goddard, WA. 2010. Dilute iota- and kappa-Carrageenan solutions with high viscosity in high salinity brines. J Petrol Sci Eng; 75: 304–311.

Iglauer, S., Wu, Y., Shuler, PJ., Tang, Y., Goddard, WA. 2010. New surfactant classes for enhanced oil recovery and their tertiary oil recovery potential. J Petrol Sci Eng; 71:23–9.

Iglauer, S., Wuelling, W., Pentland, C.H., Al-Mansoori, S.K. and M.J. Blunt (2011b) Capillary-trapping capacity of sandstones and sandpacks. SPE Journal. 16(4), 778-783.

International Energy Agency. 2010. Key world energy statistics. Paris.

Izgec, O., Demiral, B., Bertin, H. and Akin, S., 2008. CO_2 injection into saline carbonate aquifer formations I: laboratory investigation. Transport in Porous Media, 72(1), pp.1-24.

Javanbakht, G., Sedghi, M., Welch, W. and Goual, L., 2015. Molecular dynamics simulations of CO_2/water/quartz interfacial properties: impact of CO_2 dissolution in water. Langmuir, 31(21), pp.5812-5819.

Jettestuen, E., Helland, J.O., and M. Prodanovic (2013) A level set method for simulating capillary-controlled displacements at the pore scale with nonzero contact angles, Water Resources Research, 49, 4645-4661.

Juanes, R., Spiteri, E.J., Orr, F.M., and M. J. Blunt (2006) Impact of relative permeability hysteresis on geological CO_2 storage, Water Resour. Res., 42, 1–13, doi: 10.1029/2005WR004806.

Jung, J.W. and Wan, J., 2012. Supercritical CO_2 and ionic strength effects on wettability of silica surfaces: Equilibrium contact angle measurements. Energy & Fuels, 26(9), pp.6053-6059.

Karpyn, Z.T., Piri, M., and G. Singh (2010) Experimental investigation of trapped oil clusters in a water-wet bead pack using x-ray microtomography, Water Resources Research, 46, 4, W04510, doi: 10.1029/2008WR007539.

Kaveh, N.S., Rossen, W.R., Rudolph, E.S.J., Berentsen, c., 2012. Wettability Determination by Equilibrium Contact Angle Measurements Reservoir Rock - Connate Water System with Injection of CO2. SPE 154382.

Kaveh, N.S., Rudolph, E.S.J., Van Hemert, P., Rossen, W.R. and Wolf, K.H., 2014. Wettability evaluation of a CO_2/water/bentheimer sandstone system: Contact angle, dissolution, and bubble size. Energy & Fuels, 28(6), pp.4002-4020.

Keller, A.A., Blunt, M.J., Roberts, P.V. (1997) Micromodel observation of the role of oil layers in three-phase flow. Transport Porous Med. 26, 277-297.

Kim, Y., J. Wan, T. J. Kneafsey, and T. K. Tokunaga (2012) Dewetting of silica surfaces upon reactions with supercritical CO_2 and brine: Pore scale studies in micromodels, Environ. Sci. Technol., 46(7), 4228–4235.

Koschel, D., Coxam, J. Y., Rodier, L., & Majer, V. (2006). Enthalpy and solubility data of CO2 in water and NaCl (aq) at conditions of interest for geological sequestration. Fluid Phase Equilibria, 247(1), 107-120.

Kovscek, A.R. and Cakici, M.D., 2005. Geologic storage of carbon dioxide and enhanced oil recovery. II. Cooptimization of storage and recovery.Energy Conversion and Management, 46(11), pp.1941-1956.

Krevor, S. C. M., R. Pini, L. Zuo, and S. M. Benson (2012) Relative permeability and trapping of CO_2 and water in sandstone rocks at reservoir conditions, Water Resour. Res., 48, W02532, doi: 10.1029/2011WR010859.

Krevor, S., Blunt, M.J., Benson, S.M., Pentland, C.H., Reynolds, C., Al-Menhali, A. and Niu, B., 2015. Capillary trapping for geologic carbon dioxide storage–From pore scale physics to field scale implications. International Journal of Greenhouse Gas Control, 40, pp.221-237.

Kumar M, Fogden, A., Senden, T., Knackstedt M. (2012). Investigation of pore-scale mixed wettability. SPE Journal, 17, 1, 20-30.

Kumar M., Senden T., Knackstedt M., Latham S., Pinczewski W., Sok R., Sheppard A., Turner M. (2009) Imaging of Pore Scale Distribution of fluids and Wettability. Petrophysics, 50, 4, 311-321.

Kumar, A., Noh, M.H., Ozah, R.C., Pope, G.A., Bryant, S.L., Sepehrnoori, K. and Lake, L.W., 2005. Reservoir simulation of CO_2 storage in aquifers. Spe Journal, 10(03), pp.336-348.

Lackner, K.S. (2003) Climate change. A guide to CO_2 sequestration, Science, 300, 1677-1678, doi:10.1126/science.1079033.

Lagneau, V., Pipart, A., & Catalette, H. (2005). Reactive Transport modelling and Long Term Behaviour of CO_2 Sequestration in Saline Aquifers. Oil & Gas Science and Technology, 60(2), 231-247.

Lake L. W. "Enhanced Oil Recovery." SPE ATCE. Training Courses. Florence, Italy: Society of Petroleum Engineers, September 23, 2010.

Lake, LW. 2010. Enhanced oil recovery. Richardson: SPE Publications.

Lander, L. M., Siewierski, L. M., Brittain, W. J., & Vogler, E. A. (1993). A systematic comparison of contact angle methods. Langmuir, 9, 2237-2237.

Lebedev, M., Iglauer, S., Mikhaltsevitch, V. Acoustic Response of Reservoir Sandstones during Injection of Supercritical CO_2. Energy Procedia 2014; 63:4281-4288.

Li, X., E. Boek, G.C. Maitland, and J.P.M. Trusler (2012) Interfacial Tension of (Brines + CO_2): (0.864 NaCl + 0.136 KCl) at Temperatures between (298 and 448) K, Pressures between (2 and 50) MPa, and Total Molalities of (1 to 5) mol·kg-1, Journal of Chemical & Engineering Data, 57(4), 1078-1088, doi:10.1021/je201062r.

Lide, DR. CRC Handbook of Chemistry & Physics, Ohio: Chemical Rubber & Co; 2007.

Lopes, S., Lebedev, M., Mueller, T., Clennell, B., Gurevich, B. Forced imbibition into a limestone: measuring P-wave velocity and water saturation dependence on injection rate. Geophysical Prospecting 2014;62: 1126-1142.

Lorenz, C.D., and R.M. Ziff (1998) Precise determination of the bond percolation thresholds and finite-size scaling corrections for the sc, fcc, and bcc lattices, Physical Review E, 57,230-237.

Lorenz, CD, Ziff, RM. (1998) Precise determination of the bond percolation thresholds and finite-size scaling corrections for the sc, fcc, and bcc lattices. Physical Review E 57, 1, 230-236.

Love, J.C., Estroff, L.A., Kriebel, J.K., Nuzzo, R.G. and Whitesides, G.M., 2005. Self-assembled monolayers of thiolates on metals as a form of nanotechnology. Chemical reviews, 105(4), pp.1103-1170.

Madonna C., Quintal B., Frehner M., Almqvist BSG., Tisato N., Pistone M., Marone F. Saenger EH. Synchrotron-based X-ray tomographic microscopy for rock microstructure investigations. Geophysics 2013;78: D53-D64.

Mahadevan, J., 2012. Comments on the paper titled "Contact angle measurements of CO_2–water-quartz/calcite systems in the perspective of carbon sequestration": A case of contamination? International Journal of Greenhouse Gas Control, 7, pp.261-262.

McCaffery, F.G., and D.W Bennion (1974) The effect of wettability on two phase relative Permeabilities. Journal of Canadian Petroleum Engineering. 13, 4, 42-53.

McCaughan, J., Iglauer, S. and Bresme, F., 2013. Molecular dynamics simulation of water/CO 2-quartz interfacial properties: Application to subsurface gas injection. Energy Procedia, 37, pp.5387-5402.

Merath, C., 2008. Microscopic calculation of line tensions. PhD thesis, Institute for Theoretical and Applied Physics, University of Stuttgart.

Metz, B., Davidson, O., de Coninck, H., Loos, M., Meyer, L. and Working Group III of the Intergovernmental Panel on Climate Change, 2005. IPCC, 2005: IPCC special report on carbon dioxide capture and storage.

Mittal, K. L. (Ed.). (2006). Contact angle, wettability and adhesion (Vol. 4). CRC Press.

Mohamed, I.M., He, J. and Nasr-El-Din, H.A., 2011, January. Carbon Dioxide Sequestration in Dolomite Rock. In International Petroleum Technology Conference. International Petroleum Technology Conference.

Moortgat, J., Sun, S., Firoozabadi, A. (2011) Compositional modelling of three-phase flow with gravity using higher-order finite element methods. Water Resources Research. 47, W05511.

Moortgat, J., Sun, S., Firoozabadi, A. (2011) Compositional modelling of three-phase flow with gravity using higher-order finite element methods. Water Resources Research. 47, W05511.

Morrow, N, Chatzis, I, Taber, J. (1988) Entrapment and mobilization of residual oil in bead packs. SPE Reservoir Engineering. 3, 927-934.

Morrow, N. (1976) Capillary pressure correlations for uniformly wetted porous media. Journal of Canadian Petroleum Technology. 4, 49-69.

Morrow, N.R. (1990) Wettability and Its Effect on Oil Recovery. Journal of Petroleum Technology. 42(12), 1476-1484.

Naylor, M., Wilkinson, M. and Haszeldine, R.S., 2011. Calculation of CO_2 column heights in depleted gas fields from known pre-production gas column heights. Marine and Petroleum Geology, 28(5), pp.1083-1093.

Neuzil, C. E. (1994). How permeable are clays and shales? Water Resources Research, 30(2), 145-150.

Nwidee, L., Al-Anssari, S., Barifcani, A., Sarmadivaleh, M. and Iglauer, S., 2016, March. Nanofluids for Enhanced Oil Recovery Processes: Wettability Alteration Using Zirconium Oxide. In Offshore Technology Conference Asia. Offshore Technology Conference.

Nwidee, L., Al-Anssari, S., Barifcani, A., Sarmadivaleh, M. Lebedev, M., and Iglauer, S. 2016. "Nanoparticles influence on wetting behaviour of fractured limestone formation." Journal of Petroleum Science and Engineering. 149, Pages 782-788, doi: org/10.1016/j.petrol.2016.11.017.

Oak, MJ, Baker, LE, Thomas, DC. (1990) Three-phase relative permeability of Berea sandstone. J Petrol Technol. 42, 1054-1061.

Olenick, S., Schroeder, F.A., Haines, H.K. and Monger-McClure, T.G., 1993. Cyclic CO_2 injection for heavy-oil recovery in Halfmoon field: laboratory evaluation and pilot performance.

Oomole, O. and Osoba, J.S., 1983, January. Carbon Dioxide-Dolomite Rock Interaction During CO Flooding Process. In Annual Technical Meeting. Petroleum Society of Canada.

Øren, P. and S. Bakke, Process Based Reconstruction of Sandstones and Prediction of Transport Properties. Transport in Porous Media 2002. 46(2-3): p. 311-343.

Oren, P.E., Billiote, J., and W.V. Pinczewski (1992) Mobilization of waterflood residual oil by gas injection for water-wet conditions, SPE Form Eval. 7, 70-78.

Oren, PE, Pinczewski, WV. (1995) Fluid distribution and pore-scale displacement mechanisms in drainage dominated three phase flow. Transport Porous Med. 20, 105-133.

Orr, F.M. (2009) Onshore geologic storage of CO_2, Science, 325, 1656-1658, doi:10.1126/science.1175677.

Ortiz-Arango, JD, Kantzas, A. (2009) Visual study of the effect of viscosity ratio, flow rate and porous medium topology on two-phase relative permeabilities. Proc Can Int Petrol Conf; 2009.

Otsu, N. A threshold selection method from gray-level histograms. IEEE Trans Syst Man Cyber 1979; 9: 62–66.

Owens, W.W. and D.L. Archer, Effect of rock wettability on oil-water relative permeability relationships. Journal of Petroleum Technology, 1970. 23(7): p. 873-878.

Pentland, C. H., El-Maghraby, R., Iglauer, S., and M. J. Blunt (2011) Measurements of the capillary trapping of super-critical carbon dioxide in Berea sandstone, Geophys. Res. Lett., 38, L06401, doi: 10.1029/2011GL046683.

Pentland, C., S. Iglauer, O. Gharbi, K. Okada, and T. Suekane (2012) The Influence of Pore Space Geometry on the Entrapment of Carbon Dioxide by Capillary Forces, SPE 158516, SPE Asia Pacific Oil and Gas Conference and Exhibition, Perth, Australia.

Pentland, CH, Tanino, Y, Iglauer, S, Blunt, MJ. (2010) Capillary trapping in water-wet sandstone: coreflooding experiments and pore-network modelling. SPE An Tech Conf 2010, SPE 133798.

Pini, R., & Benson, S. M. (2013). Simultaneous determination of capillary pressure and relative permeability curves from core-flooding experiments with various fluid pairs. Water Resources Research, 49(6), 3516-3530.

Pinon, A.V., Wierez-Kien, M., Craciun, A.D., Beyer, N., Gallani, J.L. and Rastei, M.V., 2016. Thermal effects on van der Waals adhesive forces. Physical ReviewB, 93(3), p.035424.

Piri, M. and J.M. Blunt, Three-Dimensional Mixed-Wet Random Pore-Scale Model of Two- and Three-Phase Flow in Porous Media. II. Results. Physical Review, 2005. 71(2).

Piri, M. and M.J. Blunt, Three-Dimensional Mixed-Wet Random Pore-Scale Model of Two- and Three-Phase Flow in Porous Media. I. Model description. Physical Review, 2005. 71 026301.

Piri, M., Blunt, M.J. (2004) Three-phase capillary pressures in noncircular capillary tubes with different wettabilities including contact angle hysteresis. Physical Review E. 70, 061603.

Piri, M., Blunt, M.J. (2005a) Three-dimensional mixed-wet random pore-scale network modelling of two- and three-phase flow in porous media. I. Model description. Physical Review E. 71, 026301.

Piri, M., Blunt, M.J. (2005b) Three-dimensional mixed-wet random pore-scale network modelling of two- and three-phase flow in porous media. II. Results. Physical Review E. 71, 026301.

Pokrovsky, O.S., Golubev, S.V. and Schott, J., 2005. Dissolution kinetics of calcite, dolomite and magnesite at 25 C and 0 to 50 atm pCO_2. Chemical Geology, 217(3), pp.239-255.

Pokrovsky, O.S., Golubev, S.V., Schott, J. and Castillo, A., 2009. Calcite, dolomite and magnesite dissolution kinetics in aqueous solutions at acid to circumneutral pH, 25 to 150 C and 1 to 55 atm pCO_2: New constraints on CO_2 sequestration in sedimentary basins. Chemical geology, 265(1), pp.20-32.

Prodanovic, M., Lindquist, W.B., Seright, R.S. (2007) 3D image-based characterization of fluid displacement in a Berea core. Advances in Water Resources. 30, 214–226.

Qi, R, LaForce, TC, Blunt, MJ. (2009) A three-phase four-component streamline-based simulator to study carbon dioxide storage. Comput Geosci. 13, 493-509.

Qi, R., LaForce, T.C. and Blunt, M.J., 2009. Design of carbon dioxide storage in aquifers. International journal of greenhouse gas control, 3(2), pp.195-205.

Rahman, T., Lebedev, M., Barifcani, A. and Iglauer, S., 2016. Residual trapping of supercritical CO 2 in oil-wet sandstone. Journal of Colloid and Interface Science, 469, pp.63-68.

Roof, J.G. (1970) Snap-off of oil droplets in water-wet pores, SPE Journal, 10(1), 85-90.

Roshan, H., Al-Yaseri, A.Z., Sarmadivaleh, M. and Iglauer, S., 2016. On wettability of shale rocks. Journal of Colloid and Interface Science, 475, pp.104-111.

Saenger, EH., Lebedev, M., Uribe, D., Osorno, M., Vialle, S., Duda, M., Inglauer, S., Steeb, H. Analysis of high resolution X-ray CT images of Bentheim Sandstone under elevated confining pressures. Geophysical prospecting 2016; 64:848-859.

Sahimi, M., 2011. Flow and transport in porous media and fractured rock: from classical methods to modern approaches.

Salathiel, R.A., 1973. Oil recovery by surface film drainage in mixed-wettability rocks, Journal of Petroleum Technology, p. 1216-1224.

Saraji, S., Goual, L., Piri, M. and Plancher, H., 2013. Wettability of supercritical carbon dioxide/water/quartz systems: simultaneous measurement of contact angle and interfacial tension at reservoir conditions. Langmuir, 29(23), pp.6856-6866.

Saraji, S., Piri, M. and Goual, L., 2014. The effects of SO_2 contamination, brine salinity, pressure, and temperature on dynamic contact angles and interfacial tension of supercritical CO_2/brine/quartz systems. International Journal of Greenhouse Gas Control, 28, pp.147-155.

Sarmadivaleh, M., Al-Yaseri, A.Z. and Iglauer, S., 2015. Influence of temperature and pressure on quartz–water–CO_2 contact angle and CO_2–water interfacial tension. Journal of Colloid and Interface Science, 441, pp.59-64.

Schaef, H.T. and McGrail, B.P., 2004. Direct measurements of pH in H2O-CO_2 brine mixtures to supercritical conditions. In Proceedings of the 7th International Conference on Greenhouse Gas Control Technologies (GHGT-7).

Schlüter, S., Sheppard, A., Brown, K., and D. Wildenschild (2014) Image processing of multiphase images obtained via microtomography: a review. Water Resources Research. WR015256. 3615-3639, doi: 10.1002/2014WR015256.

Sedghi, M., Piri, M. and Goual, L., 2014. Molecular dynamics of wetting layer formation and forced water invasion in angular nanopores with mixed wettability. The Journal of chemical physics, 141(19), p.194703.

Shulakova, V., Pervukhina, M., Müller, M., Lebedev, M., Mayo, S., Schmid, S., Golodoniuc, P., De Paula, O.P., Clennell, M.B., Gurevich, B. Computational elastic up-scaling of sandstone on the basis of X-ray micro-tomographic images. Geophysical Prospecting 2013; 61:287-301.

Siddiqui, S., Grader, A. S., Touati, M., Loermans, A. M., Fun, J. J., Techniques for Extracting Reliable Density and Porosity Data From Cuttings, SPE 96918.Proceedings of the SPE Annual Technical Conference and Exhibition, 2005, Dallas, Texas.

Sleep, B.E., McClure, P.D. (2001) Removal of volatile and semivolatile organic contamination from soil by air and steam flushing. Journal of Contaminant Hydrology. 50, 21-40.

Slobod, R.L. and Blum, A, H., 1952. Method for Determining Wettability of Reservoir Rocks. Petroleum Transactions AIME., 195: p. 1-4.

Soll, WE, Celia, MA, Wilson, JL. (1993) Micromodel studies of three-fluid porous media systems: pore-scale processes relating to capillary pressure-saturation relationships. Water Resour Res. 29, 2963-2974.

Stauffer, D. (1979) Scaling theory of percolation clusters. Phys Rep. 54, 1-74.

Suekane, T., Mizumoto, A., Nobuso, T., Yamazaki, M., Tsushima, S., Hirai, S. (2006). Solubility and residual gas trapping of CO_2 in geological storage, Proceedings of the 8th International Conference on Greenhouse Gas Control Technologies GHGT-8

Suekane, T., Nobuso, T., Hirai, S., and M. Kiyota (2008) Geological storage of carbon dioxide by residual gas and solubility trapping, Int. J. Greenhouse Gas Control, 2(1), 58-64.

Takei, Y.G., Aoki, T., Sanui, K., Ogata, N., Sakurai, Y. and Okano, T., 1994. Dynamic contact angle measurement of temperature-responsive surface properties for poly (N-isopropylacrylamide) grafted surfaces. Macromolecules, 27(21), pp.6163-6166.

Tanino, Y., and M. J. Blunt (2013) Laboratory investigation of capillary trapping under mixed-wet conditions. Water Resources Research. 49, 7, 4311–4319.

Thomas, D. C., & Benson, S. M. (Eds.). (2015). Carbon dioxide capture for storage in deep geologic formations-results from the CO_2 Capture Project: Vol 2. Geologic Storage of Carbon Dioxide with Monitoring and Verification. Elsevier.

Tokunaga, T.K., and J. Wan (2013) Capillary pressure and mineral wettability influences on reservoir CO_2 capacity, Reviews in Mineralogy and Geochemistry, 77, 481-503.

Valvatne, P.H. and M.J. Blunt, Predictive pore-scale modeling of two-phase flow in mixed wet media. Water Resources Research, 2004. 40(7) W07406, doi:10.1029/2003WR002627

Van Dijke, M.I.J., McDougall, S.R., Sorbie, K.S. (2011) Three-phase capillary pressure and relative permeability relationsships in mixed-wet systems. Transport in Porous Media. 44, 1-32.

Wardlaw, N.C., and L. Yu (1988) Fluid topology, pore size and aspect ratio during imbibition, Transport in Porous Media, 3(1), 17-34.

Wildenschild, D., Sheppard, A.P. (2013) X-ray imaging and analysis techniques for quantifying pore-scale structure and processes in subsurface porous medium systems. Advances in Water Resources. 51, 217–246.

Xie, X., and N.R. Morrow (1998) Wetting of Quartz by Oleic/Aqueous Liquids and Adsorption from Crude Oil, Colloids and Surfaces, 138, 97-108.

Xu, T., Apps, J. A., & Pruess, K. (2001). Analysis of mineral trapping for CO_2 disposal in deep aquifers. Lawrence Berkeley National Laboratory.

Yang, D., Gu, Y. and Tontiwachwuthikul, P., 2008. Wettability determination of the crude oil− reservoir brine− reservoir rock system with dissolution of CO_2 at high pressures and elevated temperatures. Energy & Fuels, 22(4), pp.2362-2371.

Yang, D., Gu, Y., and P. Tontiwachwuthikul (2007) Wettability determination of the reservoir brine− reservoir rock system with dissolution of CO_2 at high pressures and elevated temperatures, Energy & Fuels, 22(1), 504-509.

Young, T., 1805. An essay on the cohesion of fluids. Philosophical Transactions of the Royal Society of London, 95, pp.65-87.

Youssef, S., Bauer, D., Bekri, S., Rosenberg, E., Vizika, O., 2010. 3D in-situ fluid distribution imaging at the pore scale as a new tool for multiphase flow studies. Paper 135194 presented at SPE Annual Technical Conference and Exhibition, Florence, Italy, September 19 -- 22.

Zhang, Y., Lebedev, M., Sarmadivaleh, M., Barifcani, A., Iglauer, S. 2016a. Swelling-induced changes in coal microstructure due to supercritical CO_2 injection. Geophysical Research Letters;43: doi:10.1002/2016GL070654

Zhang, Y., Lebedev, M., Sarmadivaleh, M., Barifcani, A., Rahman, T., Iglauer, S. 2016b. Swelling effect on coal micro structure and associated permeability reduction. Fuel;182:568-576.

Zhang, Y., Xu, X., Lebedev, M., Sarmadivaleh, M., Barifcani, A., Iglauer, S. 2016. Multi-scale x-ray computed tomography analysis of coal microstructure and permeability changes as a function of effective stress. International Journal of Coal Geology;165:149-156

Appendices

Appendix 1: Statement of Contributions of Others

Appendix 1.1: Statement of Contributions of Others for

Al-Yaseri, Roshan, H., A., Zhang, Y., **Rahman, T**., Barifcani, A., Iglauer, S., 2017. Effect of Temperature on CO2/Brine/Dolomite Wettability: Hydrophilic vs Hydrophobic Surfaces. Journal of Energy & Fuels.

Statement of Contribution of Others for "Effect of Temperature on CO2/Brine/Dolomite Wettability: Hydrophilic vs Hydrophobic Surfaces"

09 October 2017

To Whom It May Concern

I, Dr. Hamid Roshan, contributed by samples preparation, and measurement to the paper publication entitled

Al-Yaseri, Roshan, H., A., Zhang, Y., **Rahman, T**., Barifcani, A., Iglauer, S., 2017. Effect of Temperature on CO2/Brine/Dolomite Wettability: Hydrophilic vs Hydrophobic Surfaces. Journal of Energy & Fuels.

Undertaken with Taufiqurrahman

(Signature of Co-author 1)
Roshan, H

(Signature of First author)
Ahmed Al-Yaseri

Statement of Contribution of Others for “Effect of Temperature on CO2/Brine/Dolomite Wettability: Hydrophilic vs Hydrophobic Surfaces”

09 October 2017

To Whom It May Concern

I, Mr. Yihuai Zhang., contributed by samples preparation to the paper publication entitled

Al-Yaseri, Roshan, H., A., Zhang, Y., **Rahman, T**., Barifcani, A., Iglauer, S., 2017. Effect of Temperature on CO2/Brine/Dolomite Wettability: Hydrophilic vs Hydrophobic Surfaces. Journal of Energy & Fuels.

Undertaken with Taufiqurrahman

(Signature of Co-author 2)
Yihuai Zhang

(Signature of First author)
Ahmed Al-Yaseri

Statement of Contribution of Others for "Effect of Temperature on CO2/Brine/Dolomite Wettability: Hydrophilic vs Hydrophobic Surfaces"

09 October 2017

To Whom It May Concern

I, Mr. Taufiqurrahman., contributed by manuscript editing to the paper/publication entitled

Al-Yaseri, Roshan, H., A., Zhang, Y., **Rahman, T**., Barifcani, A., Iglauer, S., 2017. Effect of Temperature on CO2/Brine/Dolomite Wettability: Hydrophilic vs Hydrophobic Surfaces. Journal of Energy & Fuels.

Undertaken with Taufiqurrahman

(Signature of Co-author 3)
Rahman, T

(Signature of First author)
Ahmed Al-Yaseri

Statement of Contribution of Others for "Effect of Temperature on CO2/Brine/Dolomite Wettability: Hydrophilic vs Hydrophobic Surfaces"

09 October 2017

To Whom It May Concern

I, Prof Barifcani A., contributed by specialist technical advice and manuscript editing to the paper/publication entitled

Al-Yaseri, Roshan, H., A., Zhang, Y., **Rahman, T**., Barifcani, A., Iglauer, S., 2017. Effect of Temperature on CO2/Brine/Dolomite Wettability: Hydrophilic vs Hydrophobic Surfaces. Journal of Energy & Fuels.

Undertaken with Taufiqurrahman

(Signature of Co-author 4)
Barifcani, A

(Signature of First author)
Ahmed Al-Yaseri

Statement of Contribution of Others for “Effect of Temperature on CO2/Brine/Dolomite Wettability: Hydrophilic vs Hydrophobic Surfaces”

09 October 2017

To Whom It May Concern

I, Prof Stefan Iglauer, contributed by specialist technical advice and manuscript editing to the paper/publication entitled

Al-Yaseri, Roshan, H., A., Zhang, Y., **Rahman, T**., Barifcani, A., Iglauer, S., 2017. Effect of Temperature on CO2/Brine/Dolomite Wettability: Hydrophilic vs Hydrophobic Surfaces. Journal of Energy & Fuels.

Undertaken with Taufiqurrahman

(Signature of Co-author 5)
Iglauer, S

(Signature of First author)
Ahmed Al-Yaseri

Appendix 1.2: Statement of Contributions of Others for

M Lebedev, Y Zhang, V Mikhaltsevitch, S Iglauer, **T Rahman**, “Residual trapping of supercritical CO2: direct pore-scale observations using a low cost pressure cell for micro computer tomography”, Energy Procedia, 114, 4967-4974, 2017

Statement of Contribution of Others for “Residual trapping of supercritical CO2: direct pore-scale observations using a low cost pressure cell for micro computer tomography”

09 October 2017

To Whom It May Concern

I, Yihuai Zhang, contributed by samples preparation, and measurement to the paper publication entitled

M Lebedev, Y Zhang, V Mikhaltsevitch, S Iglauer, **T Rahman**, “Residual trapping of supercritical CO2: direct pore-scale observations using a low cost pressure cell for micro computer tomography”, Energy Procedia, 114, 4967-4974, 2017

Undertaken with Taufiqurrahman

(Signature of Co-author 1)
Yihuai Zhang

(Signature of First author)
Lebedev, M

Statement of Contribution of Others for “Residual trapping of supercritical CO2: direct pore-scale observations using a low cost pressure cell for micro computer tomography”

09 October 2017

To Whom It May Concern

I, Vassili Mikhaltsevitch, contributed by samples preparation, and measurement to the paper publication entitled

M Lebedev, Y Zhang, V Mikhaltsevitch, S Iglauer, **T Rahman**, “Residual trapping of supercritical CO2: direct pore-scale observations using a low cost pressure cell for micro computer tomography”, Energy Procedia, 114, 4967-4974, 2017

Undertaken with Taufiqurrahman

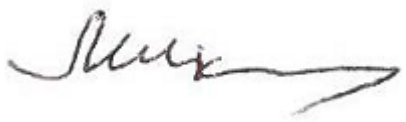

(Signature of Co-author 2)
V, Mikhaltsevitch

(Signature of First author)
Lebedev, M

Statement of Contribution of Others for “Residual trapping of supercritical CO2: direct pore-scale observations using a low cost pressure cell for micro computer tomography”

09 October 2017

To Whom It May Concern

I, Stefan Iglauer, contributed by specialist technical advice and manuscript editing to the paper/publication entitled

M Lebedev, Y Zhang, V Mikhaltsevitch, S Iglauer, **T Rahman**, “Residual trapping of supercritical CO2: direct pore-scale observations using a low cost pressure cell for micro computer tomography”, Energy Procedia, 114, 4967-4974, 2017

Undertaken with Taufiqurrahman

(Signature of Co-author 3)
Iglauer, S

(Signature of First author)
Lebedev, M

Statement of Contribution of Others for “Residual trapping of supercritical CO2: direct pore-scale observations using a low cost pressure cell for micro computer tomography”

09 October 2017

To Whom It May Concern

I, Taufiqurrahman, contributed by all analysis of residual CO_2 trapping data to the paper publication entitled

M Lebedev, Y Zhang, V Mikhaltsevitch, S Iglauer, **T Rahman**, “Residual trapping of supercritical CO2: direct pore-scale observations using a low cost pressure cell for micro computer tomography”, Energy Procedia, 114, 4967-4974, 2017

Undertaken with Taufiqurrahman

(Signature of Co-author 4)
Rahman, T

(Signature of First author)
Lebedev, M

Appendix 1.3: Statement of Contributions of Others for

Rahman, T., Lebedev, M., Barifcani, A. and Iglauer, S., 2016. Residual trapping of supercritical CO_2 in oil-wet sandstone. *Journal of colloid and interface science*, *469*, pp.63-68.

Statement of Contribution of Others for "Residual trapping of supercritical CO_2 in oil-wet sandstone"

09 October 2017

To Whom It May Concern

I, Prof Maxim Lebedev, contributed by samples preparation, and measurement to the paper publication entitled

Rahman, T., Lebedev, M., Barifcani, A. and Iglauer, S., 2016. Residual trapping of supercritical CO_2 in oil-wet sandstone. *Journal of colloid and interface science*, *469*, pp.63-68.

Undertaken with Taufiqurrahman

(Signature of Co-author 1)
Lebedev, M

(Signature of First author)
Rahman, T

Statement of Contribution of Others for "Residual trapping of supercritical CO_2 in oil-wet sandstone"

09 October 2017

To Whom It May Concern

I, Prof Ahmed Barifcani, contributed by specialist technical advice and manuscript editing to the paper/publication entitled

Rahman, T., Lebedev, M., Barifcani, A. and Iglauer, S., 2016. Residual trapping of supercritical CO_2 in oil-wet sandstone. *Journal of colloid and interface science*, *469*, pp.63-68.

Undertaken with Taufiqurrahman

(Signature of Co-author 2)
Barifcani, A

(Signature of First author)
Rahman, T

Statement of Contribution of Others for "Residual trapping of supercritical CO_2 in oil-wet sandstone"

09 October 2017

To Whom It May Concern

I, Prof Stefan Iglauer, contributed by specialist technical advice and manuscript editing to the paper/publication entitled

Rahman, T., Lebedev, M., Barifcani, A. and Iglauer, S., 2016. Residual trapping of supercritical CO_2 in oil-wet sandstone. *Journal of colloid and interface science*, *469*, pp.63-68.

Undertaken with Taufiqurrahman

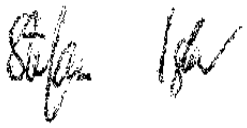

(Signature of Co-author 3)
Iglauer, S

(Signature of First author)
Rahman, T

Appendix 1.4: Statement of Contributions of Others for

Iglauer, S., **Rahman, T**., Sarmadivaleh, M., Al-Hinai, A., Fernø, M.A. and Lebedev, M., 2016. Influence of wettability on residual gas trapping and enhanced oil recovery in three-phase flow: a pore-scale analysis by use of microcomputed tomography. *SPE Journal*.

Statement of Contribution of Others for “Influence of wettability on residual gas trapping and enhanced oil recovery in three-phase flow: a pore-scale analysis by use of microcomputed tomography”

09 October 2017

To Whom It May Concern

I, Mr. Taufiqurrahman, contributed by samples preparation, measurement and all analysis of contact angle data to the paper publication entitled

Iglauer, S., **Rahman, T**., Sarmadivaleh, M., Al-Hinai, A., Fernø, M.A. and Lebedev, M., 2016. Influence of wettability on residual gas trapping and enhanced oil recovery in three-phase flow: a pore-scale analysis by use of microcomputed tomography. *SPE Journal*.
Undertaken with Taufiqurrahman

(Signature of Co-author 1)
Rahman, T

(Signature of First author)
Iglauer, S

Statement of Contribution of Others for "Influence of wettability on residual gas trapping and enhanced oil recovery in three-phase flow: a pore-scale analysis by use of microcomputed tomography"

09 October 2017

To Whom It May Concern

I, Dr. Mohammad Sarmadivaleh, contributed by specialist technical advice and manuscript editing to the paper/publication entitled

Iglauer, S., **Rahman, T**., Sarmadivaleh, M., Al-Hinai, A., Fernø, M.A. and Lebedev, M., 2016. Influence of wettability on residual gas trapping and enhanced oil recovery in three-phase flow: a pore-scale analysis by use of microcomputed tomography. *SPE Journal*.

Undertaken with Taufiqurrahman

(Signature of Co-author 2)
Sarmadivaleh, M

(Signature of First author)
Iglauer, S

Statement of Contribution of Others for “Influence of wettability on residual gas trapping and enhanced oil recovery in three-phase flow: a pore-scale analysis by use of microcomputed tomography”

09 October 2017

To Whom It May Concern

I, Dr. Adnan Al-Hinai, contributed by specialist technical advice and image processing to the paper/publication entitled

Iglauer, S., **Rahman, T**., Sarmadivaleh, M., Al-Hinai, A., Fernø, M.A. and Lebedev, M., 2016. Influence of wettability on residual gas trapping and enhanced oil recovery in three-phase flow: a pore-scale analysis by use of microcomputed tomography. *SPE Journal*.

Undertaken with Taufiqurrahman

(Signature of Co-author 3)
Al-Hinai, A

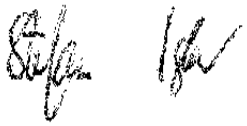

(Signature of First author)
Iglauer, S

Statement of Contribution of Others for "Influence of wettability on residual gas trapping and enhanced oil recovery in three-phase flow: a pore-scale analysis by use of microcomputed tomography"

09 October 2017

To Whom It May Concern

I, Prof Martin A Fernø, contributed by specialist technical advice and image processing to the paper/publication entitled

Iglauer, S., **Rahman, T**., Sarmadivaleh, M., Al-Hinai, A., Fernø, M.A. and Lebedev, M., 2016. Influence of wettability on residual gas trapping and enhanced oil recovery in three-phase flow: a pore-scale analysis by use of microcomputed tomography. *SPE Journal*.

Undertaken with Taufiqurrahman

(Signature of Co-author 4)
Fernø, M.A

(Signature of First author)
Iglauer, S

Statement of Contribution of Others for “Influence of wettability on residual gas trapping and enhanced oil recovery in three-phase flow: a pore-scale analysis by use of microcomputed tomography”

09 October 2017

To Whom It May Concern

I, Prof Maxim Lebedev, contributed by specialist image processing and manuscript editing to the paper/publication entitled

Iglauer, S., **Rahman, T**., Sarmadivaleh, M., Al-Hinai, A., Fernø, M.A. and Lebedev, M., 2016. Influence of wettability on residual gas trapping and enhanced oil recovery in three-phase flow: a pore-scale analysis by use of microcomputed tomography. *SPE Journal*.

Undertaken with Taufiqurrahman

(Signature of Co-author 5)
Lebedev, M

(Signature of First author)
Iglauer, S

Appendix 2: Copyright Forms

Appendix 2.1.

This appendix contains the copyright agreements between the author and Journals to reuse the author's own published material in this thesis.

Chapter 3, Article: "Effect of Temperature on CO_2/Brine/Dolomite Wettability: Hydrophilic vs Hydrophobic Surfaces"

Copyright Clearance Center RightsLink®

Home | Create Account | Help

ACS Publications
Most Trusted. Most Cited. Most Read.

Title: Effect of the Temperature on CO2/Brine/Dolomite Wettability: Hydrophilic versus Hydrophobic Surfaces
Author: A. Z. Al-Yaseri, H. Roshan, Y. Zhang, et al
Publication: Energy & Fuels
Publisher: American Chemical Society
Date: Jun 1, 2017
Copyright © 2017, American Chemical Society

LOGIN
If you're a copyright.com user, you can login to RightsLink using your copyright.com credentials. Already **a RightsLink user** or want to learn more?

PERMISSION/LICENSE IS GRANTED FOR YOUR ORDER AT NO CHARGE

This type of permission/license, instead of the standard Terms & Conditions, is sent to you because no fee is being charged for your order. Please note the following:

- Permission is granted for your request in both print and electronic formats, and translations.
- If figures and/or tables were requested, they may be adapted or used in part.
- Please print this page for your records and send a copy of it to your publisher/graduate school.
- Appropriate credit for the requested material should be given as follows: "Reprinted (adapted) with permission from (COMPLETE REFERENCE CITATION). Copyright (YEAR) American Chemical Society." Insert appropriate information in place of the capitalized words.
- One-time permission is granted only for the use specified in your request. No additional uses are granted (such as derivative works or other editions). For any other uses, please submit a new request.

BACK | CLOSE WINDOW

Copyright © 2017 Copyright Clearance Center, Inc. All Rights Reserved. Privacy statement. Terms and Conditions.
Comments? We would like to hear from you. E-mail us at customercare@copyright.com

Appendix 2.2.

This appendix contains the copyright agreements between the author and Journals to reuse the author's own published material in this thesis.

Chapter 4, Article: "Residual trapping of supercritical CO_2: direct pore-scale observation using a low cost pressure cell for micro-computer tomography"

Appendix 2.3.

This appendix contains the copyright agreements between the author and Journals to reuse the author's own published material in this thesis.

Chapter 5, Article: "Residual Trapping of Supercritical CO_2 in oil-wet sandstone"

Thank you for your order.

This Agreement between Mr. Taufiq Rahman ("You") and Elsevier ("Elsevier") consists of your license details and the terms and conditions provided by Elsevier and Copyright Clearance Center.

Your confirmation email will contain your order number for future reference.

Printable details.

License Number	4127511439607
License date	Jun 14, 2017
Licensed Content Publisher	Elsevier
Licensed Content Publication	Journal of Colloid and Interface Science
Licensed Content Title	Residual trapping of supercritical CO2 in oil-wet sandstone
Licensed Content Author	Taufiq Rahman,Maxim Lebedev,Ahmed Barifcani,Stefan Iglauer
Licensed Content Date	Jan 1, 0001
Licensed Content Volume	469
Licensed Content Issue	n/a
Licensed Content Pages	6
Type of Use	reuse in a thesis/dissertation
Portion	full article
Format	both print and electronic
Are you the author of this Elsevier article?	Yes
Will you be translating?	No
Order reference number	
Title of your thesis/dissertation	Pore-Scale Investigations of Rock and Fluid Microstructure and Fluid Displacement Processes in Geological Porous Media
Expected completion date	Jul 2017
Estimated size (number of pages)	200
Elsevier VAT number	GB 494 6272 12
Requestor Location	Mr. Taufiq Rahman 77 Lyrebird Way Thornlie, WA 6108 Australia Attn: Mr. Taufiq Rahman
Total	0.00 AUD

Appendix 2.4.

This appendix contains the copyright agreements between the author and Journals to reuse the author's own published material in this thesis.

Chapter 6, Article: "Influence of wettability on residual gas trapping and enhanced oil recovery in three-phase flow: a pore-scale analysis using micro-computed tomography"

Thank you for your order.

This Agreement between Mr. Taufiq Rahman ("You") and Society of Petroleum Engineers ("Society of Petroleum Engineers") consists of your license details and the terms and conditions provided by Society of Petroleum Engineers and Copyright Clearance Center.

Your confirmation email will contain your order number for future reference.

Printable details.

License Number	4127521159649
License date	Jun 14, 2017
Licensed Content Publisher	Society of Petroleum Engineers
Licensed Content Publication	SPE Journal
Licensed Content Title	Influence of Wettability on Residual Gas Trapping and Enhanced Oil Recovery in Three-Phase Flow: A Pore-Scale Analysis by Use of Microcomputed Tomography
Licensed Content Author	Stefan Iglauer, Curtin University;Taufiq Rahman, Curtin University;Mohammad Sarmadivaleh, Curtin University et al
Licensed Content Date	Jan 1, 2016
Licensed Content Volume	21
Licensed Content Issue	06
Type of Use	Thesis/Dissertation
Requestor type	author of the original work
SPE member	no
Format	print and electronic
Portion	full article
Will you be translating?	no
Distribution	1
Order reference number	
Title of your thesis / dissertation	Pore-Scale Investigations of Rock and Fluid Microstructure and Fluid Displacement Processes in Geological Porous Media
Expected completion date	Jul 2017
Estimated size (number of pages)	200
Requestor Location	Mr. Taufiq Rahman 77 Lyrebird Way Thornlie, WA 6108 Australia Attn: Mr. Taufiq Rahman
Billing Type	Invoice
Billing address	Mr. Taufiq Rahman 77 Lyrebird Way Thornlie, Australia 6108 Attn: Mr. Taufiq Rahman
Total	0.00 USD